FACULDADE DE ENGENHARIA DA UNIVERSIDADE DO PORTO

# PhysioIntent: Towards Biosignal-based Robot Awareness Identification of Human Movement Intentions

**Ana Filipa de Sousa Ferreira**

Mestrado em Bioengenharia - Engenharia Biomédica

Supervisor: João Paulo Trigueiros da Silva Cunha, PhD.

September 18, 2022

# PhysioIntent: Towards Biosignal-based Robot Awareness Identification of Human Movement Intentions

**Ana Filipa de Sousa Ferreira**

Mestrado em Bioengenharia - Engenharia Biomédica

September 18, 2022

# Resumo

Ao longo das últimas décadas, os robôs têm vindo a integrar progressivamente a vida humana. São cada vez mais os casos de uso que envolvem a interação homem-máquina, seja desde a indústria à reabilitação clínica.

Na indústria, os robôs colaborativos são utilizados para realizar tarefas de colaboração. No entanto, a maioria desses sistemas são reativos e não antecipam o movimento humano, o que por vezes pode causar acidentes. Assim, surge a importância em prever a intenção humana.

Relativamente à reabilitação, os robôs são utilizados principalmente para ajudar ou dificultar a execução de exercícios de reabilitação. Espera-se que estes robôs detetem a intenção do movimento humano e forneçam biofeedback informativo através de várias interfaces homem-máquina.

Atualmente, a deteção da intenção de movimento é feita principalmente com análise vídeo ou sensores de movimento; por conseguinte, há algum atraso na sua deteção. Este estudo visa ultrapassar este problema através da análise de sinais fisiológicos. Assim, o objetivo é provar que, através do EEG, é possível tornar esta deteção rápida e eficaz, tornando a interação homem-robô mais natural.

Para provar isto, foi construído um dataset (*PhysioIntent*) com nove sujeitos saudáveis. Cada sujeito realizou uma sequência de ensaios que consistiu em pensar e executar três movimentos: agarrar uma garrafa, supinação do pulso, e apanhar e colocar um objeto no sitio. O EMG, EEG, e ECG foram adquiridos durante a experiência com a *Cyton board* do OpenBCI. Os dados inerciais foram também registados com um dispositivo do INESC TEC chamado iHandU. Foi também utilizada uma câmara para gravar o vídeo da sessão do participante, apoiando assim o pós-processamento dos dados gravados, verificando por exemplo, se o sujeito executou ou não o movimento. Todos os dados foram então sincronizados com a ajuda de um foto-resistência que permitiu correlacionar os estímulos visuais apresentados ao utilizador com os sinais adquiridos através do openBCI. Para além do foto-resistência, foi pensada outra metodologia para sincronizar o iHandU com o resto dos dados. Assim, no início de cada sessão, o sujeito toca três vezes no dispositivo iHandU, provocando uma mudança abrupta no acelerómetro.

O passo seguinte consistiu no pré-processamento dos sinais. O EMG e a IMU foram utilizados para detectar o inicio dos movimentos. Entre os dois, a IMU teve uma maior precisão na deteção destes.

Neste trabalho, foi utilizado o método *event-related (des)synchronization (ERD/ERS)* para analisar a sincronização ou dessincronização na banda mu e beta do EGG durante a execução, preparação, ou imaginação das ações motoras.

Os resultados foram promissores, uma vez que a intenção de movimento foi descodificada em alguns sujeitos antes do início do próprio movimento, o que mostra que o EEG está intrinsecamente correlacionado com a intenção de movimento. O uso do EEG pode permitir assim o uso de novas abordagens em situações de interação homem-máquina.

# Abstract

Over the last decades, robots have been progressively integrating daily human life. Thanks to scientific advances in robotics research, human-machine interaction is nowadays considered a feasible activity. Humans and robots can interact in many ways, from industry to clinical rehabilitation. In industry, collaborative robots are used to perform collaborative tasks. However, most of those systems are reactive and do not anticipate human movement, which sometimes can cause accidents, bringing up the importance of predicting human intent.

Regarding rehabilitation, robots are mainly used to assist or hinder the execution of planned rehabilitation exercises. These robots are expected to detect human movement intention and provide informative biofeedback through various human-machine interfaces.

Currently, motion intention detection is mainly done with video analysis or motion sensors; therefore, there is some delay in detecting it. This thesis aims to explore new ways to overcome this problem through the analysis of physiological signals. Thus, the goal is to obtain clear indications that, through EEG, it is possible to make this detection quickly and effectively, faster than the above-mentioned current approaches, making the human-robot interaction more predictive and natural.

To explore new approaches to this problem, a dataset with 9 healthy subjects was built. Each subject performed a sequence of trials that consisted of thinking and executing 3 different movements: hand-grasping, wrist supination, and pick and place. Biosignals (EMG, EEG, and ECG) were acquired during the experiment with the openBCI system. Inertial data was also recorded with a proprietary device from INESC TEC named iHandU. A camera was also used to record the participant's session video, thus better supporting the labeling and post-processing of the recorded data and the agreement between the protocol and the participant activity. All data were then synchronized with the aid of a photoresistor, correlating the visual stimuli presented to the user with the acquired signals. Besides the photoresistor, another methodology was thought to synchronize the iHandU with the rest of the data. Thus, at the beginning of each session, the subject touches the iHandU device three times, causing an easily detectable abrupt change on the accelerometer, also visible in the video, thus being used to synchronize all data streams.

The next step consisted of pre-processing the signals. The EMG and IMU were used to detect the movements onsets. Between the two, the IMU had a higher accuracy.

In this work, an event-related (de)synchronization (ERD/ERS) method was used to analyze the synchronization or desynchronization in the EEG mu and beta band during the execution, preparation, or imagination of motor actions. It was explored as a valid approach for our aimed detection method for the human intention of movement in man-robot interaction scenarios.

Results were very encouraging as motion intention was successfully decoded before the onset of motion itself, which shows that EEG is intrinsically correlated with motion intention and is a feasible technique for the aimed robot-awareness of human motion intention for novel improved human-robot interaction approaches.

# Agradecimentos

E assim se passaram 5 anos, entre risos, longas conversas, noites mal dormidas e bons amigos. Mas tudo valeu a pena. Não poderia acabar este caminhada sem agradecer aos meus amigos, em especial à Margarida e à Joana por todas as gargalhadas nos anfiteatros.

Deixo também um abraço a todos os membros do IEEE UP SB, em especial do EMBS por me terem ajudado bastante a crescer e a deixar de lado a minha timidez.

A todo o grupo do BRAIN por toda a ajuda prestada. Em especial ao Vitor por me ter acompanhado em todo o trabalho, pelas suas dicas e por simplificar os meus problemas. Ao Duarte Dias por mostrar-se sempre prestável e por me ensinar a soldar. Por fim, ao Professor João Paulo Cunha, por nunca me deixar desanimar, nunca vou esquecer o seu conselho: "KISS- Keep it simple and stupid".

Quero deixar também um agradecimento muito especial à minha família! Ao meu pai por sempre acreditar no meu futuro. E em especial à minha mãe por me ajudar sempre que preciso, e por ser a minha cobaia nos meus testes com elétrodos.

Por fim, agradeço ao meu namorado Jorge por todo o acompanhamento durante estes 5 anos. Obrigada por todas as palavras de incentivo, por todas as chamadas, por me ajudares a passar circuitos e acima de tudo por todo o amor e carinho ao longo destes anos.

Ana Filipa de Sousa Ferreira

# Contents


**1 Introduction** **1**
- 1.1 Context . . . 1
- 1.2 Motivation . . . 1
- 1.3 Objectives . . . 2
- 1.4 Contributions . . . 3
- 1.5 Dissertation outline . . . 4

**2 Biosignals and sensors used in human motion intent** **5**
- 2.1 Electromyography (EMG) . . . 5
  - 2.1.1 Movements and related muscles . . . 6
  - 2.1.2 EMG acquisition . . . 7
- 2.2 Electroencephalography(EEG) . . . 8
  - 2.2.1 Brain organization . . . 9
  - 2.2.2 Brain activity interpretation . . . 10
  - 2.2.3 EEG acquisition . . . 12
- 2.3 Inertial Measurement Unit (IMU) . . . 13
- 2.4 Biosignals noise sources . . . 13
  - 2.4.1 EMG . . . 14
  - 2.4.2 EEG . . . 14

**3 State-of-the-art** **17**
- 3.1 Data acquisition . . . 17
  - 3.1.1 Acquisition devices . . . 18
- 3.2 Signal Processing . . . 19
  - 3.2.1 EMG . . . 20
  - 3.2.2 EEG . . . 23
- 3.3 Classification . . . 24
  - 3.3.1 Data splitting . . . 26
  - 3.3.2 Classifiers used to predict human intention . . . 27
  - 3.3.3 Evaluation Metrics . . . 30
- 3.4 Protocols and datasets found in literature . . . 32
  - 3.4.1 BCI 2000 EEG Motor Movement/Imagery Dataset . . . 34
- 3.5 Brief review . . . 34

**4 Biosensing Devices** **37**
- 4.1 OpenBCI . . . 37
  - 4.1.1 EMG, ECG, and EEG Setup . . . 40
- 4.2 iHandU device . . . 43

**5 Methodology** **45**
5.1 Experimental protocol . . . 46
5.1.1 Participants . . . 46
5.1.2 Experimental paradigm . . . 47
5.1.3 Environment . . . 49
5.1.4 Data recording . . . 50
5.1.5 ECG, EEG, and EMG setup . . . 53
5.1.6 Photoresistor setup . . . 55
5.2 Pre-processing . . . 57
5.2.1 Photoresistor - edge detection . . . 58
5.2.2 EMG processing . . . 60
5.2.3 ECG processing . . . 63
5.2.4 EEG processing . . . 63
5.2.5 iHandU processing . . . 65
5.3 Synchronization . . . 67
5.4 Event-Related Desynchronization/Synchronization . . . 68

**6 Results and discussion** **71**
6.1 Collected Dataset and its Open Access publication . . . 71
6.1.1 Data Format and Structure . . . 72
6.1.2 Dataset open access publication . . . 73
6.2 Synchronization and Labeling . . . 73
6.2.1 Synchronization . . . 73
6.2.2 Labeling . . . 80
6.3 Movements onsets . . . 82
6.4 ERD/ERS maps . . . 85
6.4.1 Results for BCI 2000 dataset . . . 85
6.4.2 Results for PhysioIntent dataset . . . 88

**7 Conclusion** **93**
7.1 Future Work . . . 94

**A Code Organization** **95**

**B Written Consent** **99**

**C ERD/ERS** **103**
C.1 ERD/ERS maps . . . 103
C.2 ERD/ERS line plots . . . 112

**References** **129**

# List of Figures


1.1 Use case simulation record on iiLab from INESC TEC with UR3 robot. . . . . 3

2.1 Example of a raw EMG signal. . . . . 6
2.2 Main muscles on the superficial layer of the left arm and forearm [11]. . . . . 6
2.3 Example of electrodes placed on the arm[1]. . . . . 8
2.4 Brainwave frequencies and associated mental states (adapted) [2]. . . . . 8
2.5 Brain cortex [18]. . . . . 9
2.6 Body maps of the primary motor cortex and somatosensory cortex of the cerebrum (homunculus map)[2] . . . . . 10
2.7 Event-Related Desynchronization and Event-Related Synchronization [24] . . . . 11
2.8 Waveforms and terminology of movement-related cortical potentials (MRCPs) from a single healthy subject [25]. . . . . 12
2.9 The 10-10 international system of EEG electrode placement. The blue circles represent the location of 10-20 EEG electrodes [26]. . . . . 13
2.10 Physiological artifacts in EEG signals [29]. . . . . 14

3.1 Human Intention prediction state-of-the-art pipeline. . . . . 17
3.2 Example of RMS envelope.[3] . . . . . 22
3.3 TKEO example [44]. . . . . 22
3.4 K-Fold Cross-Validation[4]. . . . . 26
3.5 Figure adapted from Lopez-Larraz et al. (2014) [13] . . . . . 27
3.6 Support Vector Machine [62]. . . . . 28
3.7 LDA classifier example. . . . . 29
3.8 General structure of the ANN [66]. . . . . 29
3.9 LSTM cell [68]. . . . . 30
3.10 Area under the ROC curve[5]. . . . . 31
3.11 Scheme of each trial in López-Larraz et al. work. . . . . 32
3.12 Movements performed on Jeong et al. work. . . . . 33
3.13 Scheme of each trial in Jeong et al. work. . . . . 33

4.1 OpenBCI hardware. . . . . 37
4.2 OpenBCI GUI: (a) represents a time series example. The right top square plots the FFT in real time, and the right bottom square is showing the analog read. The user can select which layout they prefer. (b) example of the GUI when the impedance is being measure. . . . . 38
4.3 OpenBCI Cyton board channels. . . . . 39
4.4 Electrodes placement on the subject . . . . . 40
4.5 Electrodes utilized for EMG and ECG acquisition . . . . . 41
4.6 EEG electrode systems . . . . . 42

4.7 EEG cables and adapters. . . . 42
4.8 EEG cap reference channel. . . . 43
4.9 iHandU device. . . . 44
4.10 iHandU - Device Dashboard . . . 44

5.1 Methodology overview. . . . 45
5.2 Data recording scheme. . . . 46
5.3 Set of movements that each participant must perform. . . . 48
5.4 Acquisition protocol (one session). . . . 49
5.5 Environment setup. . . . 50
5.6 Libraries used during the development of the experiment. . . . 51
5.7 Schematic illustration of the general outline of the experimental setup (Phase 1). . 52
5.8 Schematic illustration of the general outline of the experimental setup (Phase 2). . 53
5.9 Electrodes placement in our study for acquiring EMG data (Phase 1) [8] (adapted). 53
5.10 EEG electrodes utilized in phase 1 (10-10 system). . . . 54
5.11 EEG electrodes chosen for phase 2 (10-10 system). . . . 55
5.12 Photoresistor circuit utilized to synchronize stimulus presentation and biosignals data. . . . 56
5.13 Photoresistor utilized for iHandU-OpenBCI synchronization. . . . 56
5.14 Example of photoresistor data Run 2 subject 6. . . . 57
5.15 OpenBCI data processing scheme. . . . 58
5.16 Edge detection on the photoresistor data of subject 6. The red crosses represent the edges found. . . . 59
5.17 EMG filtering (Subject 2). . . . 60
5.18 ECG filtering (Subject 7). . . . 63
5.19 EEG pre-processing subject 6. . . . 64
5.20 iHandU processing pipeline. . . . 65
5.21 iHandU processing (subject 7) . . . 66
5.22 HandU onsets (subject 7)i . . . 66
5.23 Synchronization pipeline . . . 67
5.24 Ransac representation. The offset represents the distance between the iHandU onset sample and the correspondent EMG onset. The x-axis represents the sample index of the EMG onset. The blue points are the inliers (points used for line estimation), and the green points represent the outliers (points with abnormal distance from other values). . . . 68
5.25 ERD/ERS methodology . . . 69
5.26 ERD/ERS maps examples. . . . 70

6.1 Data storage info . . . 72
6.2 Example of photoresistor signal, Run 1, subject 6. Each peak represents the beginning of a screen. . . . 75
6.3 Photoresistor reading wrong (subject 2). . . . 76
6.4 (a): iHandU sync maneuver; (b), (c), (d): iHandU accelerometer data. The blue line represents the x-axis, the orange represents the y-axis, and the green the z-axis. The horizontal axis of the graphics represents the timestamp of each sample. 77
6.5 Synchronization subject 3. . . . 78
6.6 iHandU cumulative delay regarding openBCI data (subject 6). . . . 79
6.7 Missing iHandU data (subject 6). . . . 80
6.8 iHandU data for all runs (subject 7). . . . 80

6.9 File example of the .csv output generated during protocol acquisition. . . . . 81
6.10 File example of the .csv created with the segmentation indexes of each screen. . . 82
6.11 EMG activation segments detection (subject 3) . . . . . 82
6.12 Muscle activation detection through EMG signal or acceleration data (subject 7). 83
6.13 iHandU vs EMG onsets detection. . . . . 84
6.14 ERD/ERS maps examples from BCI 2000 . . . . . 86
6.15 ERD/ERS maps on subject 5 from BCI 2000. . . . . 87
6.16 ICA components (subject 6). . . . . 88
6.17 ICA components scores. . . . . 89
6.18 EEG signal from subject 6. Left: band-pass 7-30 Hz; Right: after removing the ICA components related with ocular artifacts. . . . . 89
6.19 ERD/ERS maps before and after remove some ICA components (subject 4). . . . 90

A.1 Code organization. . . . . 96
A.2 Files used in each step of methodology. . . . . 97

C.1 ERD/ERS maps subject 2. . . . . 103
C.2 ERD/ERS maps subject 3. . . . . 104
C.3 ERD/ERS maps subject 4. . . . . 105
C.4 ERD/ERS maps subject 6. . . . . 106
C.5 ERD/ERS maps subject 7. . . . . 107
C.6 ERD/ERS maps subject 7 with iHandU marking the onsets (t = 0). . . . . 108
C.7 ERD/ERS maps subject 8. . . . . 109
C.8 ERD/ERS maps subject 9. . . . . 110
C.9 ERD/ERS maps subject 9 with iHandU marking the onsets (t = 0). . . . . 111
C.10 ERD/ERS line plot subject 2 for $\mu$ band [10, 12] Hz . . . . . 112
C.11 ERD/ERS line plot subject 2 for $\beta$ band [18, 23] Hz . . . . . 113
C.12 ERD/ERS line plot subject 4 for $\mu$ band [10, 12] Hz . . . . . 114
C.13 ERD/ERS line plot subject 4 for $\beta$ band [18, 23] Hz . . . . . 115
C.14 ERD/ERS line plot subject 6 for $\mu$ band [10, 12] Hz . . . . . 116
C.15 ERD/ERS line plot subject 6 for $\beta$ band [18, 23] Hz . . . . . 117
C.16 ERD/ERS line plot subject 7 for $\mu$ band [10, 12] Hz . . . . . 118
C.17 ERD/ERS line plot subject 7 for $\beta$ band [18, 23] Hz . . . . . 119
C.18 ERD/ERS line plot subject 7 for $\mu$ band [10, 12] Hz (with iHandU onsets as t= 0) 120
C.19 ERD/ERS line plot subject 7 for $\beta$ band [18, 23] Hz (with iHandU onsets as t= 0) 121
C.20 ERD/ERS line plot subject 8 for $\mu$ band [10, 12] Hz . . . . . 122
C.21 ERD/ERS line plot subject 8 for $\beta$ band [18, 23] Hz . . . . . 123
C.22 ERD/ERS line plot subject 9 for $\mu$ band [10, 12] Hz . . . . . 124
C.23 ERD/ERS line plot subject 9 for $\beta$ band [18, 23] Hz . . . . . 125
C.24 ERD/ERS line plot subject 9 for $\mu$ band [10, 12] Hz (with iHandU onsets as t= 0) 126
C.25 ERD/ERS line plot subject 9 for $\beta$ band [18, 23] Hz (with iHandU onsets as t= 0) 127

# List of Tables


2.1 Compilation of some similar works and their chosen muscles to detect the desired movements. . . . 7

3.1 Acquisition devices used in some works. . . . 18
3.2 List of devices and data that they can measure . . . 19
3.3 Summary of EMG filter found in literature . . . 20
3.4 Threshold defined in some works. . . . 21
3.5 Summary of EEG signal processing techniques applied in some literature similar to this work. . . . 24
3.6 Some examples of machine learning techniques applied to similar scenarios of this thesis. . . . 25
3.7 Confusion Matrix . . . 30
3.8 TP, FP, TN and FN definition on Lopez-Larraz work. . . . 31
3.9 Tasks performed during the protocol. . . . 34
3.10 Annotation present in each task . . . 34

4.1 OpenBCI board characteristics . . . 39
4.2 Channel setting commands . . . 40

5.1 Participants description. . . . 47
5.2 Number of runs and trials on each acquisition phase. . . . 48
5.3 Values tested to obtain the best results for EMG segments activation detection. . . . 61

6.1 Specifications of the dataset. . . . 72
6.2 Label for each movement . . . 81
6.3 Number of movements detected in each subject's session. For phase 1 each movement should be performed 20 times, and for phase 2 30 times. . . . 84

# Abbreviations

| | |
|---|---|
| ANN | Artificial Neural Network |
| API | Application Programming Interface |
| AUC | Area Under the Curve |
| BCI | Brain-Machine Interfaces |
| BMI | Brain-Machine interfaces |
| BLE | Bluetooth Low Energy |
| CSP | Common Spatial Pattern |
| ECG | Electrocardiography |
| EEG | Electroencephalography |
| EF | Elbow flexion-extension |
| EMG | Electromyography |
| EOG | Electrooculography |
| ERD | Event-Related Desynchronization |
| ERS | Event-Related Synchronization |
| ES | Elbow supination-pronation |
| FFT | Fast Fourier Transform |
| FN | False Negative |
| FP | False Positive |
| GND | Ground |
| GUI | Graphical User Interface |
| ICA | Independent Component Analysis |
| LDA | Linear Discriminant Analysis |
| LSTM | Long Short-Term Memory |
| LSTM-RNN | Long Short-Term Memory Recurrent Neural Network |
| ME | Motor Execution |
| MI | Motor Imagery |
| MRCP | Movement-Related Cortical Potential |
| NTP | Network Time Protocol |
| REF | Reference |
| RLDA | Regularized linear discriminant analysis |
| RMS | Root Mean Square |
| RNN | Recurrent Neural Network |
| ROC | Receiver Operating Characteristics |
| SA | Shoulder abduction-adduction |
| SDA | Sparse Discriminant Analysis |
| sEMG | Surface Electromyography |
| SF | Shoulder flexion-extension |
| SR | Shoulder external-internal rotation |
| SVM | Support Vector Machine |
| TN | True Negative |
| TP | True Positive |
| WE | Wrist extension-flexion |
| WR | Wrist radial-ulnar deviation |

# Chapter 1

# Introduction

## 1.1 Context

Over the last decades, robots have been progressively integrating daily human life. Thanks to the scientific advances in robotics research, human-machine interaction is nowadays considered a feasible activity. A human and a robot can interact in many different ways, depending on the level of cooperation desired. In this sense, the human-machine interaction can be independent or shared. It is independent when the robot performs the task without human intervention (autonomous) or when the person performs it without input from the robot (manual). On the other hand, certain situations require human and machine collaboration to accomplish the desired task. Currently, human-robot interactions are applied in several fields, such as in industry, education, robot-assisted surgery, and rehabilitation [1].

In industry, collaborative robots are used to perform more complex tasks. However, it raises new significant challenges related to workers' safety since most systems are reactive and do not anticipate human movement, which sometimes can cause accidents, bringing up the importance of predicting human intention [2].

Regarding the rehabilitation field, robots are mainly used to assist or hinder the execution of planned rehabilitation movements. These robots allow more intensive repetitive movement sequences and reduce the treatment cost and the physical therapist's workload. They are expected to detect human movement intention and provide informative biofeedback through various human-machine interfaces. This feedback can trigger the actuation of robotic systems, allowing a more natural Human-Robot Interaction (HRI) [3]. Nevertheless, it would be nice to have a faster and more accurate diagnosis of human intention so that the robots can better interact with the patient.

## 1.2 Motivation

Thus, it is clear that predicting human intention in collaborative systems is essential. In this way, robots can communicate implicitly with their human partner, understand its need, and modify their actions, taking into account the information collected from the human. There are already

probabilistic models aiming to overcome these limitations, however, predicting human behavior remains highly complex [2].

The methods currently used to recognize human motion intent mainly include bio-force information (such as joint angle, plantar pressure, joint torque, etc.), video imaging, and bioelectrical signals (such as in an electrocardiogram (ECG), electrooculogram (EOG), electromyogram (EMG), electroencephalogram (EEG)) [4, 1]. Force sensors and video images can only detect the intention after the movement starts. Besides, vision sensors are typically fixed in space and present limitations, such as occlusions, that reduce their area of action [5].

On the other hand, physiological signals such as EMG and EEG are intrinsically correlated with human intention. With those signals, human intention is detected before the movement starts. However, the study of these signals is still in the preliminary stages.

To sum up, it is essential to further investigate the biosignals' ability to detect human intention, aiming to notice it more quickly and effectively, allowing, in this way, a more natural human-robot interaction.

A use case for this dissertation was simulated on the iiLab from INESC TEC (see Fig. 1.1), where the robot and the worker have a collaboration relationship. In this scenario, the robot places the objects in one place, and the human must collect them, being always coordinated with the robot. But imagine that for some reason, the worker didn't collect the object, and the robot is already placing the other. Since the robot (UR3) is reactive, he will stop when it hits the human, which may cause some injury, as exemplified in Figure 1.1a. However, if the robot is able to predict the intention, he will notice that the human will perform the movement, and if the intention is predicted earlier, the robot has time to stop, which will not cause any harm to the worker (see Fig. 1.1b).

## 1.3 Objectives

Given the motivation, this dissertation aims to prove that it is possible to detect human intention faster and more accurately using physiological signals, such as EEG and EMG. In order to do so, a multi-modal dataset was acquired and organized (containing EEG, EMG, ECG, and inertial data), followed by their processing to reach the final goal.

Thus, this dissertation can be divided into the following sub-objectives:

- Study of the acquisition devices: openBCI for biosignals and iHandU for IMU data;
- Creation of the data acquisition protocol. The protocol consists of thinking and executing some movements of the upper limb, which will be repeated several times throughout the session;
- Data recording and synchronization;
- Data pre-processing;

- Movements onset detection: evaluate the feasibility of using the iHandU device instead of the EMG signal;
- Detection of human intention.

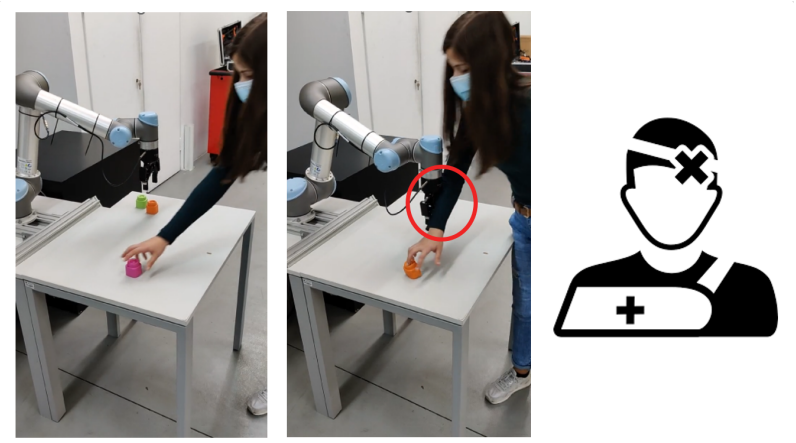

(a) Robot without intention prediction.

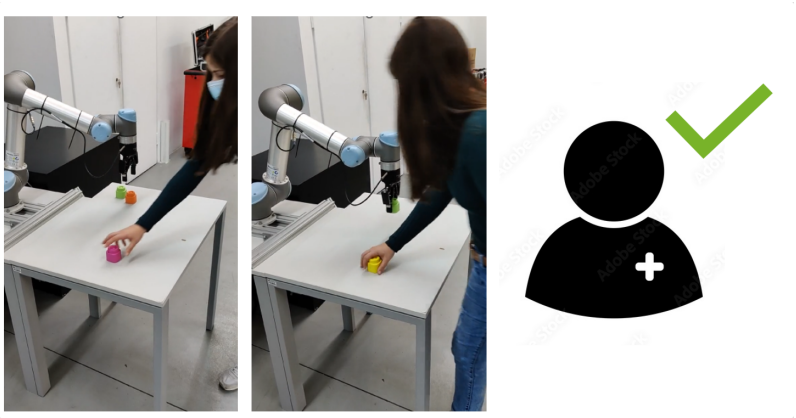

(b) Robot with intention prediction.

Figure 1.1: Use case simulation record on iiLab from INESC TEC with UR3 robot.

## 1.4 Contributions

The principal contributions of this dissertation are:

- Development of a new experimental protocol that can be used to study human movement intention.
- Creation of a dataset called *PhysioIntent*, containing 7.41 GB of data from EEG, EMG, ECG, IMU, and video from 9 healthy subjects (https://doi.org/10.25747/6101-JD30).

- The dataset was carefully structured, organized, and approved by the Ethics committee so that it could be published in open-access to the scientific community.
- Implementation of an accurate automatic synchronization algorithm between the acquired data;
- Development of optimized pre-processing techniques for all the data.
- Proof that it is possible to predict human motion intent with EEG.

## 1.5 Dissertation outline

Besides the Introduction, this document has six more chapters.

- Chapter 2 overviews the biosignals used to predict human intention, explains their main characteristics, and how they are used in literature to predict human motion intent.
- Chapter 3 describes some works found in the literature related to human intention by enhancing the methodology used in each work to process the signals and achieve the desired result.
- Chapter 4 shows an overview of the devices used to acquire data.
- Chapter 5 addresses the methodology implemented in this work. Starting by explaining the protocol and then explaining how the signals were synchronized and processed.
- Chapter 6 analysis and discuss the results obtained.
- Chapter 7 presents the conclusion and future work.

# Chapter 2

# Biosignals and sensors used in human motion intent

Nowadays, when building a robotic system that needs to interact or collaborate with humans, it is crucial to have a fast and reliable Human-Robot Interaction (HRI) so that the robot can quickly adapt to the human's needs, providing a more natural behavior. In this way, to achieve a better HRI, it is essential to predict the human intent quickly and accurately.

The biosensors commonly used to detect human intention are electromyography (EMG) and electroencephalography (EEG) [6, 7]. The EMG activity can be detected in a range of 50-100 ms before the actual movement of the limb [8]. On the other hand, the intention is noticed earlier in the EEG, being detected up to 0.5 seconds before the execution since the brain is responsible for controlling the movements [2]. Additionally, some other devices are sometimes employed, such as inertial or force sensors. The main drawback of using force or inertial sensors alone is that the detection of the intent is only noticed after a human starts realizing the movement, resulting in a delay in the intention detection [8].

This chapter aims to overview the biosignals used to predict human intention, explain their main characteristics, and how they are used in literature to predict human motion intent.

## 2.1 Electromyography (EMG)

The EMG is a biomedical signal that measures the electrical currents generated in the muscles during their contraction. Each muscle movement is made under the control of our brain. For each potential action, the brain generates an electrical signal, which passes through the nerve fibers and stimulates the muscle fibers, consequently inducing the muscles' movement [9]. EMG activity is revealed about 50-100 ms before the actual limb motion [1], which is one of the reasons why EMG is used in human motion intent. Figure 2.1 shows an example of an EMG signal. Its typical amplitude is between 0-10 mV [9].

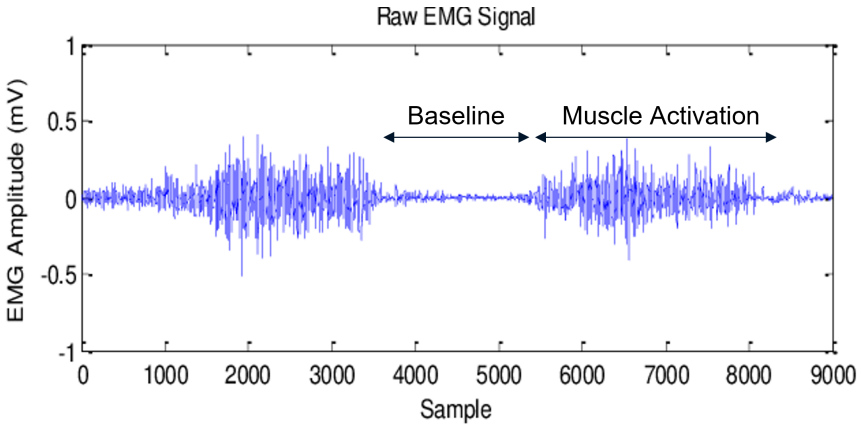


Figure 2.1: Example of a raw EMG signal, adapted from [10].

### 2.1.1 Movements and related muscles

As mentioned in Chapter 1, this work focuses on upper limb movements. In this way, to choose the best place for each electrode, it is first important to understand the muscle responsible for each type of movement and its position on the arm.

Figure 2.2 shows the superficial muscles in the upper arm and the forearm. In addition, Table 2.1 describes the movements more frequently used in the literature and the respective muscles chosen. For example, the extensor and flexor carpi muscles are responsible for wrist flexion and extension.

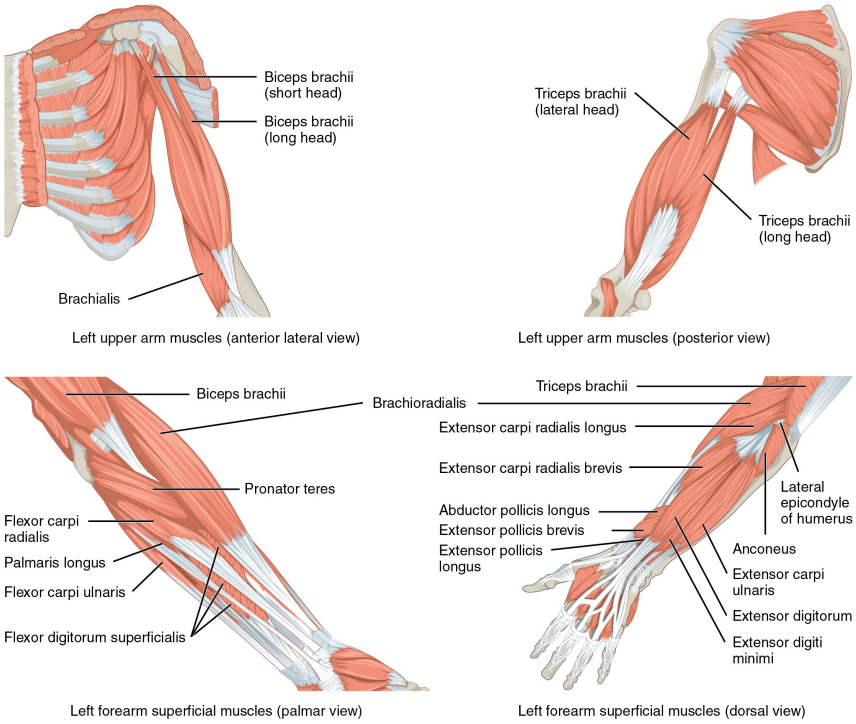


Figure 2.2: Main muscles on the superficial layer of the left arm and forearm [11].

Table 2.1: Compilation of some similar works and their chosen muscles to detect the desired movements.

| Author | Movement | Muscles |
|---|---|---|
| A. Ruiz-Olaya et al. [7] | Wrist flexion-extension;<br>Forearm pronation-supination;<br>Elbow flexion-extension | Biceps brachii long head;<br>Triceps brachii long head;<br>Five muscles around the forearm. |
| S. Guo et al. [12] | Elbow flexion-extension;<br>Forearm pronation-supination;<br>Wrist flexion-extension;<br>Wrist abduction-adduction | Flexor Carpi Radialis;<br>Flexor Carpi Ulnaris;<br>Extensor Carpi Radialis;<br>Extensor Carpi Ulnaris;<br>Biceps brachii;<br>Triceps brachii |
| E. López-Larraz et al. [13] | Shoulder abduction-adduction (SA);<br>Shoulder flexion-extension (SF);<br>Elbow flexion-extension (EF);<br>Elbow supination-pronation(ES);<br>Shoulder external-internal rotation (SR);<br>Wrist extension-flexion (WE);<br>Wrist radial-ulnar deviation (WR) | Extensor digitorum;<br>Extensor carpi ulnaris;<br>Palmaris longus;<br>Biceps brachii;<br>Triceps brachii;<br>Shoulder muscles |
| J. Jeong et al. [14] | Arm-reaching along 6 directions<br>(forward, backward, left, right, up, and down);<br>Hand-grasping of 3 objects;<br>Wrist supination-pronation | Extensor carpi ulnaris;<br>Extensor digitorum;<br>Flexor carpi radialis;<br>Flexor carpi ulnaris;<br>Biceps brachii;<br>Triceps brachii. |

### 2.1.2 EMG acquisition

Two main techniques are used to acquire muscle activity: invasive and non-invasive. The main difference is the type of electrodes used. The invasive uses needle electrodes or fine wire electrodes, which are inserted into the muscle. This type of procedure is widely used in clinical neuromuscular evaluations. On the other hand, surface EMG electrodes provide a non-invasive technique for measuring EMG signals. This approach takes advantage of the fact that current flows through the skin, by electrolytic conduction, to the electrode to capture muscle signals without requiring direct contact with the muscle [15].

Among the various known methods to acquire this signal, surface EMG (sEMG) attracts the most attention from researchers since it allows the signal to be measured in a easy, non-invasive way and directly reflects physical intentions and movement information. Regarding the positioning of the electrodes on the skin, typically, two are placed on the muscle, and one on a bone, as shown in Figure 2.3.

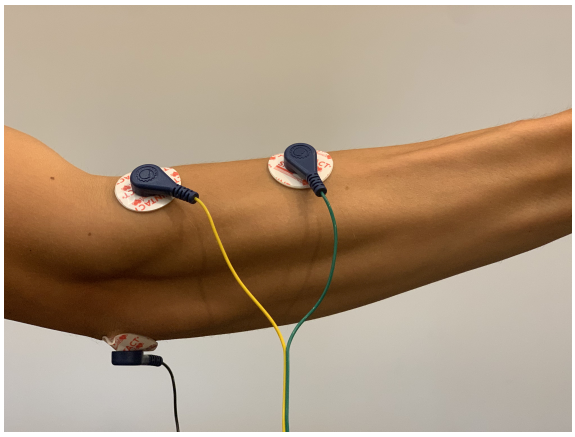

Figure 2.3: Example of electrodes placed on the arm[1].

## 2.2 Electroencephalography(EEG)

The EEG measures the brain waves over time using electrodes attached to the scalp. The raw EEG signals usually have a range of 0.5-100 µV in amplitude, and the brain waves can be classified into five different groups depending on their frequency bands [2], as shown in Figure 2.4. Human intention can be detected in the alpha and beta waves up to 0.5 seconds before the movement execution [2].

In the human-machine interaction field, the EEG signal is mainly used on Brain-Computer Interfaces (BCI) or Brain-Machine Interfaces (BMI). Such interfaces use brain signals to control equipment such as prosthetics, exoskeletons, or wheelchairs. For example, if we consider a user who cannot move his limbs, his brain may still be able to generate command signals, which can be used to drive an exoskeleton [16].

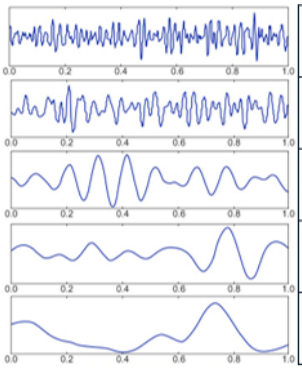

| | | |
|---|---|---|
| **Gamma** | 30 - 100 Hz | Higher Mental Activity, Alertness |
| **Beta** | 12 – 30 Hz | Active Thinking, Focus, Aware of Surroundings, Motor Functions |
| **Alpha** | 8 – 12 Hz | Motor Functions, Relaxed but not Drowsy, Tranquil, Conscious |
| **Theta** | 4 – 8 Hz | Drowsiness, Imaginary, Dream |
| **Delta** | 0.1 – 3 Hz | Deep Dreamless Sleep, Unconscious |

Figure 2.4: Brainwave frequencies and associated mental states (adapted) [2].

[1]Taken from : https://docs.openbci.com/GettingStarted/Biosensing-Setups/EMGSetup/

### 2.2.1 Brain organization

The brain can be divided into three regions: brain, cerebellum, and brain stem. The surface of the cerebrum is called the cortex (grey matter), which is connected to the inner layer (white matter). The cortex consists of four lobes: frontal, temporal, parietal, and occipital, each with a specific function assigned (Fig. 2.5). Each lobe may also be divided, once again, into areas that serve particular functions [17]:

- **Frontal:** Essential for cognitive functions and control of voluntary movements (motor cortex);
- **Temporal:** Related to sound processing;
- **Parietal:** Senses touch, pain, temperature (sensory cortex); Decodes signals from vision, hearing, motor, sensory, and memory; Performs spatial and visual perception;
- **Occipital:** Interprets vision (color, light, movement)

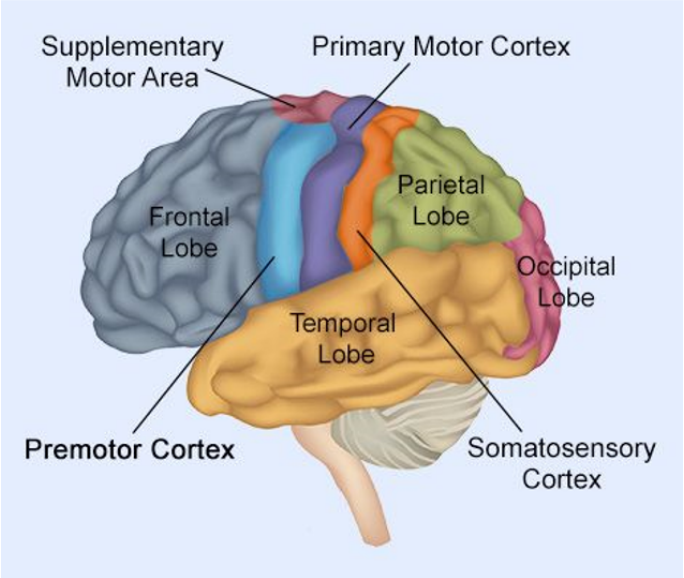


Figure 2.5: Brain cortex [18].

The motor cortex is the area in the frontal lobe responsible for planning, controlling, and executing voluntary movements. It comprises three regions: the primary motor cortex, the premotor cortex, and the supplementary motor area [19].

The **primary motor cortex** houses neurons responsible for carrying out voluntary movements of different body parts, mainly to the contralateral, or opposite, side [20]. The **premotor cortex** directly communicates with the primary motor cortex. Its function is to store and process information about the past activity, and it helps to integrate sensory and motor information for planning future voluntary movements. The **supplementary motor cortex** is a part of the primate cerebral

cortex that contributes to movement control. The primary motor cortex has been considered a first choice as the source of neural signals to control prosthetic devices for humans with paralysis [21].

Thus, focusing on the primary motor cortex, it contains an inverted representation of the opposite half of the body, known as a motor homunculus (Fig. 2.6). Therefore, the top part of the cortex stimulates leg movements, whereas the movements of the face are stimulated by the lowest part of the motor cortex. Thus, each body movement has neuronal activity associated with a specific cortex area. This is similar to the sensory homunculus of the sensory cortex, which is situated immediately behind the motor cortex.

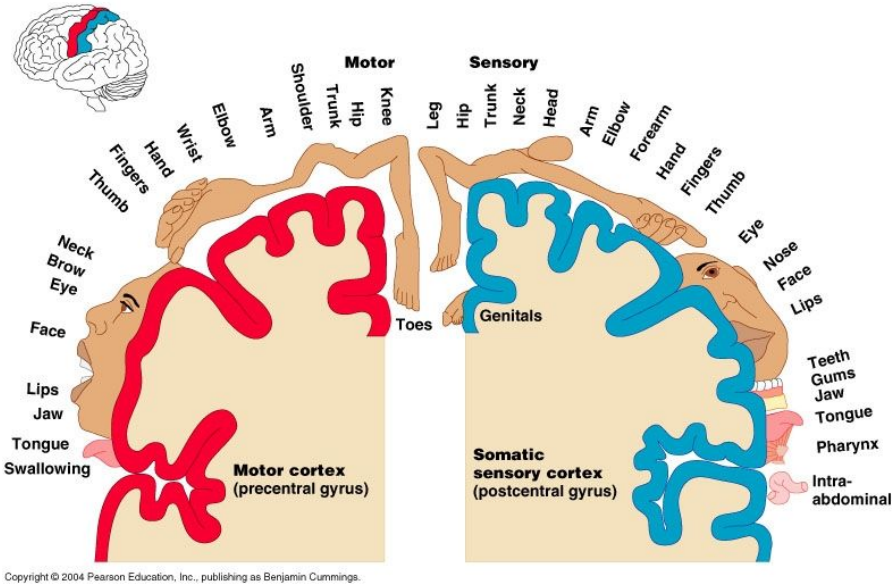


Figure 2.6: Body maps of the primary motor cortex and somatosensory cortex of the cerebrum (homunculus map)[2]

### 2.2.2 Brain activity interpretation

There are two majorly reported neural features related to detecting movement intention: the Event-Related Desynchronization/ Synchronization (ERD/ERS) and the Movement-Related Cortical Potential (MRCP) [22]. ERD/ERS and MRCP features have been used to detect motion intent, not only to distinguish rest from motion (or Motor Imagery) but also to distinguish the type of movement [13].

#### 2.2.2.1 Event-Related Desynchronization/ Synchronization (ERD/ERS)

When a movement is performed, the 8–12 Hz alpha band (mu ERD) and the 13-30 Hz beta band (beta ERD) exhibit a decrease in amplitude before the actual movement. This pre-movement suppression over sensorimotor areas can be attributed to motor preparation and execution. Conversely, when the movement ceases, the 13-30 Hz beta band (beta ERS) at the precentral region of

[2]Adapted from: https://nanopdf.com/download/cns-brain-a_pdf

the brain exhibits an increase in amplitude [23]. This phenomenon can be observed in more detail in Figure 2.7. To sum up:

- **Event-Related Desynchronization (ERD):** suppression of the rhythmic brain activity when an event occurs;
- **Event-Related Synchronization (ERS)**: enhancement of the rhythmic brain activity when an event occurs.

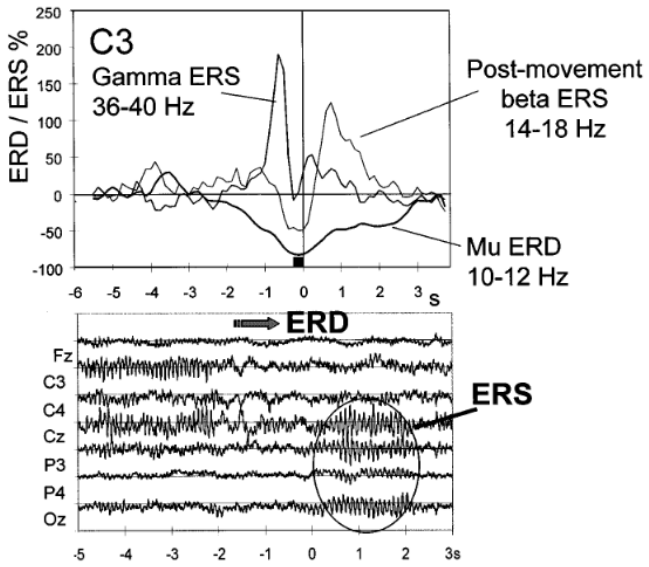


Figure 2.7: Event-Related Desynchronization and Event-Related Synchronization [24]. The graphic above presents how should be the shape of the mu, beta, and gamma-band on the C3 channel before and during the movement.

#### 2.2.2.2 Movement-Related Cortical Potential (MRCP)

The MRCP is characterized by a slight decrease in the EEG amplitude over the primary motor cortex within at least 0.5 seconds preceding the movement onset [22].

The MRCP comprises three events, as illustrated in Figure 2.8: the readiness potential (RP) or Bereitschafts potential (BP), the motor potential (MP), and the movement-monitoring potential (MMP), which are thought to reflect movement planning/preparation, execution, and control of performance [25], respectively.

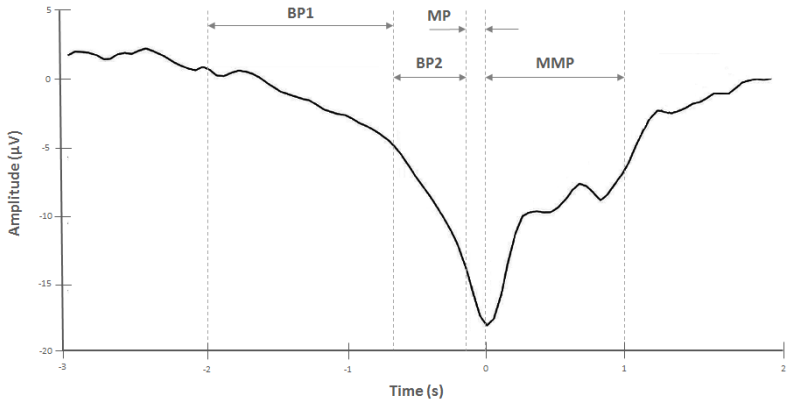


Figure 2.8: Waveforms and terminology of movement-related cortical potentials (MRCPs) from a single healthy subject [25]. BP1: early Bereitschafts potential; BP2: late Bereitschafts potential; MP: motor potential; MMP: movement-monitoring potential

The BP can be divided into two parts: the early and late BP. The early BP is a low negative slope segment that appears about 1500 ms before the movement onset. The late BP has a steeper slope and happens around 400-500 ms before the EMG onset. Its maximum amplitude is over the primary motor cortex.

### 2.2.3 EEG acquisition

Like the EMG, the EEG can be acquired either invasively (intracranial) or non-invasively. The invasive approach requires implanting electrodes directly on the exposed surface of the brain. On the other hand, a non-invasive approach, the standard EEG method, measures the activity through a set of electrodes placed on the subject's scalp.

EEG acquisition has a pre-set of electrode placement rules. The 10-20 system was the first system proposed and, consequently, was the first to set a standard location and nomenclature for each of the 21 electrodes placed on the scalp. In 1985, an extension of the original 10-20 system was proposed involving an increase in the number of electrodes from 21 to 74 (new 10-10 system) [26]. The 10-20 EEG electrode placement system is mostly used in clinical applications, while the 10-10 system, represented in Figure 2.9 is mainly used in research. The name of each electrode consists of one or two letters followed by a number. The letters refer to the region of the brain where the electrode is positioned (F: frontal, C: central, T: temporal, P: posterior, and O: occipital), and the number is related to the cerebral hemisphere with even numbers in the right hemisphere, and odd numbers in the left hemisphere [26].

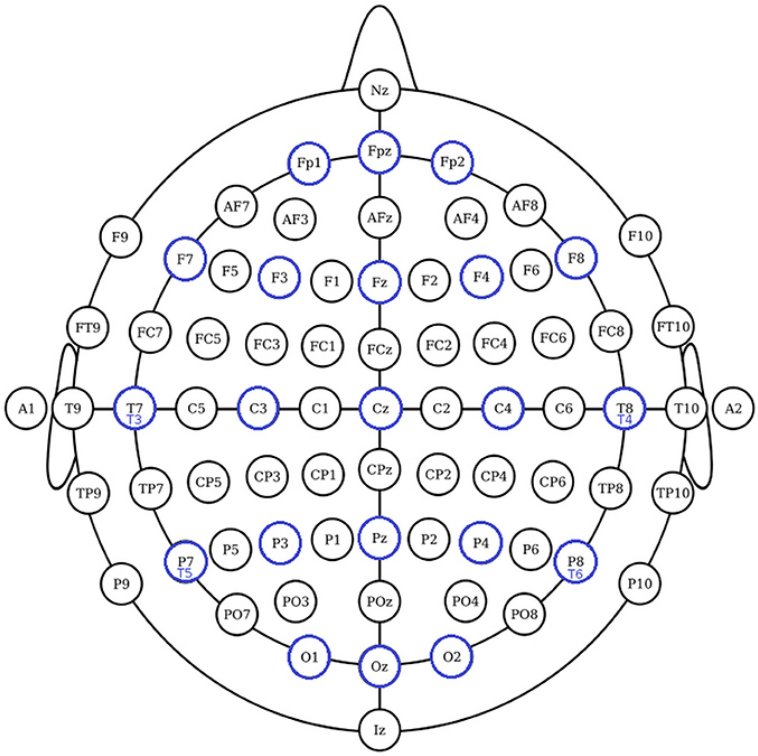


Figure 2.9: The 10-10 international system of EEG electrode placement. The blue circles represent the location of 10-20 EEG electrodes [26].

## 2.3 Inertial Measurement Unit (IMU)

An IMU is an electronic device that combines up to three sensors - an accelerometer, a gyroscope, and sometimes a magnetometer [27].

An accelerometer is a sensor that measures the linear acceleration caused by the movement and the earth's gravitational force. On the other hand, the gyroscope measures angular velocity, determining how quickly the device rotates. Lastly, a magnetometer is a device commonly used to measure the strength and direction of the earth's magnetic field [28].

The IMU sensor is often used in human intention detection and is commonly applied to remove some artifacts from the biosignals. Adding an IMU to the system makes it possible to verify whether the person effectively performed the movement.

## 2.4 Biosignals noise sources

Artifacts are unwanted signals from environmental noise, experimental error, and physiological artifacts [29]. These sources can be classified into two main groups: external and internal artifacts.

A common external source is the power line noise, which is present in all data. Regarding internal sources, these artifacts are caused by the subject. In other words, they originate from the subject's physiological activity and are more difficult to remove.

The following subsections discuss the main artifacts present in physiological signals.

### 2.4.1 EMG

The muscle activity, as described in Subsection 2.1.2 can be measured in a non-invasive way, which involves the placement of electrodes under the skin. The movement of the cable connecting the electrode to the amplifier, and the interface between the detection surface of the electrode and the skin, can create some motion artifacts [30].

Furthermore, another source of EMG contamination is the "crosstalk" between muscles, which can cause an incorrect interpretation of the signal. Crosstalk can be minimized by choosing electrodes of less than 30 mm size and by guaranteeing inter-electrode distances of at least 1-2 cm [30].

Several techniques can be applied to reduce the captured noise, such as band-pass filtering, adaptive noise cancellation filters, and filters based on the wavelet transform [31].

### 2.4.2 EEG

There are several types of artifacts in EEG signals. Noise from external sources usually results from environmental interference, recording equipment, electrode pop-up, or cable movement. Regarding physiological artifacts on EEG, the three noise sources most common result from ocular, muscle, or cardiac activity (Fig. 2.10).

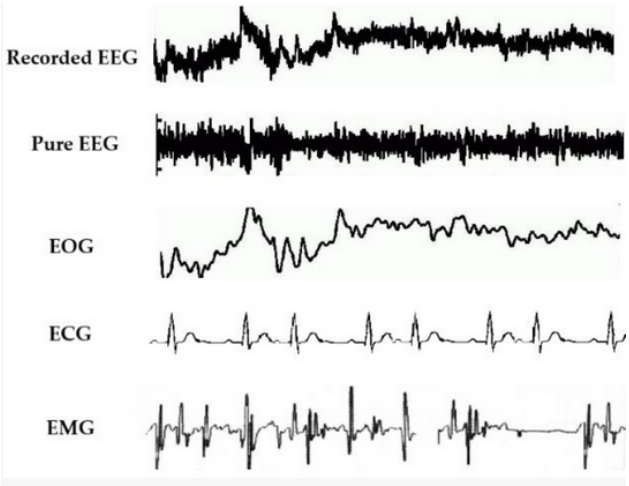


Figure 2.10: Physiological artifacts in EEG signals [29].

**Ocular artifacts** are related to eye movement and respective blinking, which propagate over the scalp and, consequently, are also recorded in the EEG activity, namely in the FP1 and FP2 channels. Typically, these artifacts have a higher amplitude than the normal EEG. While a regular EEG signal ranges from -50 to 50 µV, blink-related artifacts have amplitudes up to 100 µV [32].

The contamination of EEG data by **muscle activity** can be caused by any muscle contraction near the EEG electrodes, e.g., when the subject talks, sniffs, or swallows, among others. The degree of muscle contraction and stretch will affect the amplitude and waveform of artifacts. The Independent Component Analysis (ICA) emerges as a possible method to remove the EMG contamination in the EEG signal [29].

**Cardiac artifacts** might be introduced when the electrodes are placed on or near a blood vessel. This artifact is around 1.2 Hz [29] and can be removed with a reference waveform of the ECG signal.

Therefore, some pre-processing needs to be done to improve the quality of the signals, and it is discussed in the next Chapter, in Section 3.2.

# Chapter 3

# State-of-the-art

This chapter aims to describe some works found in the literature related to human intention by enhancing the methodology used in each work to process the signals and achieve the desired result.

Most of the papers found are based on the same pipeline (Fig. 3.1). First, data is acquired, then it is processed, starting with pre-processing followed by feature extraction and then classification.

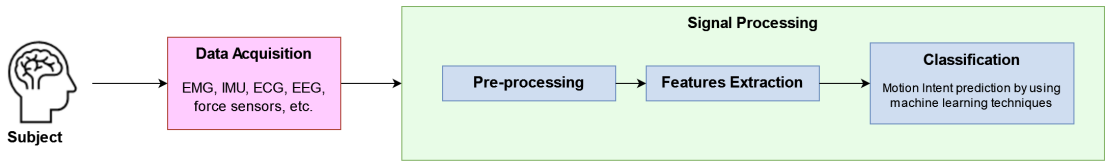


Figure 3.1: Human Intention prediction state-of-the-art pipeline.

## 3.1 Data acquisition

As mentioned above, inertial and force sensors, video-imaging, and physiological signals, such as EEG and EMG, are typically used to predict human intent. Most works use more than one type of data aiming to remove some artifacts that may occur during the acquisition.

Papers that only use EMG and IMU usually have the purpose of classifying the type of motion. For example, A. Ruiz-Olaya et al., 2016 [7] used 7 EMG channels and 3 IMUs to distinguish seven classes (six upper limb movements + one resting state). They also proved that the use of IMUs improves the detection of motion intent. D. Sirintuna et al.,2020 [8] used EMG and force sensors to predict the direction of the movement of the arm. The force sensors are only used to determine when the limb movement starts. EMG features are used for classification.

Some works use EEG combined with other signals, such as EMG and ECG, to remove some artifacts and noise. For example, V. Peterson et al.,2020 [33] used EEG and EMG. The EMG is only used to determine if any EEG trial was corrupted. In all these works, the data were acquired with different equipment, as shown in Table 3.1. Furthermore, the number of muscles and the

number o EEG channels chosen varies. Subsection 3.1.1 presents some of the devices used for data acquisition.

Table 3.1: Acquisition devices used in some works.

| | **Signals** | **Devices** |
|---|---|---|
| **E. López-Larraz et al. (2014) [13]** | 32 channels EEG;<br>8 muscles EMG | g.Tec system |
| **A. Ruiz-Olaya et al. (2016) [7]** | 7 muscles EMG;<br>3 IMUs | MPU9150 from InvenSense<br>PowerLab 8/30 system<br>from ADInstruments |
| **B. Gudino-Mendonza et al. (2016) [34]** | 21 channels EEG;<br>2 muscles EMG | Nexus- 32 electrophysiology<br>monitoring system from<br>Mind Media |
| **J. Ren et al. (2019) [35]** | 16 channels EMG;<br>2 IMUs | Myo armband |
| **D. Sirintuna et al. (2020) [8]** | 4 muscles EMG;<br>1 force sensor | sEMG sensor - MyoWare<br>Force sensor - Mini40, ATI Inc |
| **V. Peterson et al. (2020) [33]** | 15 channels EEG;<br>2 antagonic muscles EMG | OpenBCI Cyton + Daisy Module<br>Electrocap System II<br>Myoware sensors |
| **J. Jeong et al. (2020) [14]** | 60 channels EEG;<br>7 muscles EMG;<br>4 channels EOG | actiCap from BrainProduct GmbH<br>EEG signal amplifier - BrainAmp<br>from BrainProduct GmbH |

### 3.1.1 Acquisition devices

Besides the devices used in the previously mentioned studies, other devices can be used. Table 3.2 lists some of the devices found in the literature. It is important to enhance that some of those devices can acquire more than one type of data simultaneously, which facilitates data synchronization.

For sEMG acquisition, the usual method is to connect the electrode cables to the measuring equipment. There is already some specialized hardware to acquire this signal, such as Myoware [36]. There are also devices that can acquire different signals simultaneously, such as the EmotiBit [37] that records IMU, EMG, and other data.

Table 3.2: List of devices and data that they can measure

| Device | | Data acquisition |
|---|---|---|
| Myo Armband [38] | | 8 EMG channels and IMU data |
| EmotiBit [37] | | IMU, Humidity, PPG, EDA, etc. |
| iHandU [39] | | IMU and force sensors |
| OpenBCI [40] | 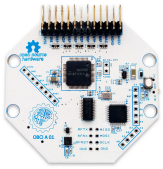 | EEG, EMG, ECG |
| Myoware [36] | | EMG |
| Emotiv Epoc [41] | | EEG |
| EEG cap by Besdatatech [42] | | EEG |

## 3.2 Signal Processing

The signal processing module is divided into different parts, as seen in Figure 3.1. The first step is to pre-process the data to reduce the noise present in the signal and prepare the data for feature extraction (second step). Lastly, the classification is done by applying some machine learning techniques.

This section describes some of the processing techniques of the signals discussed in Section 3.1, namely the EMG and EEG.

### 3.2.1 EMG

#### 3.2.1.1 Pre-processing

Most pre-processing techniques applied to EMG focus on removing the artifacts and detecting active segments.

- **Noise reduction**
  Besides the environment noise, which is removed with a notch filter of 50 Hz, there are motion artifacts which are result from electrode interfaces and electrode cables. These motion artifacts have a frequency range between 1-10 Hz [30]. To remove this type of noise, a high-pass filter of cut frequency of 10 Hz is typically applied. Table 3.3 specifies the type of filter applied in the literature. They all use a Butterworth filter changing on order and cut-off frequency.

Table 3.3: Summary of EMG filter found in literature

| **Author** | **Filter** |
|---|---|
| D. Sirintuna et al. (2020) [8] | Band-pass Butterworth filter 5-500 Hz |
| J. Ren et al. (2019) [35] | High-pass 4th order Butterworth 10 Hz |
| V. Peterson et al. (2020) [33] | High-pass 5th order Butterworth 10 Hz |
| J. Jeong et al. (2020) [14] | Band-pass 5th order Butterworth filter 10-500 Hz |

- **Active segment detection**
  Active segment detection is usually done to identify the muscle activation from the resting period. Usually, an algorithm is applied to determine the onsets of muscle activity. To achieve that, the **EMG envelope** needs to be calculated, and then a **threshold** is defined to determine the onset and offset of EMG activity. This threshold doesn't always follow the same protocol. For example, in Peterson et al. work, the onset activity threshold was calculated as the standard deviation of the envelope of a rest segment [33]. Table 3.4 describes some of the threshold defined. Other works set the threshold visually or estimated based on the mean ($\mu$) and standard deviation ($\sigma$) of the baseline signal (see Equation 3.1, where $h$ is a variable determining the threshold level) [43]. Usually, $h$ is set to 3 [44].

$$T = \mu + h\sigma \tag{3.1}$$

Table 3.4: Threshold defined in some works.

| Author | EMG onset threshold |
|---|---|
| R. Leeb et al. (2010) [45] | $th = 2\mu + \sigma$ |
| V. Peterson et al. (2020) [33] | $th = \sigma$ *(0.25 s of rest EMG envelope)* |

Regarding **EMG envelope**, the literature describes two ways of performing it: by signal rectification followed by a low-pass filter or through the root mean square (RMS) [12, 7]. The low-pass filter can be a Butterworth filter [33, 8] or moving average [14].

- **Signal rectification:** Though full-wave rectification or half-wave rectification [46]. Full-wave rectification is preferred, meaning that each data point is replaced by its absolute value. On the contrary, when half-wave rectification is performed, all negative data is discarded, and positive data is kept.
- **Low-pass filter:** One way to filter a signal is to calculate the mean value in a window that slides along the signal. This process is known as the **moving average**. Jeong et al. [14] applied a moving average on a window size of 100 ms. The larger the window size, the greater will be the smoothness [47]. Another way to low pass filter the rectified signal is to use a discrete version of a traditional low pass filter such as **Butterworth** or Chebyshev [47]. Peterson et al. performed a low-pass 3rd order Butterworth filter with a 40 Hz cut-off frequency [33]. In some works, a low-pass Butterworth filter with a cut-off frequency of 5 Hz was applied [8].
- **Root Mean Square (RMS):** Another way of performing EMG envelope is by calculating the RMS. The RMS represents the square root of the average power of the EMG signal for a given period of time. It is known as a time-domain variable because the amplitude of the signal is measured as a function of time [48]. Equation 3.2 represents how RMS is calculated, where N represents the length of the signal.

$$RMS = \sqrt{\frac{1}{N}\sum_{n=1}^{N} {x_n}^2} \tag{3.2}$$

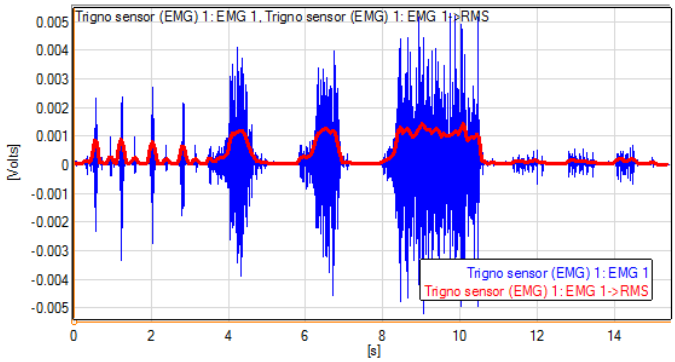


Figure 3.2: Example of RMS envelope.[1]

Besides these pre-processing techniques, it has been proved that the Teager Kaiser Energy Operator (TKEO) (Equation 3.3) improves the onset detection compared to simply filtering the EMG data [44]. The TKEO converts the amplitude signal into energy, as shown in Figure 3.3. The threshold defined is based on Equation 3.1. For this algorithm, normally, the h is set to 14 [44].

$$TKEO = x^2(n) - x(n+1)x(n-1) \tag{3.3}$$

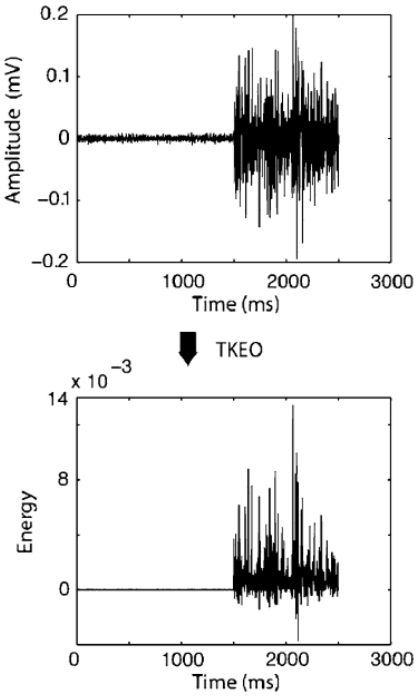


Figure 3.3: TKEO example [44].

[1]Taken from https://delsys.com/amplitude-analysis-root-mean-square-emg-envelope/

### 3.2.2 EEG

#### 3.2.2.1 Pre-processing

As mentioned in Chapter 2, Section 2.4, the EEG is a signal very susceptible to noise. Besides the extrinsic artifacts, such as the power line noise, which is easily removed with notch filtering, the intrinsic artifacts, such as ocular, muscular and cardiac artifacts, also need to be removed.

Looking to the literature, spatial filters are commonly used to improve signal-noise quality. Spatial filters give a more representative pattern of what is actually happening in each channel.

The most relevant filters described in the state-of-the-art are described below:

- **Surface Laplacian (SL):** The Surface Laplacian can reduce spatial noise and help limit potential sources of the signal [49]. The Laplacian behaves as a high-pass spatial filter. It increases focal activity from local sources and reduces distributed activity such as that resulting from EMG, eye movements, and blinking [50].

- **Common Average Reference (CAR):** CAR consists of computing the average of all the channels and subtracting it to each electrode. In this case, the average is seen as EEG noise [50].

López-Larraz et al. [13] used the SL and CAR before applying the MRCP and ERD to predict human movement intention.

#### 3.2.2.2 Features extraction and selection

Besides the methods referenced above, there are other techniques that, besides removing the noise and artifacts, are used for feature extraction and selection. These methods are explained below. Table 3.5 summarizes the main processing methods applied in some works.

- **Common Spatial Patterns (CSP):** The common spatial patterns (CSP) have been used for feature extraction in EEG signals for motor imagery (MI). The CSP algorithm uses the diagonalization of the covariance matrix to maximize the variance ratio of the two-class signal matrices [51]. Jeong et al. [14] and Peterson et al. [33] applied this method.

- **Principal Component Analysis (PCA):** PCA allows feature extraction and data reduction to a few independent components. The algorithm is based on eigenvalues of covariance matrix [29]. The algorithm's output will be the component time series and the factors representing each component's contribution to the channel. After identifying the principal components in the frequency domain, they are multiplied by their factor to enhance some components [52]. Buerkle et al. applied the PCA method after band-pass the EEG signal from 8-30 Hz (alpha and beta band) [2].

- **Independent Component Analysis (ICA):** ICA is a feature extraction method that transforms the multivariate random signal into a signal with components that are mutually independent [53]. Hence, the EEG signal is separated into independent components accounting

for different neural activities but also stereotyped nonbrain-artifact signals, including eye movements, line noise, and muscle activities [53]. J. Jeong et al. applied the infomax ICA to remove the blink artifacts.

- **Discrete Wavelet Transform (DWT):** Conventional DWT recursively decomposes the low-pass signal with the same scaling and wavelet functions to the desired decomposition level [54]. After decomposing the EEG data, a threshold is applied to discard the signal containing the artifacts. Then, using inverse DWT, the cleaned EEG signals are reconstructed. It should be noted that most wavelet-based algorithms remove artifacts from each channel individually. More recently, DWT has been used in combination with other methods, such as ICA [29].

Table 3.5: Summary of EEG signal processing techniques applied in some literature similar to this work.

| **Author** | **Signal Processing** |
|---|---|
| A. Buerkle et al. (2021) [2] | FFT 8-30 Hz<br>PCA |
| E. López-Larraz et al. (2014) [13] | Laplacian filter followed by ERD<br>CAR filtered followed by MRCP |
| V. Peterson et al. (2020) [33] | Band-pass (1-40 Hz)<br>CSP |
| J. Jeong et al. (2020) [14] | Band-pass (8-30 Hz)<br>ICA - infomax algorithm<br>CSP |

## 3.3 Classification

After processing all the data and extracting its characteristics, the machine learning algorithms are applied. Machine learning (ML) is a sub-area of artificial intelligence (AI) that allows software applications to predict accurate outcomes [55]. In order to do so, it needs a high amount of data to train, so it can make its correct classification when given a similar input. The models that can make those predictions are usually named classifiers.

This section presents an overview of the main techniques found in the literature. Table 3.6 summarizes the research made.

Table 3.6: Some examples of machine learning techniques applied to similar scenarios of this thesis.

| | Classes | Data splitting | Classifier | Evaluation metrics |
|---|---|---|---|---|
| **E. López-Larraz et al. (2014) [13]** | 0: rest<br>1: pre-movement | Leave-one-out cross-validation | Sparse Discriminant Analysis (SDA) | Shoulder flexion-extension:<br>AUC = 85.6 %<br><br>Wrist radial-ulnar deviation:<br>AUC = 64.8 % |
| **A. Ruiz-Olaya et al. (2016) [7]** | 1: wrist flexion;<br>2: wrist extension;<br>3: forearm pronation;<br>4: forearm supination;<br>5: elbow flexion;<br>6: elbow extension;<br>7: rest | Train: 2 trials<br>Test: 1 trial | Linear Discriminant Analysis (LDA) | Sensitivity: 94.07 %<br>Specificity: 89.77% |
| **B. Gudino-Mendonza et al. (2016) [34]** | 0: rest<br>1: intention | Train: 80 % trials<br>Test: 20 % | Support Vector Machine (SVM) | Accuracy: 80 % |
| **D. Sirintuna et al (2020) [8]** | Rest<br>Y direction<br>Z direction | Train: 75 % trials<br>Test: 25 % | Artificial Neural Network (ANN) | Accuracy: 96 % |
| **V. Peterson et al. (2020) [33]** | Rest<br>Motor Imagery (MI) | 10 x 10 fold cross validation | Generalized sparse discriminant analysis (GSDA) | Accuracy: 73.15 ±2.12 %<br>for CSP features |
| **J. Jeong et al. (2020) [14]** | Reach<br>Grasp<br>Twist | 10 x 10 fold cross validation | Regularized linear discriminant analysis (RLDA) | Accuracy |
| **A. Buerkle et al. (2021) [2]** | 0: rest<br>1: intention<br>2: movement | Train: 5 epochs<br>Test: 5 epochs | Long Short-Term Memory Recurrent Neural Network (LSTM-RNN) | Accuracy: 84.98 - 92.08 % |

### 3.3.1 Data splitting

The data is usually separated into training and testing and can be divided in several ways. Below are described some of the methods found in the literature.

#### 3.3.1.1 K-Fold Cross-Validation

The 10 x 10 fold cross-validation is used in most of the works [33, 14]. The k-fold cross-validation is a technique that divides the data into k groups, using k-1 to form the training set and one as the validation set. It then iterates until all possible combinations of groups are used, as seen in Figure 3.4. The model is trained in each iteration, and its performance is evaluated on the validation set [56]. Then, the performance measure reported by k-fold cross-validation is the average of the values computed in the loop.

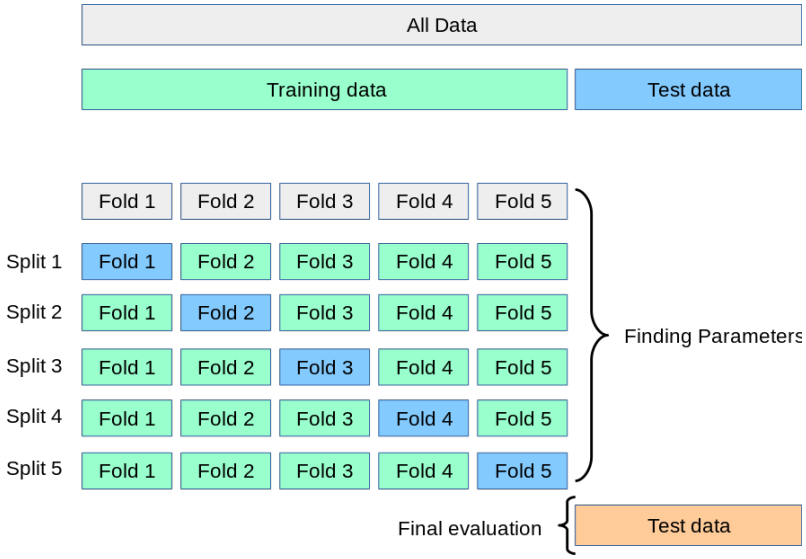


Figure 3.4: K-Fold Cross-Validation[2].

- **Leave-One-Out Cross-Validation**

Leave-one-out cross-validation is a particular case of cross-validation where the number of folds (k) is equal to the total number of data. Thus one sample of the dataset is used for test and the rest for training, iterating in the same way as in k-fold cross validation [57].

López-Larraz et al. [13] implemented this splitting method. They use windows of one second to classify between rest and intention (pre-movement state). The training set of each trial was composed of one window corresponding to movement intention, [-1, 0] s. And the rest state were the windows from -3 to -1 second with a sliding step of 0.25 s, as shown in Figure 3.5a. The classifier was trained using N – 1 trials (leave-one-out cross-validation). Regarding the test set used for evaluation, it was selected windows from -3 to 0 seconds with a sliding step of 0.125 s (Fig. 3.5b). The classifier was trained using N – 1 trials (leave-one-out cross-validation).

[2]Taken from: https://scikit-learn.org/stable/modules/cross_validation.html

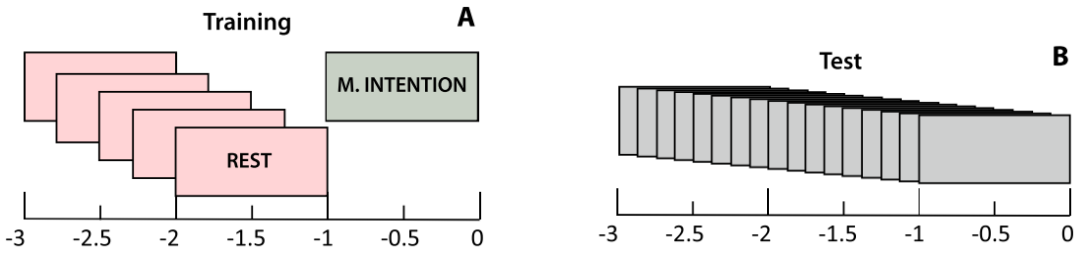


(a) Five windows of rest and one of intention extracted from one trial.

(b) Test set windows.

Figure 3.5: Figure adapted from Lopez-Larraz et al. (2014) [13]

### 3.3.2 Classifiers used to predict human intention

The Support Vector Machine (SVM) is the most common classifier to predict human intention [2]. Besides these, other classifiers such as Linear Discriminant Analysis (LDA) or derivatives are used. Table 3.6 presents the main classifiers found. A definition of those is given below.

- **Support Vector Machine (SVM)**

In SVM, the goal is to find a hyperplane (or a set of hyperplanes) in a high-dimensional space, which separates the data. A good separation is one that maximizes the distance between the boundary and the data points, called margin [58]. In 2 Dimensions, this hyperplane is a simple line, but in 3 Dimensions, it might be a plane.

In case the data is linearly separable, it is possible to find two hyperplanes parallel to the previous one, maximizing the distance between them.

However, if the classes are not linearly separable in the original input space, the SVM transforms this space into a higher dimensional features space, as seen in Figure 3.6. This transformation is done using non-linear mappings or kernels, namely polynomial, sigmoidal and gaussian radial basis function (RBF). Then, the SVM finds the optimal linear separating hyperplane in this new feature space.

The quality of an SVM model depends on the Kernel used to transform the input data and in a set of parameters, particularly the Regularization parameter (C) and Gamma [59]. C defines how the boundary allows for misclassification. This means that a high value of C gives more weight to the training data, and a lower value of C gives complexity more weight. Thus, a high value of C indicates that training data is more important and reflects the real-world data, whereas a low value is just the opposite. Gamma defines how fair a training point can influence the hyperparameter. With low gamma points far away from the separating plane are to be considered. In the other hand, with high Gamma, only closer points to the boundary are used to compute the classifier expression [60].

SVM presents some advantages in relation to other methods since it is effective in high-dimensional spaces (even if the number of dimensions is greater than the number of samples),

uses a subset of training points in the decision function, called support vectors, which are memory efficient, and versatile [61].

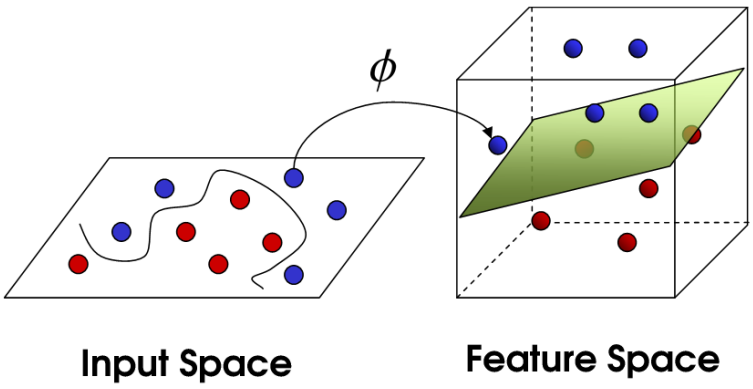


Figure 3.6: Support Vector Machine [62].

- **Linear Discriminant Analysis (LDA)**

It can be used for both dimensionality reduction and classification. The principle of this method is to find a linear combination between the features [58].

LDA uses two criteria to create the hyperplane [63]:

1. Maximize the distance between the mean value of two classes.
2. Minimize the interclass variance.

For example, the axis represented in red in Figure 3.7a will be the new axis that best fits the above criteria. After generating this new axis, all class data points are plotted on this new axis as shown in the Figure 3.7b.

These classifiers are commonly used because they are simple, easy to compute, and have no hyperparameters to tune [64]. However, it has the drawback of being linear, which can result in a lousy classification when the problem is not linearly separable [65].

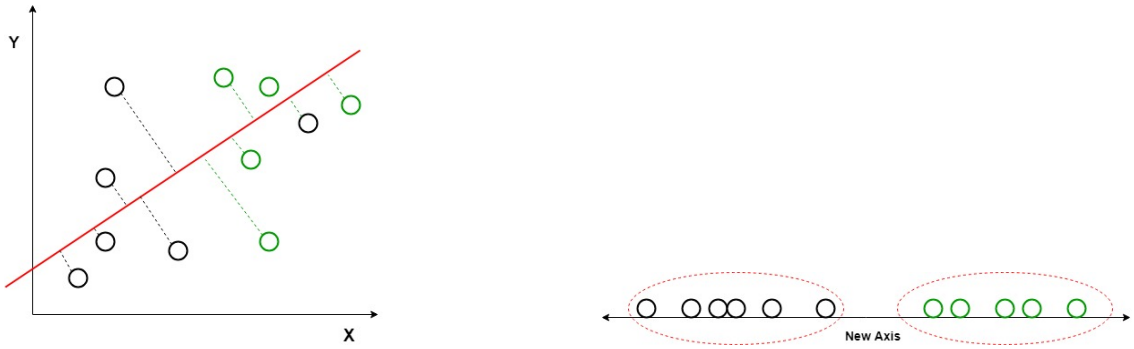


(a) Example of a 2-dimensional LDA classifier. (b) Sample projected in the new axis.

Figure 3.7: LDA classifier example.

- **Artificial Neural Network (ANN)**

Artificial neural network (ANN) is a machine learning methodology based on the structure and function of the biological neural network. Like neurons in the brain, ANN also consists of neurons arranged in various layers. The network architecture has an input layer, a hidden layer (one or more), and the output layer, as shown in Figure 3.8.

The ANN algorithm uses a training algorithm to learn the datasets, which modifies the neuron weights depending on the error rate between the target and actual output. In general, ANN also uses a backpropagation algorithm, where the error between predicted output and target output is calculated, and then gradient descent is used to update the weight values [66].

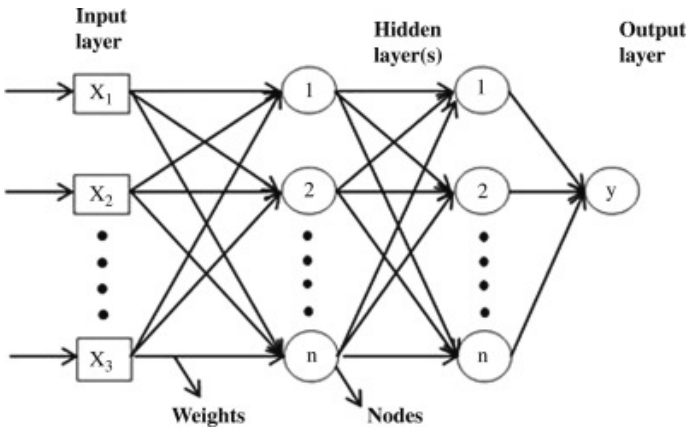


Figure 3.8: General structure of the ANN [66].

– **Long short-term memory (LSTM):** Long Short-Term Memory (LSTM) networks are a type of recurrent neural network (RNN), which means that, unlike standard feed-forward neural networks, LSTM has feedback connections [67]. An LSTM cell comprises three gates: an input gate, an output gate, and a forget gate, as shown in Figure 3.9.

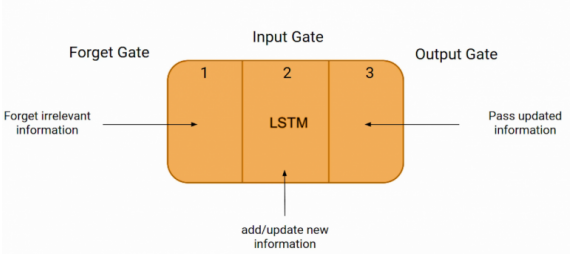


Figure 3.9: LSTM cell [68].

### 3.3.3 Evaluation Metrics

The final step consists of evaluating the performance of the models. Several metrics were found in the literature, being accuracy the most used (see Table 3.6, last column). The accuracy measures the capacity of the algorithm to detect classes correctly and can be calculated by considering the values obtained in the confusion matrix (see Equation 3.4). In this matrix, the rows represent the predicted classes while the columns represent the actual classes, as presented in Table 3.7. With this matrix, it is possible to observe:

- **True Positive (TP)** - classes predicted as positives and are really positives;
- **True Negative (TN)** - classes predicted as negatives and are really negatives;
- **False Positive (FP)** - classes predicted as positives and are negatives;
- **False Negative (FN)** - classes predicted as negatives and are positives;

Table 3.7: Confusion Matrix

| | **Predict positive class** | **Predict negative class** |
|---|---|---|
| **Actual positive class** | True Positive (TP) | False Negative (FN) |
| **Actual negative class** | False Positive (FP) | True Negative (TN) |

$$Accuracy = \frac{TP+TN}{TP+FP+TN+FN} \tag{3.4}$$

Besides the accuracy score, other metrics can be calculated, such as the ones defined below [69]:

- **Sensitivity/ Recall -** also know as true positive rate, measures the proportion of positives that are true positives (see Equation 3.5).

$$Sensitivity = \frac{TP}{TP+FN} \tag{3.5}$$

- **Specificity -** also known as true negative rate, measures the proportion of negatives that are true negatives (see Equation 3.6).

$$Specificity = \frac{TN}{TN + FP} \tag{3.6}$$

- **Precision -** measures the proportion of positives identifications that are actually correct (see Equation 3.7).

$$Precision = \frac{TP}{TP + FP} \tag{3.7}$$

#### 3.3.3.1 Receiver Operating Characteristics (ROC) curve

To visualize the classifier's performance, it is common to plot the ROC (Receiver Operating Characteristic) curve, see Figure 3.10. The curve is a probability curve obtained by plotting the sensitivity (true positive rate) against 1-specificity (false positive rate or false alarm) [70]. In order to quantitatively analyze the results of the curve, the **area under the curve (AUC)** is calculated.

AUC represents the degree of separability between classes. The higher the curve, the closer the AUC is to one, and the better the model predicts the correct labels for all observations.

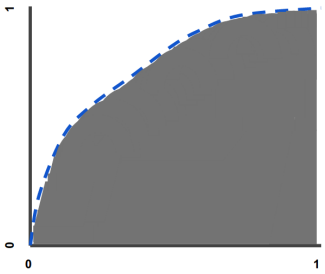


Figure 3.10: Area under the ROC curve[3].

López-Larraz et al. [13] used the ROC curve to evaluate the performance of the classifier. Their definition of TP, FP, TN, and FN is presented in Table 3.8.

Table 3.8: TP, FP, TN and FN definition on Lopez-Larraz work.

| | |
|---|---|
| **TP** | Correct onset detection between [-1, 0] |
| **FP** | At least one classifier onset misclassification during the rest phase [-3, -1] |
| **TN** | Rest periods with no false onset detections |
| **FN** | Movement intention periods with no correct onset detections |

[3]Taken from: https://developers.google.com/machine-learning/crash-course/classification/roc-and-auc

## 3.4 Protocols and datasets found in literature

In order to create a standard protocol for the data acquisition performed throughout this dissertation, a research was conducted regarding the protocols and datasets.

Most protocols follow a similar pipeline: a cross-screen followed by a visual cue of the movement to be performed or imagined (motor imagery). Then it is given an executing time, which can be cue-initiated or self-initiated movement. Self-initiated protocols ask the subject to wait a few seconds before performing the movement shown on the cue. Cue-initiated protocols are the opposite. The subject performs the movement right after the cue is shown.

Lopéz-Larraz et al. created a self-initiated multimodal acquisition protocol (EEG, EMG, and IMU) to predict human intention [13]. They created a total of 14 blocks of trials, 2 per movement. In each block, the same exercise was performed 25 times, meaning that 25 trials were conducted. Each trial was divided into two parts: movement cue and rest. The movement cue lasts 10 seconds and consists of the execution of the movement. The movement can only be executed at least 3 seconds after the start of the cue. At the end of the 10 seconds, the subject rests for 3 seconds until the start of the next cue. Figure 3.11 exemplifies how each trial was structured.

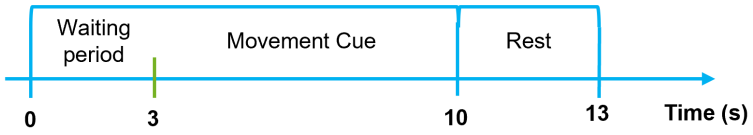


Figure 3.11: Scheme of each trial in López-Larraz et al. work.

On the opposite, Jeong et al. created, in 2020, a cue-initiated multimodal dataset (EEG, EMG, and EOG) to be used in BCI studies [14]. Of all the multimodal acquisitions, this paper was the only one found that has public data. The dataset is available on the GigaDB repository, `http://gigadb.org/dataset/100788`. This dataset includes 60 channels of EEG, 7 of EMG, and 4 of electrooculography (EOG).

During the session, the participants performed 11 different upper limb movements: arm-reaching in 6 directions (forward, backward, left, right, up, and down), hand-grasping of 3 objects, and wrist supination-pronation (Fig. 3.12).

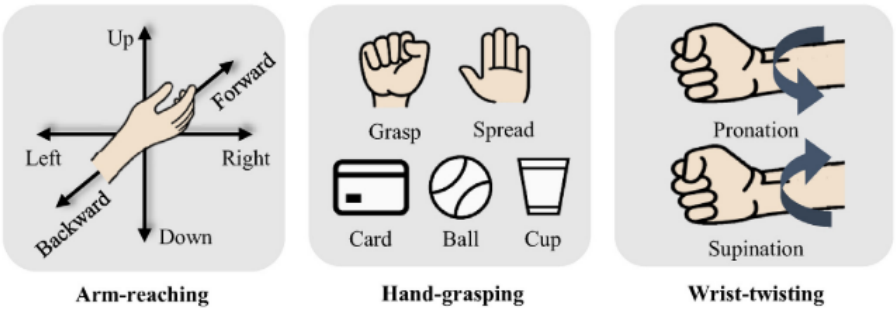


Figure 3.12: Movements performed on Jeong et al. work.

Each trial started with a fixation cross, taking 4 seconds, corresponding to the resting state. After resting, a visual cue was displayed on the monitor for 3 s with the instructions of the movement to be executed or imagined. Then the participants have 4 s to perform or imagine the motion. Figure 3.13 shows a scheme of each trial. In each session, each motion is performed or imagined 50 times.

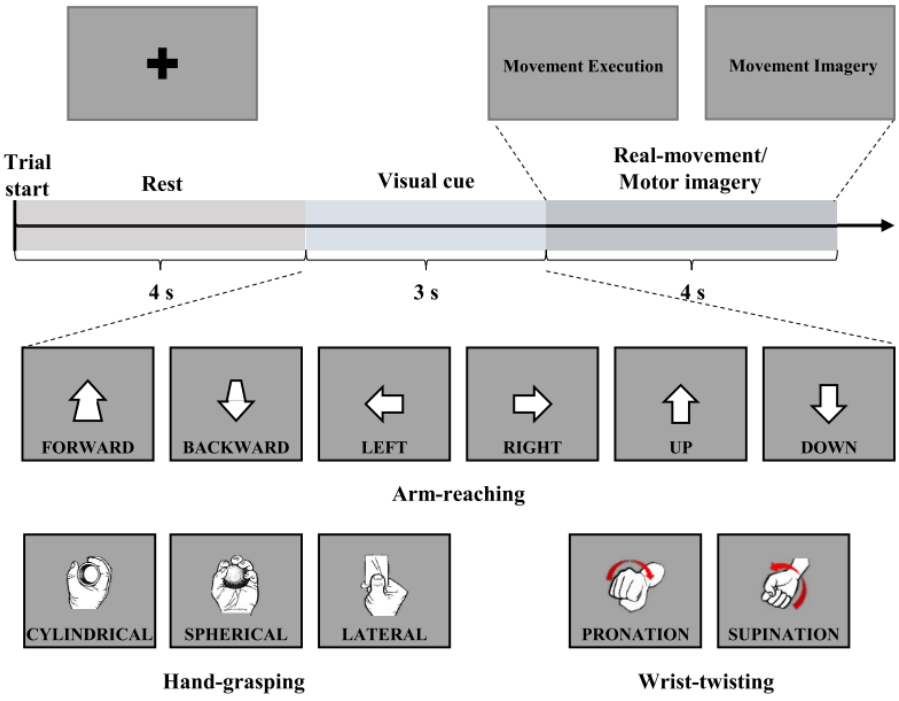


Figure 3.13: Scheme of each trial in Jeong et al. work.

A standard dataset used for BCI studies is EEG Motor Movement/Imagery Dataset[4] which was developed by the same team that created the BCI2000 instrumentation system.

From the research conducted, it can be concluded that most papers have private data, and most public databases have only the EEG data record. Of all public datasets found in literature, BCI2000

[4] https://archive.physionet.org/pn4/eegmmidb/

was chosen to be analyzed in this dissertation since it is the most used in literature. The following subsection describes this dataset in more detail.

### 3.4.1 BCI 2000 EEG Motor Movement/Imagery Dataset

The dataset records the EEG of 64 channels from 109 volunteers. It is divided into motor imagery and motor execution runs, resulting in 14 runs and 4 tasks. The first two runs consisted of the acquisition of baselines, eyes open and closed, for 1 minute each. Then the tasks start. Task 1, occurring in runs 3, 7, and 11, consists of opening or closing the left or right fist, as indicated by the cue. The subject has 4 seconds to execute the request and 4 seconds to rest. This is repeated for 2 minutes, and the same happens for the remaining tasks. Task 2 (runs 4, 8, and 12) is similar to task 1, but in this case, the subject performs the motor imagery. The remaining tasks, 3 and 4, deal with the opening and closing of both hands or feet. Task 3 consists of movement execution, and task 4 of imagery. Similarly, these tasks are repeated 3 times; task 3 is performed at runs 5, 9, and 13, and task 4 at runs 6, 10, and 14.

Regarding the labeling, three different annotations are made in each run: T0, T1, and T2. T0 corresponds to the rest period, whereas T1 and T2 change their meaning depending on the run. For example, in run 6 corresponding to task 4, T1 corresponds to both fists and T2 to both feet. Table x shows the meaning of annotations in each run.

Table 3.9: Tasks performed during the protocol.

| | **Description** | **Runs** |
|---|---|---|
| **Task 1** | Open and Close left or right fist | 3, 7, 11 |
| **Task 2** | Imagine opening and closing left or right fist | 4, 8, 12 |
| **Task 3** | Open and Close both fists or both feet | 5, 9, 13 |
| **Task 4** | Imagine opening and closing both fists or both feet | 6, 10, 14 |

Table 3.10: Annotation present in each task

| | **Task 1 & 2** | **Task 3 & 4** |
|---|---|---|
| **T0** | rest | rest |
| **T1** | left fist | both fists |
| **T2** | right fist | both feet |

## 3.5 Brief review

After conducting a short review on the subject of "Human Movement Intention," it is now even clearer that in recent years the number of studies in this area has been increasing. However, there is still much to be done and studied so that, in the future, the human-robot interaction can be more effective.

Some of the works use force sensors, inertial sensors, and EMG to classify movement intention [7, 8, 35, 12]. However, there is some delay in the robot's response because the intention is only

detected when the movement is initiated. Thus, in recent years, more studies have used EEG to predict movement intention with the help of other signals, such as EMG, to determine muscle activation [2, 13, 14, 34].

Seeing that with the use of biosignals, the results are more promising, a detailed analysis of the main methods implemented in this was then made, leading to conclude that:

- Regarding the detection of the EMG activity, there is no consensus yet on the chosen threshold.
- Related to the EEG segments, there is no conformity in the choice of $t = 0$ s. In some works, it is considered the time when the cue is presented on the screen [14], and in others, the time when the movement starts [13].
- Besides that, most works use more than one type of data acquired on different devices, and almost the works did not describe how the synchronization was done, except Lopéz-Larraz's work [13]. They described briefly that the synchronization was done manually, which is not very efficient. Since the detection of the movements' intention is done milliseconds before the movement, the ideal would be an automatic method with minimal synchronization errors.

Regarding the datasets and protocols, most of the data acquired are private. And most of the public databases only have the EEG data record. As discussed before, it is necessary to have some extra data, such as the one obtained from the EMG or IMU, indicating when the movement is being executed.

Therefore, this thesis work intends to address all of the counterfactuals presented here. Starting by:

- Creating a protocol and record EEG, ECG, EMG, and IMU data. This dataset will be public available to the scientific community:
- Make an accurate automatic synchronization algorithm between the acquisition devices;
- Find a threshold for EMG activity adapted to all subjects;
- Lastly, analyse the possibility of predicting human motion intention with EEG.

# Chapter 4

# Biosensing Devices

This chapter aims to overview the devices used in this dissertation. The openBCI system was used for biosignal acquisition, and the iHandU was employed for inertial measurements. This chapter also presents the most suitable electrode systems for each biosignal (EMG, ECG, EEG) and their setup.

## 4.1 OpenBCI

OpenBCI is an open-source, versatile and affordable biosensing system that can acquire EEG signals and measure the electrical activity of muscle (EMG) and heart (ECG). Two different battery-powered boards (amplifiers), named Cyton and Ganglion (Fig. 4.1), have been developed by the OpenBCI team [40]. These boards can be wirelessly connected to PCs, laptops, smartphones, or any Bluetooth-compatible device. The board communicates wirelessly with any computer via Bluetooth with the OpenBCI USB dongle (Fig. 4.1d).

The OpenBCI data can be recorded in two different ways: using the OpenBCI Graphical User Interface (GUI) (Fig. 4.2a), which displays data in real-time and allows users to measure the impedance of each channel (Fig. 4.2b), or through BrainFlow[1], which is a library intended to interact and obtain data from biosensors.

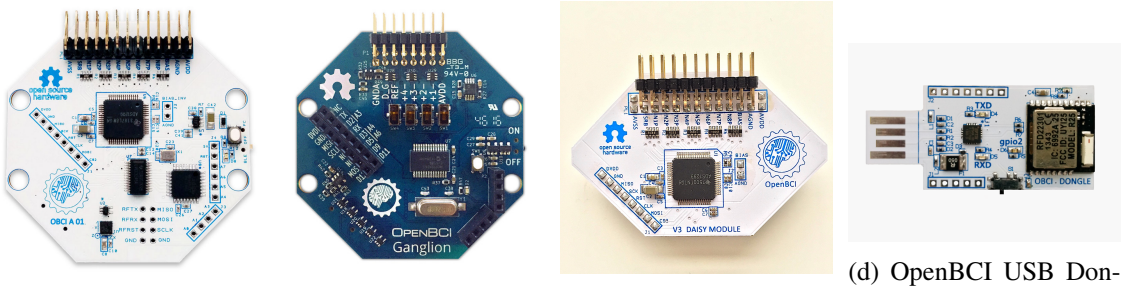


(a) Cyton Board (b) Ganglion Board (c) Daisy Module (d) OpenBCI USB Dongle

Figure 4.1: OpenBCI hardware[2].

[1] https://brainflow.readthedocs.io/en/stable/index.html

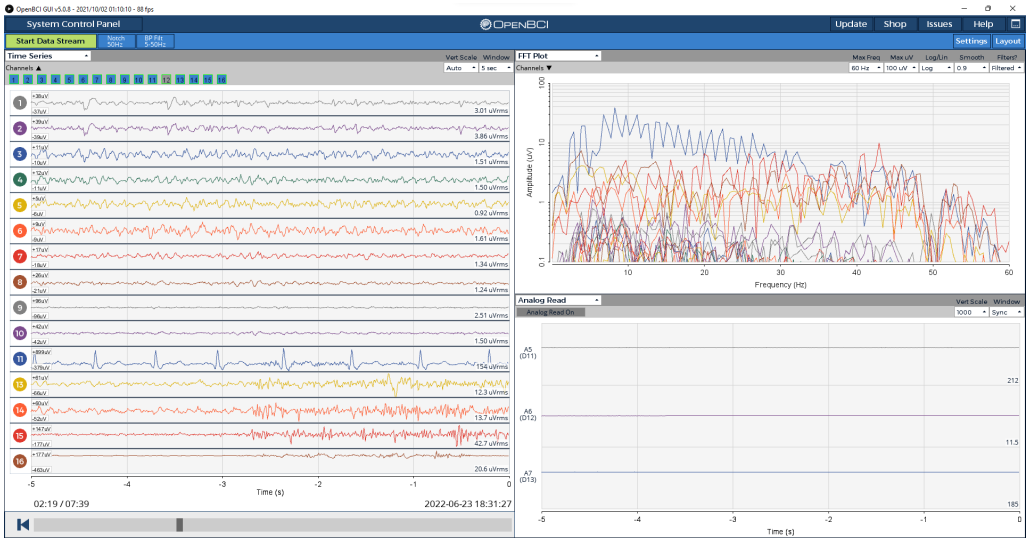


(a) Time series

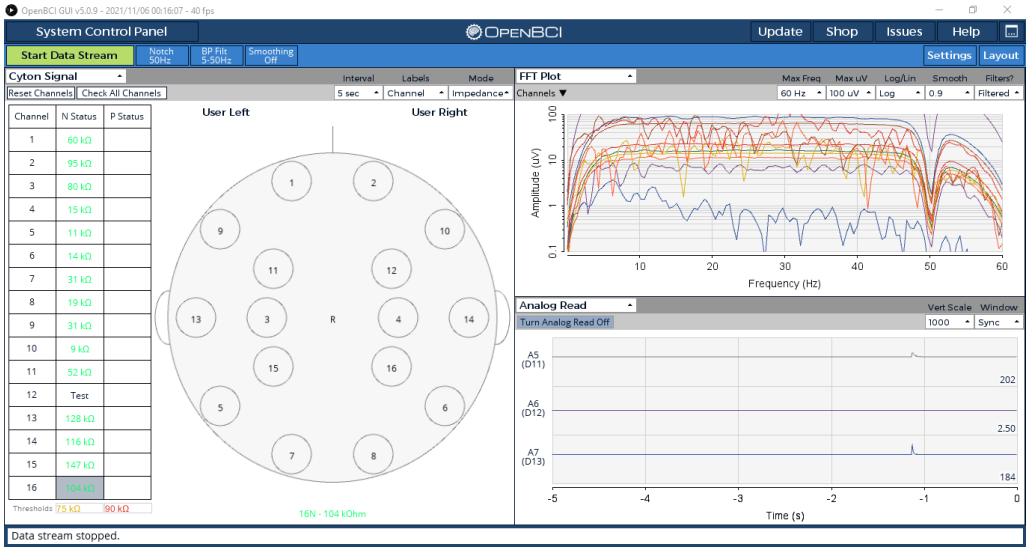


(b) Impedance measurement

Figure 4.2: OpenBCI GUI: (a) represents a time series example. The right top square plots the FFT in real time, and the right bottom square is showing the analog read. The user can select which layout they prefer. (b) example of the GUI when the impedance is being measure.

Cyton board, used in this dissertation, can acquire data at 250 Hz in eight channels. Besides that, an extra Daisy Module (Fig. 4.1c) can be added, increasing the number of channels to 16 but reducing the sample rate to 125 Hz. The main characteristics of these boards are presented below in Table 4.1.

[2] https://docs.openbci.com/GettingStarted/GettingStartedLanding/

Table 4.1: OpenBCI board characteristics

| Specifications | Cyton Board | Cyton + Daisy module |
|---|---|---|
| **Number of channels** | 8 channels | 16 channels |
| **Sampling rate** | 250 Hz | 125 Hz |

Figure 4.3 shows the indicated label for each channel. The BIAS, AGND, and SRB are considered reference channels. The data channels are N1P-N8P.

The reference channels needed for each biosignal are:

- **EEG**: two reference channels - **one SRB and one BIAS**. Additionally, it should be noted that both SRB pins must be connected to the same reference if the EEG data is acquired using the Cyton board and the Daisy module. A Y-Splitter cable can be used for this;
- **EMG**: one reference channel - **AGND**;
- **ECG**: one reference channel - **BIAS**.

The SRB pin is the reference for all EEG channels, and the AGND pin is the common ground for measuring voltage activity. Finally, BIAS is used for noise-canceling; it combines the common noise on all channels and subtracts it from the data channels [71].

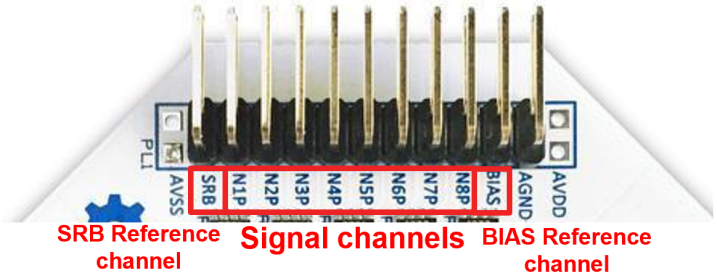


Figure 4.3: OpenBCI Cyton board channels.

Different channel requirements must be set depending on the signal to be acquired. For example, the default settings for EEG acquisition should be kept: SRB and BIAS on and gain x24. However, for EMG and ECG, the SRB2 parameter must be off. Also, the amplitude of both signals is higher than EEG, which means that ECG gain x1 and EMG gain x2 are enough.

As mentioned, these settings can be set using the OpenBCI GUI or the BrainFlow library. The former presents a simple user interface and allows any setting to be changed quite intuitively. On the other hand, if the BrainFlow library is used, any change to be applied must be transformed into an ASCII sequence and sent to the device, respecting the following format:
**x( CHANNEL, POWER_DOWN, GAIN_SET, INPUT_TYPE_SET, BIAS_SET, SRB2_SET, SRB1_SET)X**

For example, if someone wants channel 2 to record EEG data, he/she should send 'x2060111X'. Table 4.2 explains the meaning of each byte.

Table 4.2: Channel setting commands[3]

| | |
|---|---|
| **CHANNEL** | **1 2 3 4 5 6 7 8** for selecting channels in the Cyton board<br>**Q W E R T Y U I** for selecting channels on the Daisy Module |
| **POWER_DOWN** | 0 = ON (default)<br>1 = OFF |
| **GAIN_SET** | 0 = Gain 1<br>1 = Gain 2<br>2 = Gain 4<br>3 = Gain 6<br>4 = Gain 8<br>5 = Gain 12<br>6 = Gain 24 (default) |
| **INPUT_TYPE_SET** | 0 ADSINPUT_NORMAL (default)<br>1 ADSINPUT_SHORTED<br>2 ADSINPUT_BIAS_MEAS<br>3 ADSINPUT_MVDD<br>4 ADSINPUT_TEMP<br>5 ADSINPUT_TESTSIG<br>6 ADSINPUT_BIAS_DRP<br>7 ADSINPUT_BIAS_DRN |
| **BIAS_SET** | 0 = Remove BIAS<br>1 = Include BIAS (default) |
| **SRB2_SET** | 0 = Disconnect this input from SRB2<br>1 = Connect this input to SRB2 (default) |
| **SRB1_SET** | 0 = Disconnect all N inputs from SRB1 (default)<br>1 = Connect all N inputs to SRB1 |

### 4.1.1 EMG, ECG, and EEG Setup

#### 4.1.1.1 EMG

Starting with the EMG acquisition setup and taking into account the openBCI documentation, it is recommended to use one channel for each muscle. Therefore, one electrode cable is connected to the top pin of the channel and the other one to the bottom. Besides that, the ground electrode should be placed on the elbow (bone area) and connected to the AGND bottom pin, acting as a universal ground. Figure 4.4 shows an example of electrode placement on the upper limb muscles of a subject.

Some aspects need to be considered to improve the signal quality, such as the electrode configuration and placement. Regarding the electrodes used, SENIAM[4] recommends the pre-gelled Ag/AgCl electrodes. According to the literature, sEMG electrodes' size varies

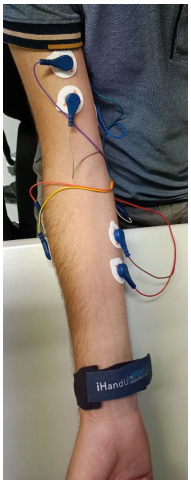

Figure 4.4: Electrodes placement on the subject

[3] https://docs.openbci.com/Cyton/CytonSDK/
[4] http://www.seniam.org/

from 1 $mm^2$ to a few $cm^2$. Considering the material available in the laboratory, the Dormo SX-30 electrodes, with 30 mm diameter, were used (Fig. 4.5a). Before placing the electrodes, the skin contact area should be cleaned with alcohol. The sensors' placement should be parallel to the muscle fiber, and the inter-electrode distance should be at least 2 cm to avoid crosstalk.

#### 4.1.1.2 ECG

Regarding the ECG, a 3-lead ECG configuration must be set up for one channel acquisition. One snap electrode acts as the ground and should be connected to the BIAS on the board and stuck to the bony part of the chest. The remaining two electrodes must be placed on opposite sides of the subject's chest and connected to the top and bottom pins of the same channel.

Like in the EMG, sticky electrodes should also be used. In this case, the Ambu® BlueSensor VL[5] electrodes (Fig. 4.5b) are recommended for ECG signal acquisition.

(a) sEMG electrode used: Dormo SX-30 electrodes, with 30 mm diameter.

(b) ECG electrodes used: Ambu® BlueSensor VL, with a contact size of 68 mm.

Figure 4.5: Electrodes utilized for EMG and ECG acquisition

#### 4.1.1.3 EEG

Finally, focusing now on the EEG setup, the three setups illustrated in Figure 4.6 could be used:

- Gold cup electrodes [72] (Fig. 4.6a), which already come together with the OpenBCI kit;
- Ultracortex "Mark IV" EEG headset [73] (Fig. 4.6b), which also comes in the OpenBCI kit;
- EEG cap by Besdatatech [42] (Fig. 4.6c).

Regarding the three possibilities, a comparative study was recently done by V. Minhoto [65] to determine the best option. The Ultracortex "Mark IV" headset led to signals with a higher impedance and was therefore immediately discarded. Among the remaining two, since the impedance is similar, the Besdatatech EEG cap was chosen due to being simpler to set up.

[5] https://www.ambu.com/cardiology/ecg-electrodes/product/ambu-bluesensor-vl

(a) Gold Cup Electrodes [72]

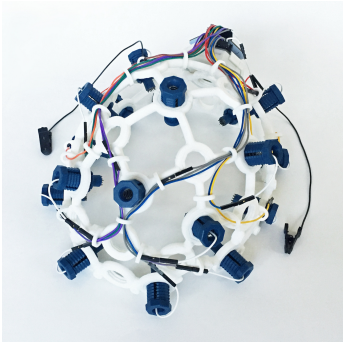

(b) Ultracortex "Mark IV" [73]

(c) EEG cap by Besdatatech [42]

Figure 4.6: EEG electrode systems

Focusing on the EEG cap chosen for this work, the connection procedure consists of four steps:

1. First, adjust the cap to the subject's scalp;
2. Then, connect the electrodes on the cap to the openBCI channels through a cable adapter, as shown in Figure 4.7;
3. After that, connect each electrode to one channel of the openBCI board. The GND must be on channel AFZ, and the REF must be wired to the SRB pin (Fig. 4.8);
4. Finally, fill with an electroconductive gel, e.g. the Electro-Cap Electro-Gel[6], each channel chosen for data recording. This step ends once all the selected channels have acceptable impedance values, checking with the OpenBCI GUI (Fig. 4.2b).

(a) EEG cap cable.

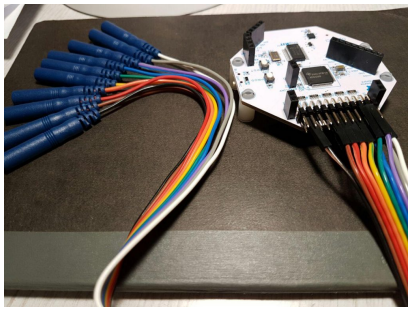

(b) OpenBCI - EEG electrode adapter.

(c) Adapter connection to GND cap electrode.

Figure 4.7: EEG cables and adapters.

[6] https://shop.openbci.com/collections/frontpage/products/electrodegel

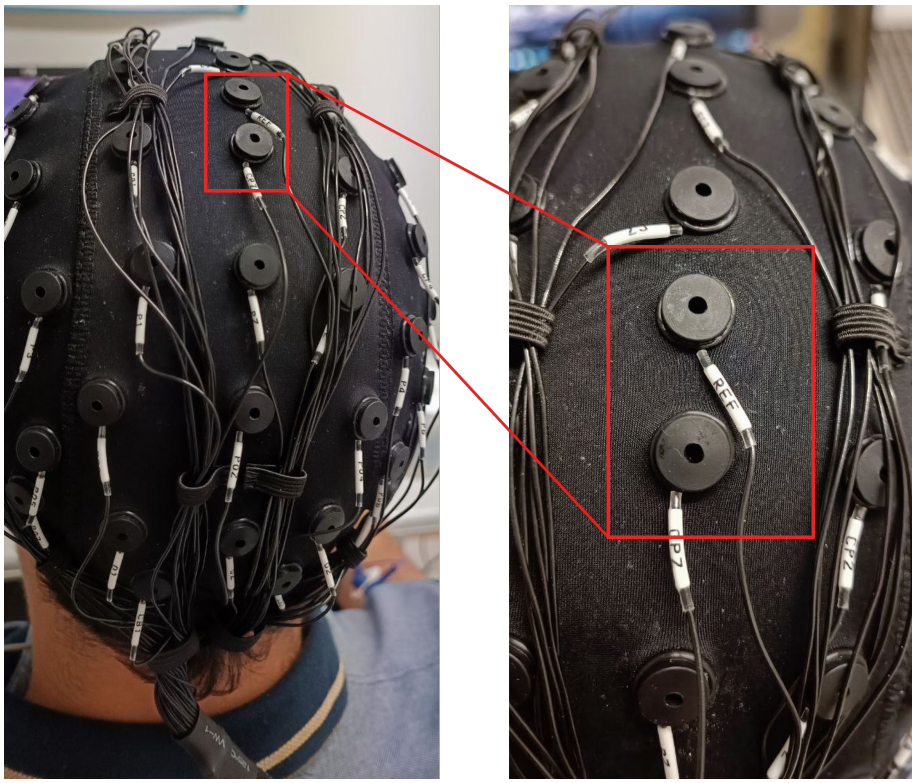


Figure 4.8: EEG cap reference channel.

## 4.2 iHandU device

While biosignals are being collected, it is also important to gather information about the position of the limbs. For this, a device known as iHandU (Fig. 4.9) can be used. This device has been developed in the BRAINLab group of INESC-TEC and is a wearable device that comprises a hardware sensing unit integrated into a textile band [74]. The device acquires data from four different sensors: an accelerometer, a gyroscope, a magnetometer, and a temperature sensor (all compacted in an Inertial Measurement Unit: ICM-20948[7] which establishes an I2C communication with the microcontroller) [39]. Additionally, the iHandU device has an integrated Bluetooth Low Energy (BLE) module to exchange data with other devices. The IMU and the analog data are measured at a frequency of 50Hz. This dissertation only requires the data coming from the accelerometer and the gyroscope.

The connection with the device and the data recording can be made through a web platform, using Google's Web Bluetooth API (Application Programming Interface) methods to connect the BLE devices with the Google Chrome browser.

The web page is illustrated in Figure 4.10. It consists of a dashboard containing two main buttons: a "Connect"/"Disconnect" to start or stop the data stream from the device and a "Record"

[7] https://invensense.tdk.com/wp-content/uploads/2016/06/DS-000189-ICM-20948-v1.3.pdf

button to save the received data into a *.csv* file. Additionally, it contains six charts that illustrate the sensor data in real time.

Considering that the chosen movements focus on the forearm, it is enough to use only one iHandU on the wrist, as shown in Figure 4.9b.

(a) iHandU device

(b) iHandU on the subject forearm.

Figure 4.9: iHandU device.

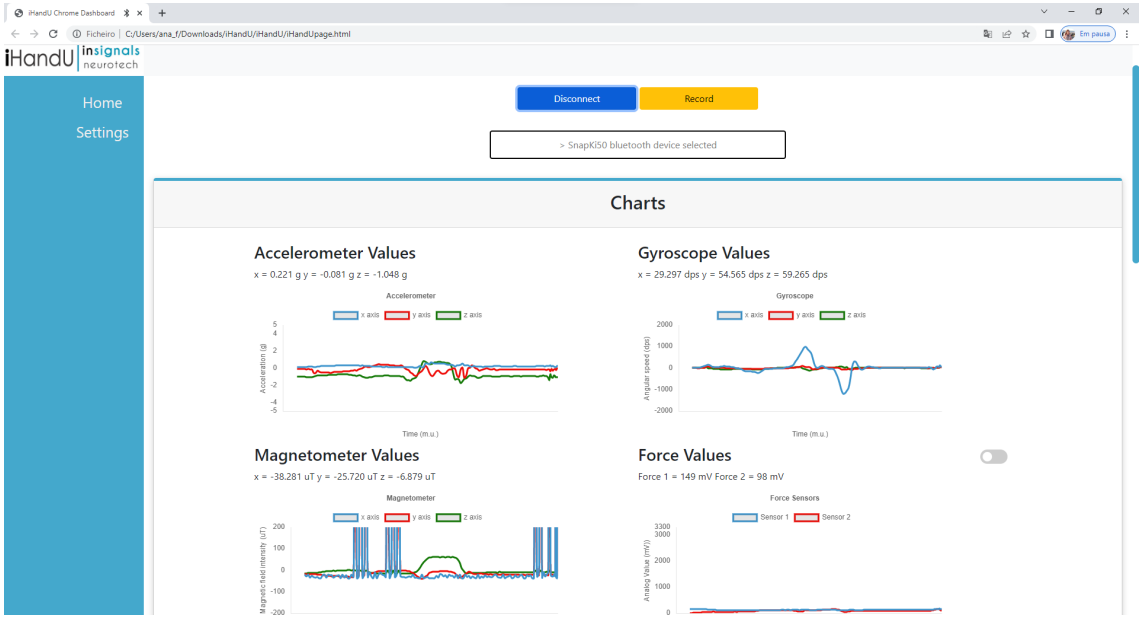


Figure 4.10: iHandU - Device Dashboard

# Chapter 5

# Methodology

This chapter addresses the methodology implemented in this thesis. Section 5.1 describes the experimental protocol developed to acquire the data. Section 5.2 the methods applied to each data type are presented, and finally, Section 5.3 describes how all data was synchronized. A summary of the entire pipeline is shown in Figure 5.1. The code structure is explained in Appendix A and is available on GitLab from INESC TEC: https://gitlab.inesctec.pt/brain-lab/human-machine-symbiosis/machine-human-awareness.

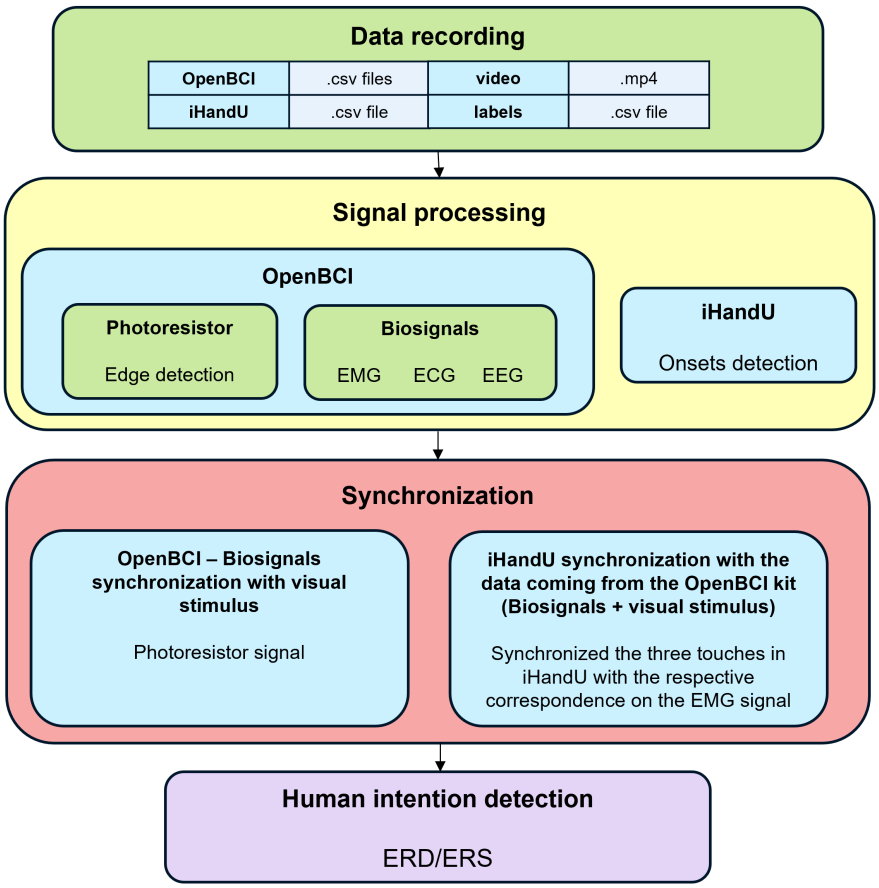


Figure 5.1: Methodology overview.

## 5.1 Experimental protocol

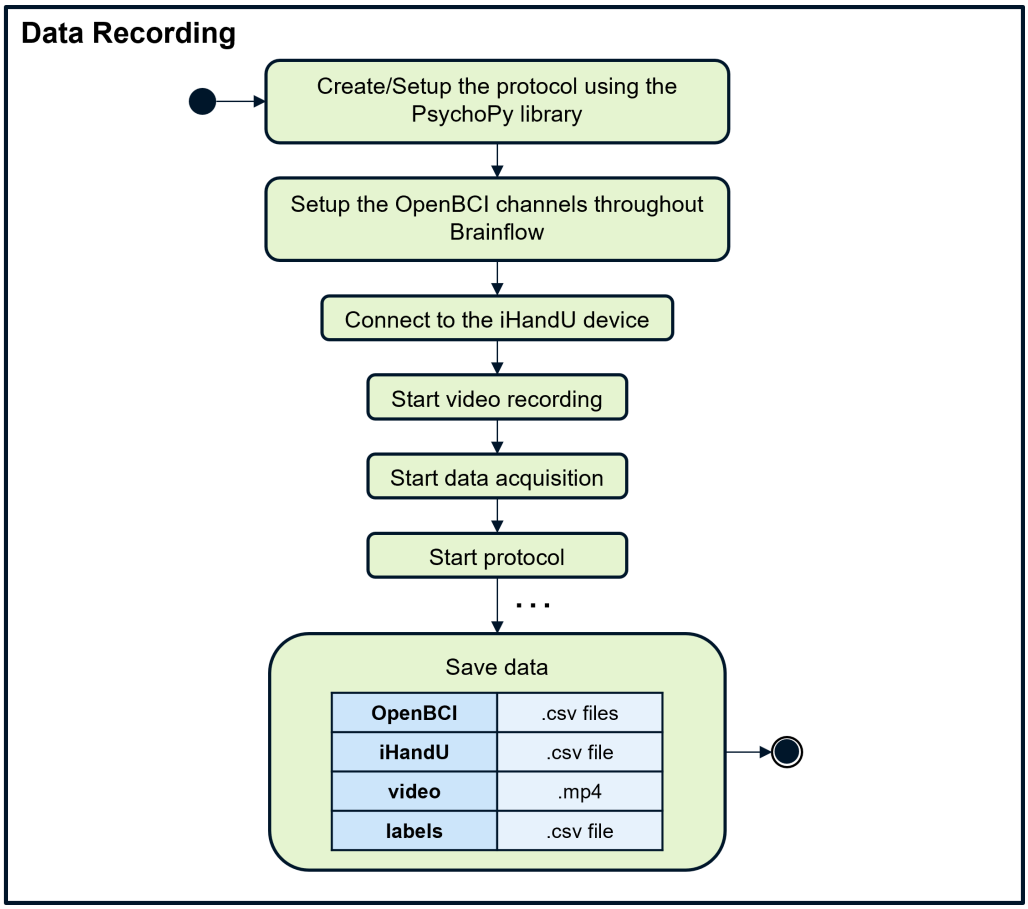


Figure 5.2: Data recording scheme.

The protocol was established based on similar experiments found in the literature and in some existing databases also built to predict human motion intent [14, 75, 76, 13, 33].

Figure 5.2 summarizes the main steps performed to obtain the dataset. The following subsections detail each step of the implemented protocol. Subsection 5.1.4 explains the frameworks used.

### 5.1.1 Participants

All participants were healthy individuals with no known neurophysiological anomalies or musculoskeletal disorders. Before the experiments, the participants were informed about the experimental protocols, paradigms, and purpose. After ensuring they understood the information, the participants signed a written consent form. In addition to the explanation, each participant tried a tiny version of the protocol (with only two runs totaling six trials) to relax and become familiar with what they had to perform next.

The acquisitions were divided into two phases. The second phase emerged to improve some setbacks encountered in phase 1, such as data loss and synchronization problems, after analysing the results from phase 1. These problems are explained in more detail in Chapter 6.

The first phase of tests had six healthy volunteers, aged 22 to 25, two males and four females, all right-handed (see Table 5.1). During these trials, some setbacks occurred: First, on Subject 1, the iHandU sync maneuver was not recorded. Then, the protocol crashed at the end of the second run of the Subject 3' session. Furthermore, the EEG data from Subject 5 was not recorded by mistake.

Regarding phase 2, three additional healthy volunteers (aged 20 to 26, two males and one female, all right-handed) participated in the experiment.

Table 5.1: Participants description.

| | **Phase 1** | **Phase 2** |
|---|---|---|
| **Number of participants** | 6 | 3 |
| **Age (years ± std)** | 22.3±0.9 | 22.6±2.5 |
| **Gender** | 4 females; 2 males | 1 female; 2 males |

### 5.1.2 Experimental paradigm

Each session starts with a Welcome Screen followed by the "iHandU sync maneuver" screen, which consists of touching 3 times in the iHandU device placed on the wrist. This is done to help synchronize the data between the devices. After that, starts the baseline recording, which consists of a 30-second "Eyes Open" window, followed by another 30-second "Eyes Closed". After these two blocks, "Jaw Clenching" and "Eye Movement" are performed to capture the noise that may contaminate the EEG. Then, the protocol enters a loop that runs $n$ times (depending on the acquisition phase), consisting of a Run and a 1-minute short break. Each run is composed of $m$ trials of a random class. The random algorithm is implemented so that having three classes, each class is performed $k$ times, preventing class imbalance.

The number of runs and trials varies depending on the acquisition phase. Table 5.2 describes the number of runs and trials of each phase.

Each trial follows the subsequent sequence:

1. **Rest**: A cross-screen shows up for 4 seconds. It includes an audible signal 1 second before the end of the screen.

2. **Visual Cue**: A movement video is played for 4 seconds.

3. **Rest**

4. **Movement Imagery**: The user thinks, for 6 seconds, about the task that should perform.

Table 5.2: Number of runs and trials on each acquisition phase.

| | **Phase 1** | **Phase 2** |
|---|---|---|
| **Runs *(n)*** | **4** | **5** |
| **Different movements** | 3 | 3 |
| **Number of movements per run *(k)*** | 5 | 6 |
| **Trials per run *(m)*** | **15** | **18** |
| **Total movements** | **60** | **90** |

5. **Rest**

6. **Real Movement**: The participant has 6 seconds to perform the movement. He must perform and hold the position. An audible cue is displayed 1 second before the end, so the participant knows that he should return to the rest position.

Figure 5.4 illustrates the session pipeline. The rest screens were implemented to accurately separate the screens and the classes. During the rest screens, the participants were asked to avoid executing or imagining any movement.

The movements that each participant must perform were chosen based in literature, namely:

- **Hand-grasping**: The participants should grasp a water bottle, an object of daily use (see Fig. 5.3a).
- **Wrist-twisting (supination)**: The participants rotate their wrists to the right, if they are right-handed, otherwise to the left (see Fig. 5.3b).
- **Pick and place**: The participants grab an object and place it on the opposite side (see Fig. 5.3c).

(a) Hand-grasping.

(b) Wrist-twisting (supination)

(c) Pick and place

Figure 5.3: Set of movements that each participant must perform.

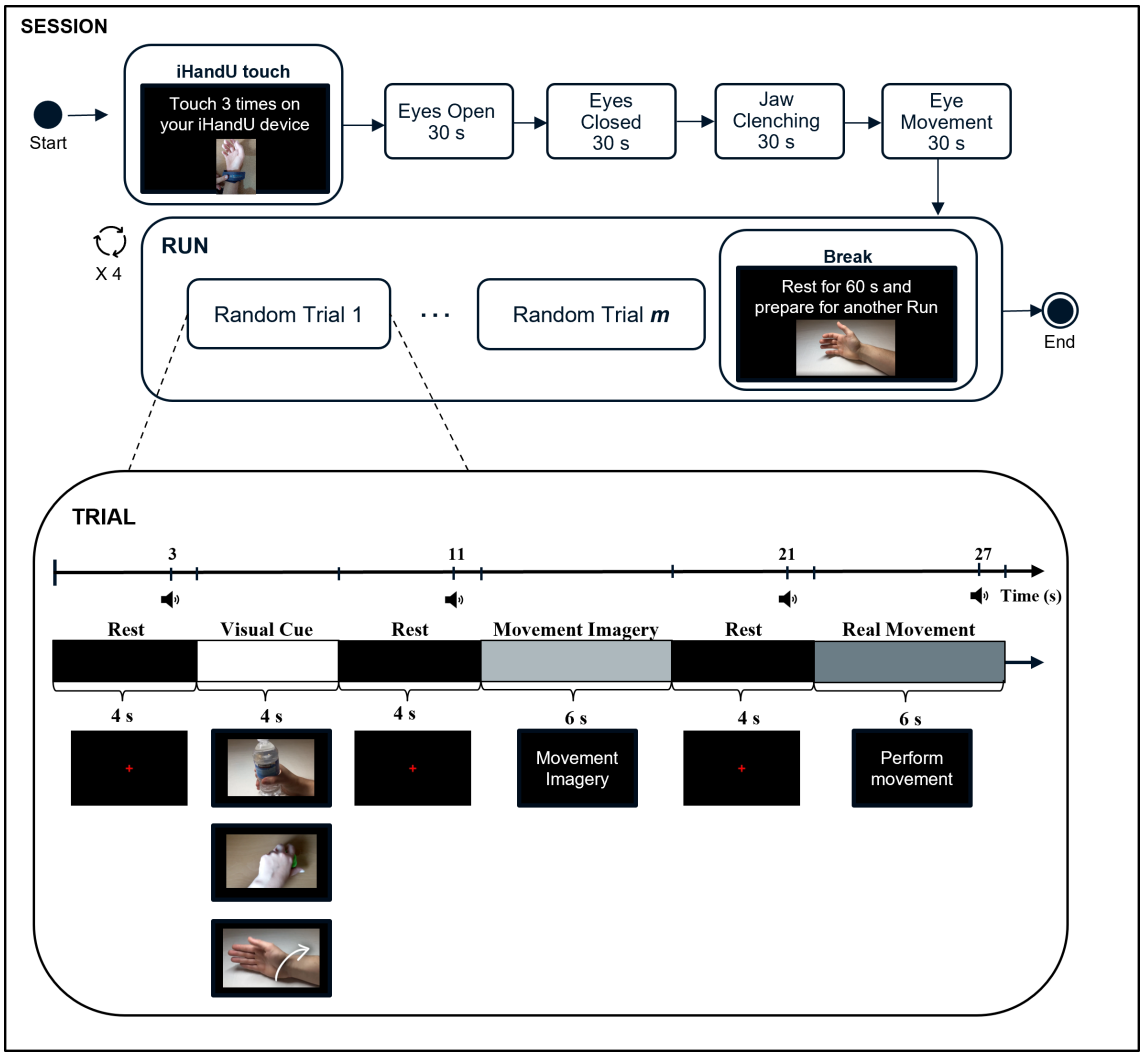


Figure 5.4: Acquisition protocol (one session).

### 5.1.3 Environment

During the experiments, each participant was comfortably seated in a chair with armrests approximately 60 cm from the monitor. Figure 5.5 shows some images taken during the experiment protocol.

An EEG cap (Fig. 4.8) with 64 channels was placed on each participant's head, and the EMG and ECG electrodes were attached to pre-assigned locations. The impedances of the EMG, EEG, and ECG electrodes were also checked and kept below 100 KΩ. Besides the physiological data, the IMU data and video were also recorded. During the data recording, participants were asked to perform the movements with minimum eye and body movements.

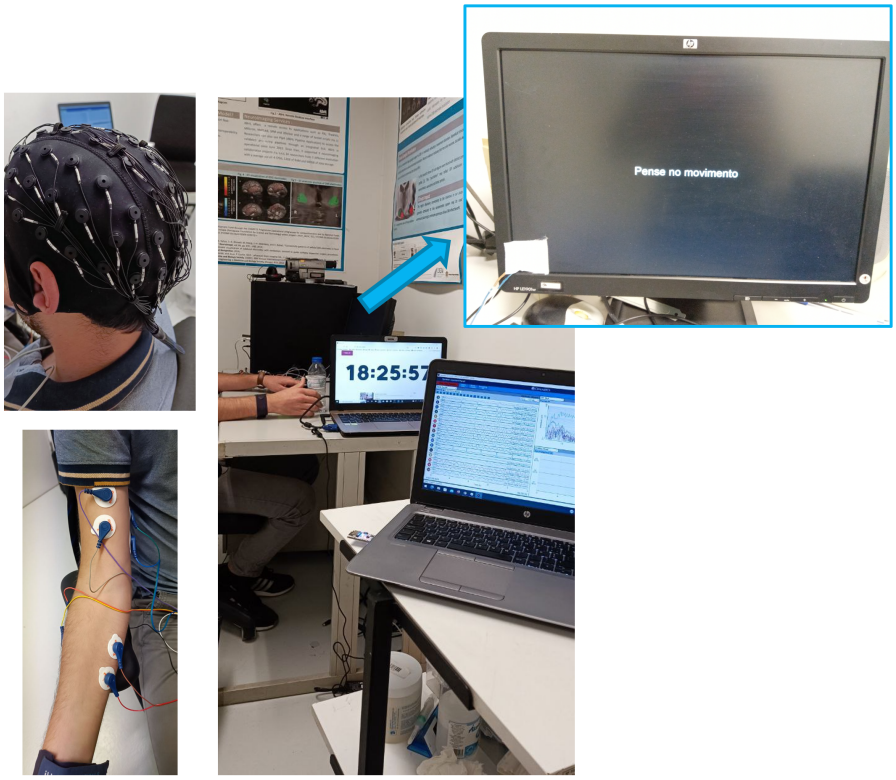


Figure 5.5: Environment setup.

### 5.1.4 Data recording

During the execution of the protocol, data from the openBCI (EEG, ECG, EMG, photoresistor signal) and iHandU (IMU data) were recorded. The ECG was used for artifact removal. The EMG and IMU were used for movement onset detection. Both are used to evaluate the feasibility of using iHandU instead of EMG since it is simpler to use. In addition, a camera (Logitech C270 HD) is also used to record the participant's session in video, thus better supporting the post-processing of the recorded data. All the code was developed in Python language. Figure 5.6 shows the libraries used to process and handle each data type.

The protocol was implemented using the PsychoPy Library[1], which is a cross-platform package that allows to build and run a wide range of experiments in the behavioral sciences (neuroscience, psychology, psychophysics, linguistics, among others). Furthermore, it stores the information related to the trials on a .csv file, e.g., what stimuli were presented to the participant and in what order, which means that the protocol-related data can be easily accessed and processed.

Focusing on the biosignals acquisition, the same device was used, the OpenBCI system (Cyton board + Daisy module - Section 4.1), which means that the ECG, the EEG, and the EMG are acquired simultaneously. Besides that, the OpenBCI Cyton board was also used to sample the output signal of the photoresistor circuit. These data were recorded with the Brainflow library's

[1] https://www.psychopy.org/

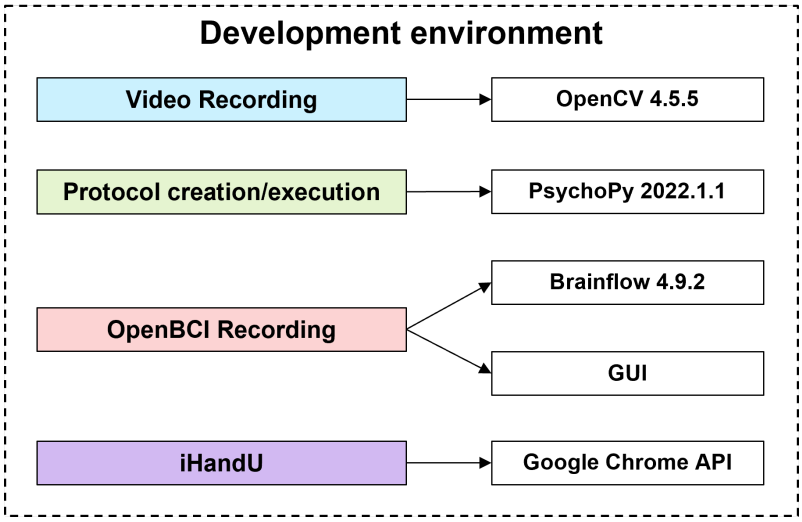


Figure 5.6: Libraries used during the development of the experiment.

help and saved on a .csv file. The impedance checking was done using the GUI developed by the openBCI team. The Brainflow is a library intended to interact and obtain data from openBCI boards (see Section 4.1).

The IMU data was acquired using the iHandU device and the Google Chrome API (see Fig. 4.10) and saved on a .csv file. Regarding the camera video, it was captured with an ordinary webcam and saved on a .mp4 file with the help of the OpenCV library[2], which is an open source computer vision and machine learning software library.

All the code was developed on an ASUS A541UJ Intel Core i3 (PC 2 of the schemes below) running on Windows 10. The experiment routine is presented to the participants through a second monitor, on an HP EliteDisplay E231 23-inch monitor, with a 60 Hz refresh rate connected via VGA cable to the PC 2. A second computer, an HP EliteBook 850 G3 laptop (PC 1 of the schemes below), was used to reduce the average computational load required from each processor.

Each computer had different tasks assigned, depending on the acquisition phase. The schematic in Figure 5.7 corresponds to the organization of phase 1. In this first approach, one computer was responsible for recording the video (PC 1) and the other for performing the experiment and recording the biosignals, the photoresistor signal, and the IMU data (PC 2). It should be noted that all biosignals (ECG, EEG, and EMG) and the photoresistor signal are stored in the same file, and each run has a new file associated. Despite all these efforts to reduce the computational load, some errors and data loss were still observed when analyzing the recorded output.

[2] https://opencv.org/

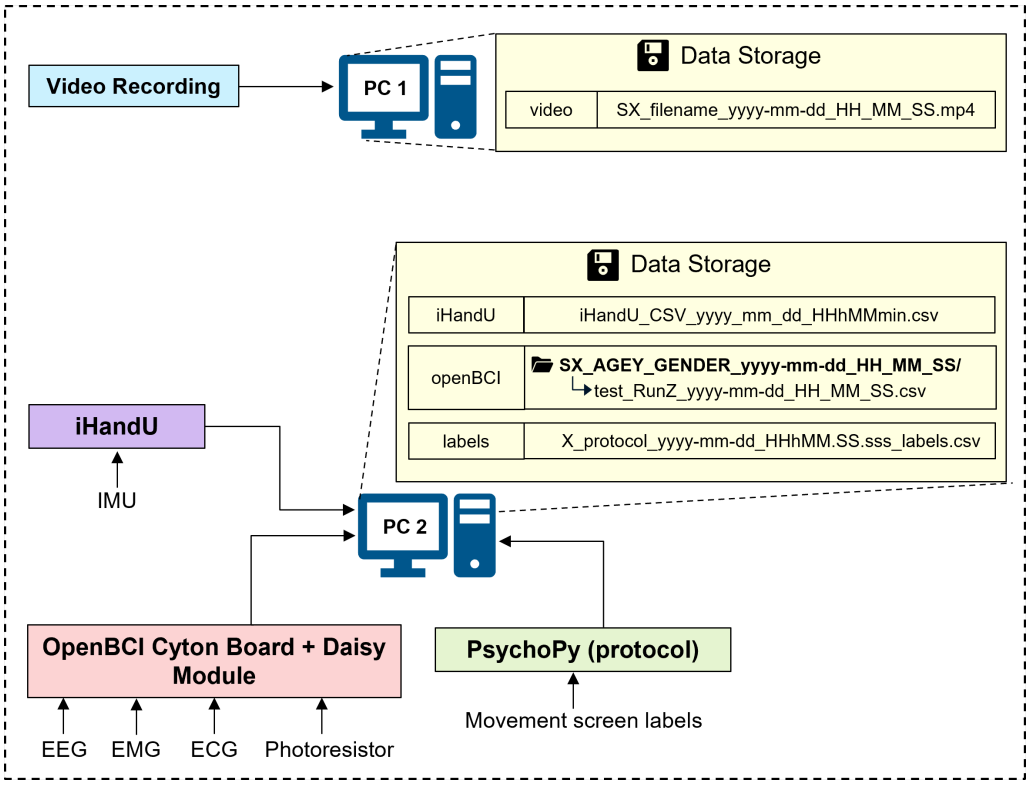


Figure 5.7: Schematic illustration of the general outline of the experimental setup (Phase 1).

In order to solve these issues, a new approach to data recording was considered. On this new setup, the IMU and OpenBCI data (biosignals + photoresistor) were recorded using different computers but synchronized by the same NTP server [77], *time.windows.com*, as depicted in the schematic of Figure 5.8.

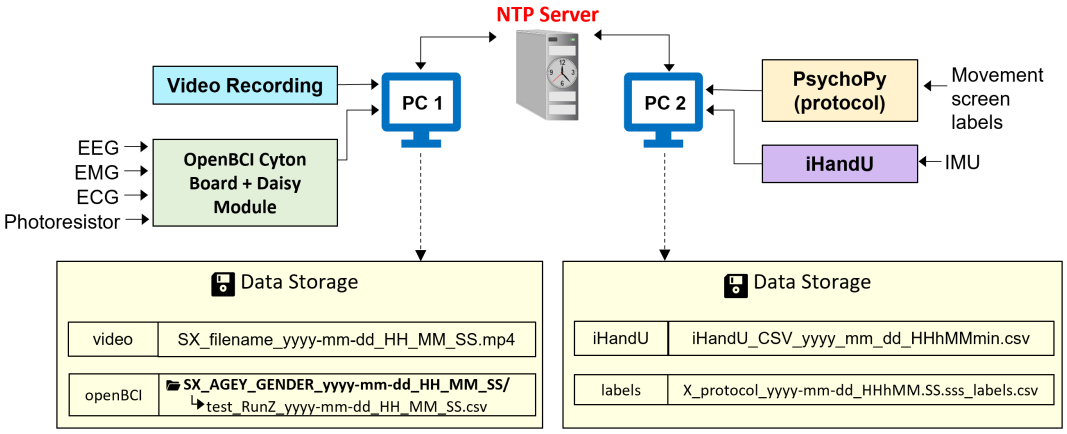


Figure 5.8: Schematic illustration of the general outline of the experimental setup (Phase 2).

### 5.1.5 ECG, EEG, and EMG setup

As stated above, the biosignals were acquired at 125 Hz with the openBCI system (Cyton board + Daisy module). The number of brain channels used and muscle activity recorded was different in each acquisition phase, however, for both phases, the 3-lead ECG was set up, which led to only one channel being used. Subsection 4.1.1 reviews how the openBCI channels must be configurated for each type of signal.

#### 5.1.5.1 Phase 1

Regarding phase 1, only 15 channels were used. Based on what was found in the literature and the relation between the muscles and the movements performed (Subsection 2.1.1), 4 muscles were chosen: *bicep brachii*, *tricep brachii*, *flexor carpi radialis*, and *extensor digitorum* (see Fig. 5.9), resulting in 4 channels connected to the Daisy Module.

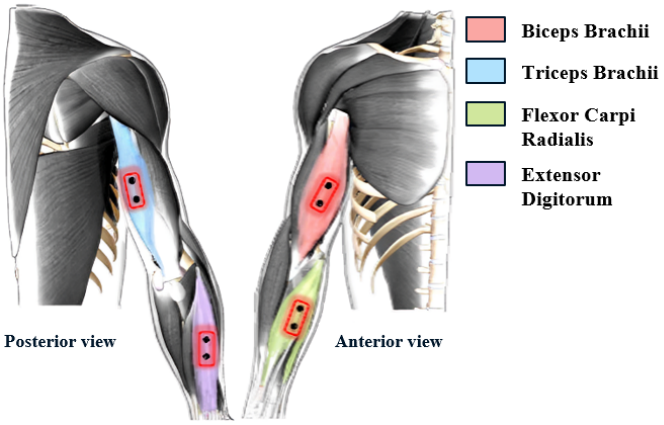


Figure 5.9: Electrodes placement in our study for acquiring EMG data (Phase 1) [8] (adapted).

The EEG channels were chosen according to the regions related to the motor area, regions in pre-motor, primary motor, and somatosensory (Fig. 2.5 Subsection 2.2.1). The channels used were FP1 and FP2 to capture eye blink, and FCZ, C3, CZ, C4, CP3, CP4, P3, and P4 (see Fig. 5.10).

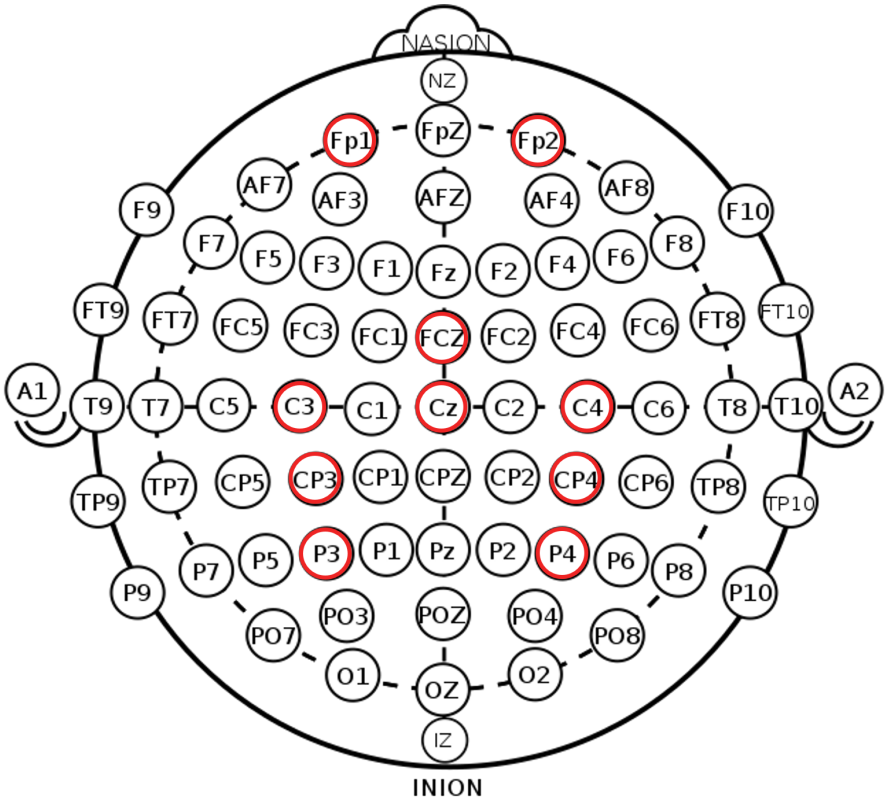


Figure 5.10: EEG electrodes utilized in phase 1 (10-10 system).

#### 5.1.5.2 Phase 2

Since a new round of data acquisitions was necessary, it was decided to make some changes regarding the channels utilized. For example, from the analysis of the first phase data, it was verified that the *extensor digitorum* muscle could reveal muscle activation for all movements, which does not happen with the other muscles. Therefore, it was decided to reduce the number of EMG channels in this new phase of acquisitions and increase the number of EEG channels, hence obtaining more EEG features. In this way, the EEG channels considered in phase 2 are: FP1, FP2, FC3, FCz, FC4, C1, C3, Cz, C2, C4, CP3, CP4, P3, and P4 (see Fig. 5.11).

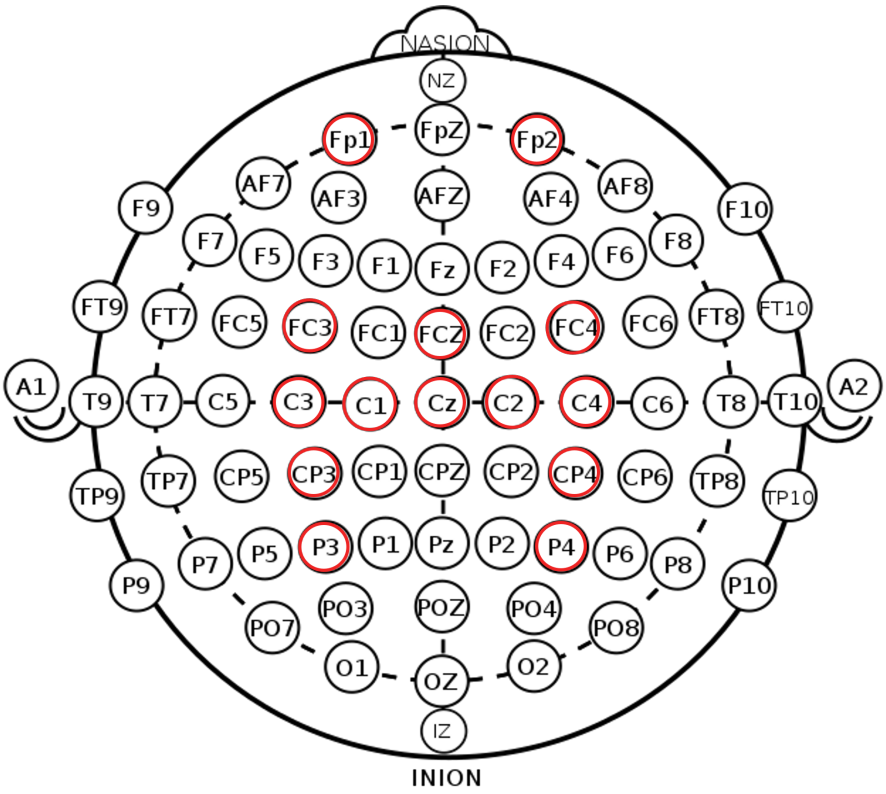


Figure 5.11: EEG electrodes chosen for phase 2 (10-10 system).

### 5.1.6 Photoresistor setup

As mentioned above, a photoresistor signal was also recorded on the Cyton board to help synchronize the openBCI data with the visual stimulus. This section explains in more detail how the photoresistor works and how it was configured on the openBCI board.

The photoresistor circuit is depicted in Figure 5.12 and can directly connect to the OpenBCI cyton board. The VDD and the ground (GND) pins are connected to the voltage divider's input and ground. The A5 (D11) pin (or any other analog pin available in the OpenBCI board) is connected to the output of the circuit, as exemplified in Figure 5.13a.

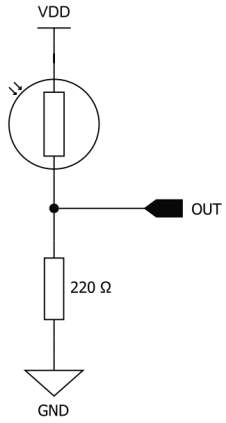


Figure 5.12: Photoresistor circuit utilized to synchronize stimulus presentation and biosignals data.

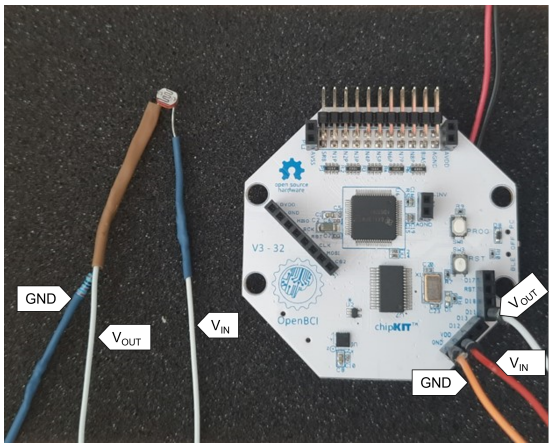


(a) Photoresistor setup on Cyton Board.

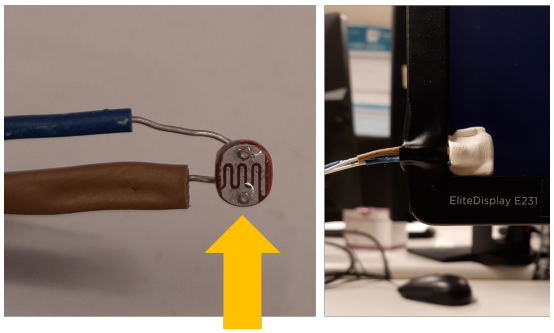


(b) Photoresistor placed on the bottom-left corner of the external monitor.

Figure 5.13: Photoresistor utilized for iHandU-OpenBCI synchronization.

The photoresistor was attached to the bottom left corner of the screen (see Fig. 5.13b) so that the output of the voltage divider increases with the screen brightness. To detect screen changes, the protocol built with PsychoPy displays a small square in the bottom left corner, which is represented with different grey levels depending on the trial topic currently running. The square is only displayed while the screen is active, allowing a stricter segmentation of the data. For example, the square shown on the Visual Cue screen is white; in Movement Imagery, the square is light gray, while in the Real Movement screen, it is a darker gray (see Fig. 5.14). This way, it is possible to know which screen is active by looking at the photoresistor data and knowing the order in which the screens appear.

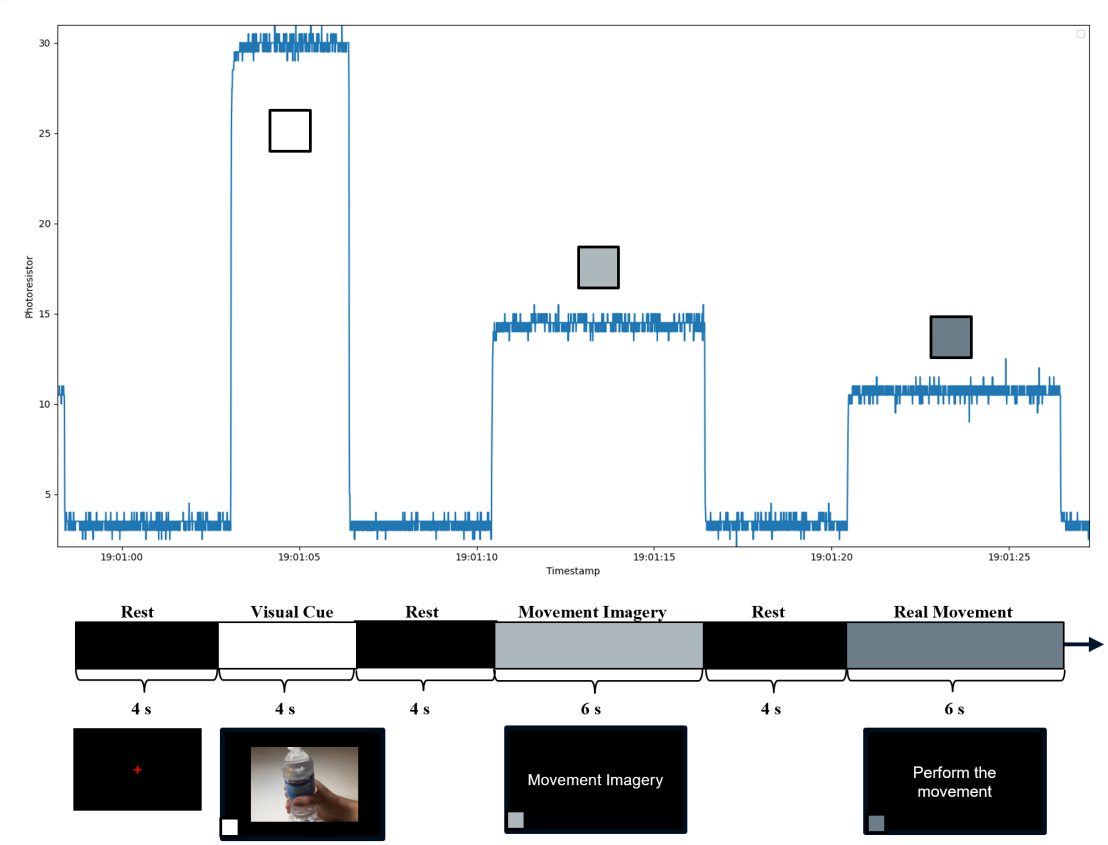


Figure 5.14: Example of photoresistor data Run 2 subject 6.

## 5.2 Pre-processing

This section focuses on the main processing steps applied for each type of data.

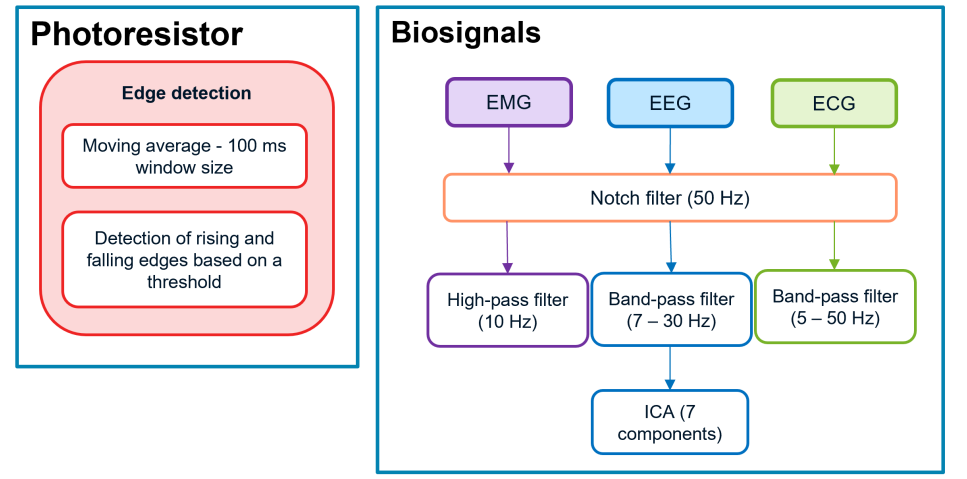


Figure 5.15: OpenBCI data processing scheme.

### 5.2.1 Photoresistor - edge detection

Starting with the photoresistor, this sensor was used to detect the occurrence of a screen change more accurately. For this, after acquiring the signal (Fig. 5.16), it was necessary to detect the high slope points of the signal, which correspond to moments when a new square appeared (rising edge), or the screen went completely dark (falling edge). In this way, when the screen brightness increases, the value read by the photoresistor also increases. On the other hand, when there is no square, the screen is black, so the brightness level is very low, and consequently, the output of the voltage divider circuit is also near zero, as represented in the example in Figure 6.2. Thus, detecting the steep gradient points becomes crucial for synchronizing and labeling the data.

Firstly a moving average of a small window size (100 ms) was applied to the raw signal to remove some outliers and reduce the noise (see Algorithm 1 to follow the algorithm description). Then, two boolean variables, *last_low* and *last_high*, were defined, and two thresholds were set, one to find the rising edges (*th_rising_edge*) and the other to find the falling edge samples (*th_falling_edge*).

The variable *last_low* was initialized to True, meaning we are looking for a rising edge. In contrast, *last_high* was initialized to False. Then a loop was executed to go through all the signal samples and save the indices corresponding to the rising and falling edges. If the value of the photoresistor is greater than *th_rising_edge*, then it is a rising edge if *last_low* is true. If the value of the photoresistor is greater than *th_rising_edge*, but a *rising_edge* sample has already been found (*last_low* = False), then nothing happens. On the other hand, if the value is less than *th_falling_edge* and *last_high* = True (rising edge found, looking for a falling edge), then the sample corresponds to a falling edge. After finding the falling edge, the boolean variables are again updated to look for a rising edge and so on (*last_low*= True; *last_high*= False).

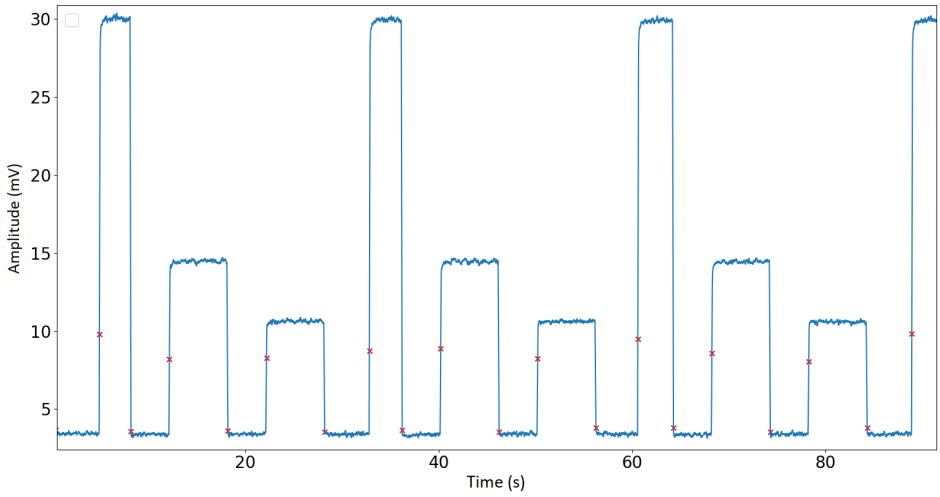


Figure 5.16: Edge detection on the photoresistor data of subject 6. The red crosses represent the edges found.

**Algorithm 1** Edge detection

```
last_low ← True
last_high ← False
while not in the end of the signal do
    if photoresistor >= th_rising_edge then                ▷ Possible rising edge
        if last_low then                                   ▷ Found rising edge
            Save sample index
            last_low ← False
            last_high ← True
        end if
    else if photoresistor <= th_falling_edge then          ▷ Possible falling edge
        if last_high then                                  ▷ Found falling edge
            Save sample index
            last_low ← True
            last_high ← False
        end if
    end if
end while
```

### 5.2.2 EMG processing

Regarding EMG, all the processing techniques were implemented with the help of BioSPPy[3], a Python toolbox for biosignal processing.

Two filters were applied to the raw EMG data: a 5th-order high-pass Butterworth filter with a cutoff frequency of 10 Hz and a notch filter with a cutoff frequency equal to 50 Hz. Figure 5.17 illustrates an EMG signal before and after filtering.

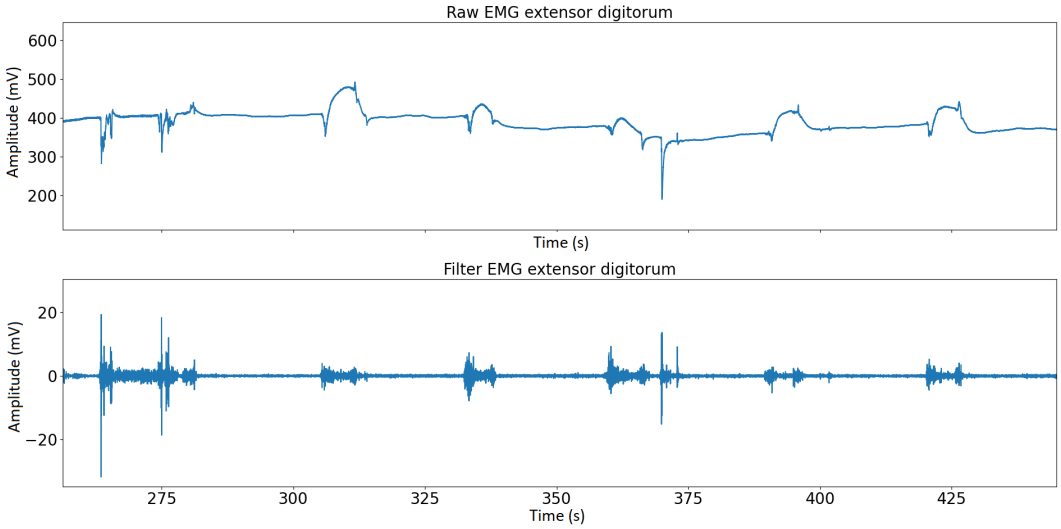


Figure 5.17: EMG filtering (Subject 2). The top graph represents the raw signal. The bottom one illustrates the EMG signal already filtered.

#### 5.2.2.1 EMG onsets detection

After filtering the signal and eliminating the noise, several implementations found in the literature were tested to find the one that provides the most accurate active segments of the EMG signal. The algorithm defined by M. Lidierth [78] presented the best results. Nevertheless, some changes were still made to improve these results even more.

Like the other state-of-the-art solutions, this algorithm (see Algorithm 2) is based on using a defined threshold to find the possible onsets. This implementation stands out from all the others because it analyzes if it is a "true" onset since a few points above the threshold may not be enough to consider that a muscle activation occurred. Thus, the implemented algorithm employs two extra variables: *minimum_state_duration* and *fail_size*. The first refers to the minimum time needed to consider an activation (true onset). The latter aims to ignore some noisy samples that may be below the threshold after the onset point. If some samples are below the threshold and if they last less than *fail_size* they are ignored. In opposition, if the EMG value is below the threshold during more than *fail_size* samples, then it is considered that the EMG activation period is over (offset).

[3] https://biosppy.readthedocs.io/en/stable/

The threshold is applied on a filtered EMG signal that passes through a full-wave rectification, followed by a moving average with a window size of 0.1 seconds. The value set for the threshold was: $\mu + 4 * \sigma$, based on Equation 3.1. Regarding the other two parameters (*minimum_state_duration* and *fail_size*), it was defined that each "true" onset point must have the next 0.4 seconds of data above the threshold, with a maximum duration of 0.2 seconds of samples below the threshold.

For defining these parameters, the values usually applied in literature were firstly tested, and based on qualitative analysis (visual analysis), the parameters were adjusted until obtaining satisfying results. Table 5.3 compiles some of the values tested for each associated parameter.

Table 5.3: Values tested to obtain the best results for EMG segments activation detection. Bold indicates the values choose for each parameter.

| **Parameter** | **Values** |
|---|---|
| Moving average window (s) | 0.005 [78]; **0.1** |
| Threshold - *h* value | 3; **4**; 5 |
| minimum_state_duration (s) | 0.3; **0.4**; 0.5; 0.6 |
| fail_size (s) | 0.02 [78]; 0.1; **0.2** |

**Algorithm 2** EMG onsets detection

```
Remove baseline offset
Perform a full-wave rectification, followed by a moving average - EMG Envelope
threshold ← μ + 4 * σ
alarm ← False
finding_onset ← True
finding_offset ← False
for sample in emg_envelope do
    if finding_offset then
        if alarm is False and sample < threshold then                ▷ Possible offset detected
            alarm ← True
            Save sample index
        else if alarm is True then
            if sample < threshold then
                state_duration ← state_duration + 1
                if state_duration == active_state_duration then      ▷ "True" offset detected
                    Add previously saved index to the offsets list
                    finding_onset ← True                             ▷ Search now for an onset
                    finding_offset ← False
                    alarm ← False
                    state_duration ← 0
                end if
            else if number of samples above the threshold > fail_size then
                alarm ← False                                        ▷ Ignore false offsets
                state_duration ← 0
            end if
        end if
    else if finding_onset then
        if alarm is False and sample >= threshold then               ▷ Possible onset detected
            alarm ← True
            Save sample index
        else if alarm is True then
            if sample >= threshold then
                state_duration ← state_duration + 1
                if state_duration == active_state_duration then      ▷ "True" onset detected
                    Add previously saved index to the "true" onsets list
                    finding_offset ← True                            ▷ Search now for an offset
                    finding_onset ← False
                    alarm ← False
                    state_duration ← 0
                end if
            else if number of samples below the threshold > fail_size then
                alarm ← False                                        ▷ Ignore false onsets
                state_duration ← 0
            end if
        end if
    end if
end for
```

- **EMG activation of each execution trial**

As described in Subsection 5.1.2, each trial contains a "Movement Execution" screen. As such, it is important to know if the movement was actually performed or not and, if so when it began and how much time it took. In a valid situation, the EMG onset corresponding to the "Movement Execution" screen and obtained with the photoresistor edge detection algorithm (Subsection 5.2.1) is near the beginning of that screen. The EMG onset closest to the beginning of the "Movement Execution" screen should be within the runtime, not later than the end of the execution screen, and not much earlier than the start of the screen (lower than 2 seconds). The trial is ignored if no EMG onset accomplishes these conditions (wrong labeling). Otherwise, the EMG onset will be used to extract the epochs to analyze the EEG data.

### 5.2.3 ECG processing

The ECG was only acquired to remove some cardiac artifacts that may appear on the EEG signal. The processing applied to the raw ECG signal was very simple and consisted of a notch filter of 50 Hz followed by a band-pass filter from 5 to 50 Hz. It was automatically performed using the BioSPPy library.

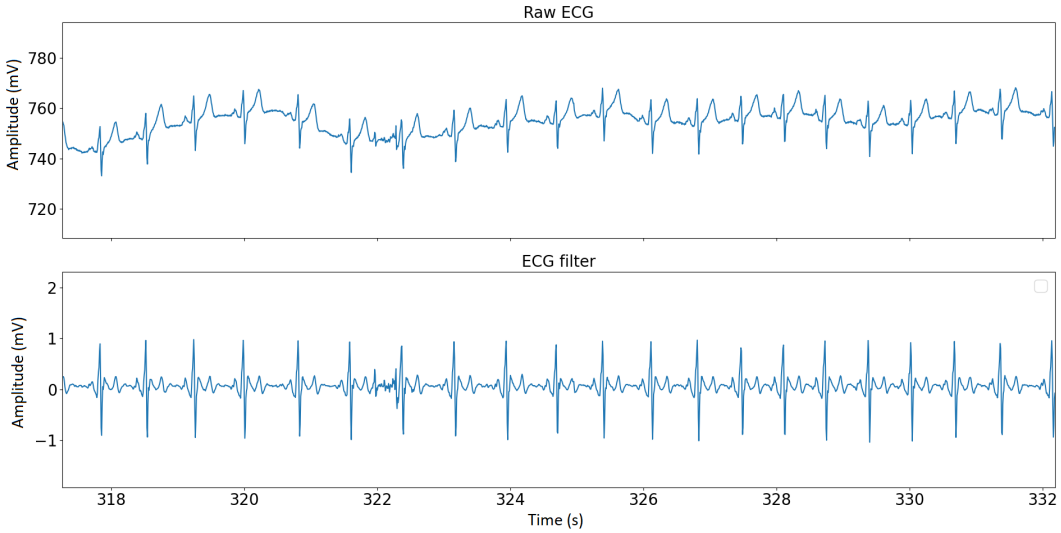


Figure 5.18: ECG filtering (Subject 7). The top graph represents the raw signal. The bottom one illustrates the filtered signal.

### 5.2.4 EEG processing

The EEG processing was performed with the help of some functions from the MNE library[4].

The first step involved applying a notch filter followed by a fourth-order Butterworth band-pass filter with cut-off frequencies of 7 and 30 Hz (mu and beta bands). Then, based on what was

[4] https://mne.tools/stable/index.html

found in the state-of-the-art analysis (Subsection 3.2.2.2), the ICA technique was employed to find the ocular and cardiac artifacts components. For this, the FP1, FP2, and ECG channels were used as a "pattern" to check the ICA components (ICs) with higher scores (higher similarity). The number of components was manually set to 7. The ICA components to be removed were those in which the score (similarity to FP1, FP2, and ECG signals) was higher than 75 %. Subsequently, the remaining ICs were projected back into the scalp channel space to be reconstructed as the corrected EEG data.

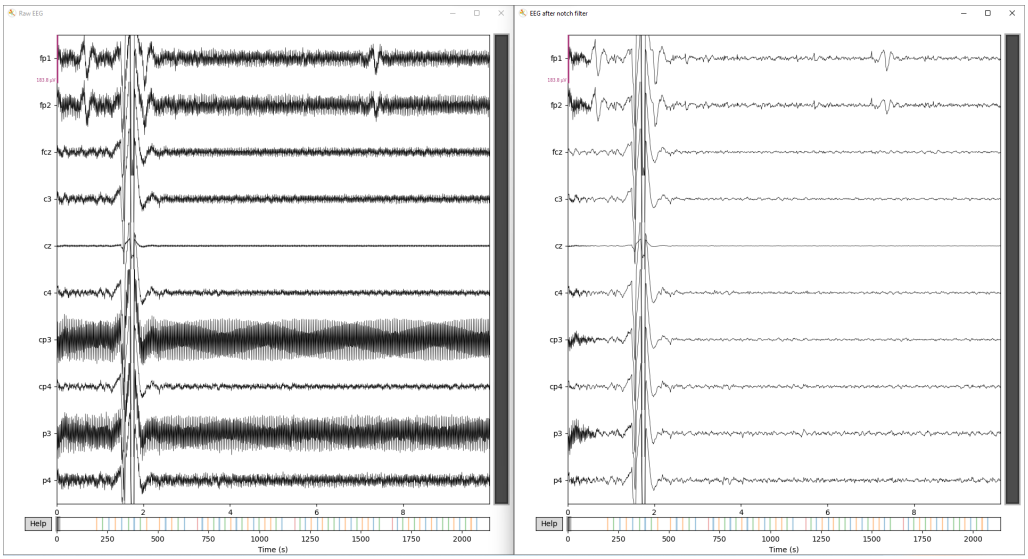


(a) Left: raw EEG; Right: EEG signals after applying a 50 Hz notch filter

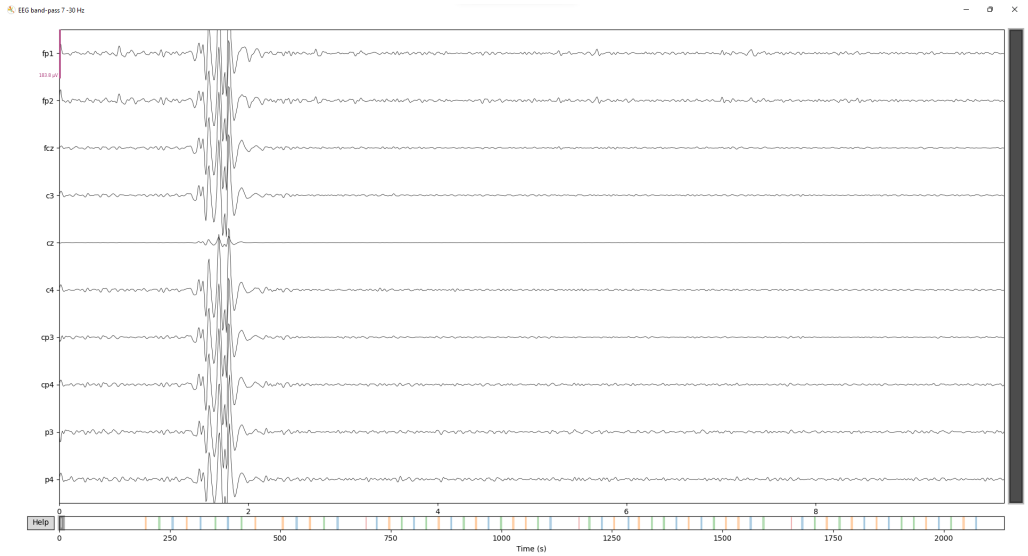


(b) EEG signal after applying the band-pass filter (7-30 Hz).

Figure 5.19: EEG pre-processing subject 6. The plots were generated using the *plot()* method from the MNE library. Each signal represents an EEG channel, the first two rows correspond to the FP1 and FP2 channels.

### 5.2.5 iHandU processing

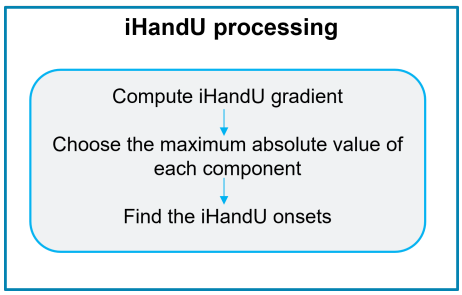


Figure 5.20: iHandU processing pipeline.

Regarding the iHandU, this device was employed to analyze the possibility of detecting the beginning and end of each movement execution with inertial signals. Furthermore, by functioning as a simple wristband and being much more practical than the placement of EMG electrodes, it may replace the use of muscle signals (EMG).

In this way, the iHandU accelerometer data was processed to detect the temporal segments in which the participant was moving his wrist. Essentially, six operations were performed:

- First, in order to highlight the points of most significant muscle activity, the gradient of each accelerometer component (x, y, and z) was computed using the Numpy library[5]. This function implements the gradient following a second-order accurate central differences approach;
- Then, the peaks present in each gradient signal were detected;
- Afterwards, the three gradient signals were merged into one, considering at each moment the component with the highest absolute value;
- Then, the gradient signal obtained in step 3 was filtered through a moving average filter with a 100 ms window size;
- Next, it was performed a search for the peak associated with the first iHandU touch (regarding the three touches sequence) using the gradient signal;
- Finally, the onsets and offsets in the gradient signal were detected, using the same approach applied in the EMG data (Algorithm 2).

Figure 5.21 represents the gradients results, and then Figure 5.22 represents the movements onsets.

[5] https://numpy.org/doc/stable/reference/generated/numpy.gradient.html

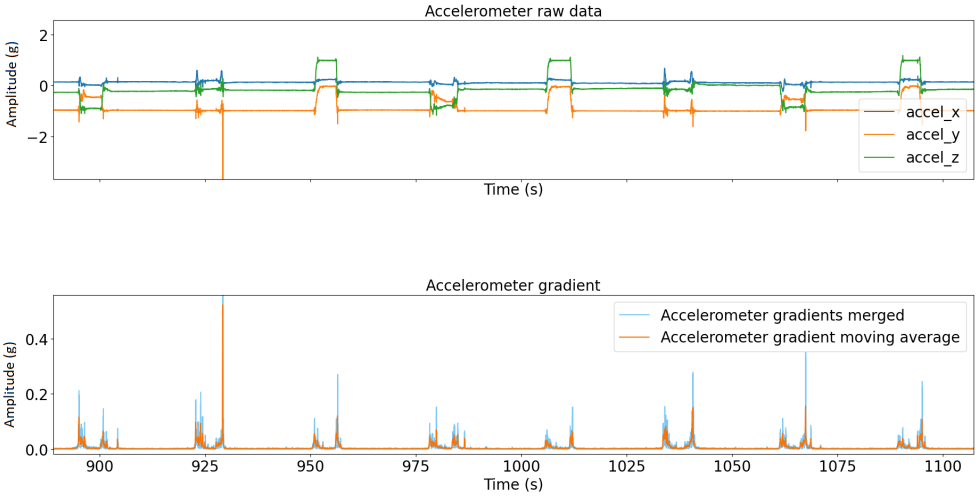


Figure 5.21: iHandU processing (subject 7). The top graph represents the three accelerometer axis. The bottom graph represents the result of the merged gradients and the moving average.

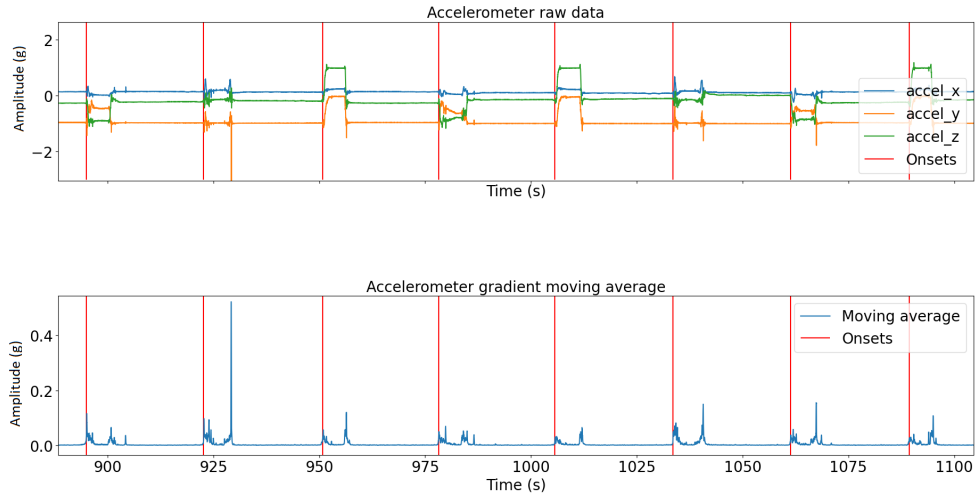


Figure 5.22: HandU onsets (subject 7).

## 5.3 Synchronization

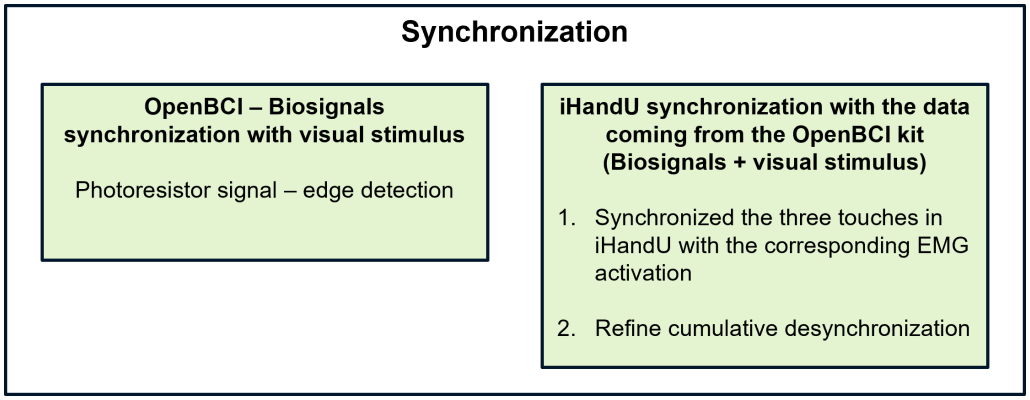


Figure 5.23: Synchronization pipeline

The synchronization between all the devices was a critical step to ensure an accurate segmentation and labeling of data. Therefore, the data from the iHandU, the openBCI system, and the protocol must be synchronized. Two strategies were tried to accomplish this inter-devices synchronization:

The first approach was to synchronize the iHandU and OpenBCI data by the timestamp of each sample. Using this method, it was only necessary to record the time instant when each screen appeared. However, there was some delay between sending a command to refresh the screen and the time instant in which the screen actually refreshes, due to, for example, the monitor's refresh rate. So it was decided to use an analog sensor to determine when the screen content changes.

After some research, it was found that a light sensor (photoresistor) is widely used to synchronize the OpenBCI data (ECG, EEG, and EMG) with the visual stimulus. In addition, since the photoresistor data read on the OpenBCI device is automatically synchronized with the biosignals, and considering that the light sensor registers the screen changes, then, consequently, the biosignals are automatically synchronized with the visual stimulus. So, all that remains is ensuring that the iHandU data is synchronized with the OpenBCI sensors.

In order to synchronize the iHandU data with the information acquired with the openBCI board, an extra screen was added to the protocol (iHandU screen). In the first phase of the acquisitions, the iHandU screen was only presented at the beginning of each session. In contrast, in the second phase of acquisitions, the iHandU screen was added at the beginning of each run. This screen asks the participant to touch three consecutive times on the device, thus causing a sudden change in the accelerometer. Finding these peaks and knowing the moment the screen appeared (recorded on the photoresistor) makes it possible to find the shift and synchronize all the data.

The iHandU-OpenBCI synchronization was performed in two steps: the first estimates a rough synchronization between the two devices. The second step aims to refine the synchronization obtained in the first step, seeking better results.

The first iHandU-OpenBCI synchronization calculates the deviation between the peak of the first iHandU touch and the beginning of the EMG closest to the edge of the photoresistor associated

with the iHandU display. At the end of this step, an approximate synchronization between the signals of the iHandU and the openBCI data was obtained.

The second step aims to tune the synchronization obtained in the previous step by estimating the line equation that relates the difference between each iHandU and EMG onset with the temporal index. In other words, it tries to estimate the time difference between each pair of iHandU and EMG onsets and use that information to correct the iHandU signals, making them coincide as well as possible with those from the EMG. This synchronization refinement step was necessary because it was found that although the signal was synchronized at the beginning, after some time, there was a considerable delay in the iHandU onsets relative to the EMG onsets, and this delay increased with time. Thus, to obtain the line equation mentioned above, the RANSAC algorithm [79] was employed. This implementation obtains more robust results than, for example, a linear regression since it eliminates the outliers before searching for the line that best fits the points, as presented in Figure 5.24. As it can be seen, over time, the iHandU gets further away from the corresponding onset EMG.

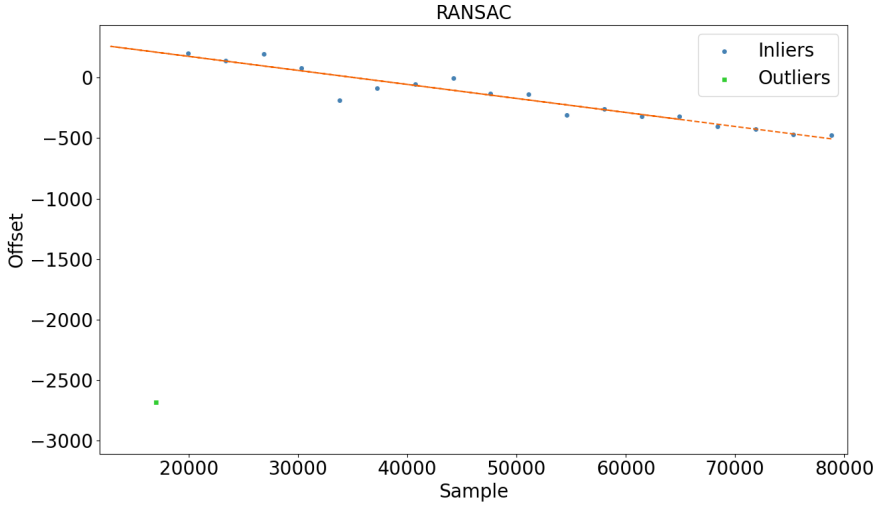


Figure 5.24: Ransac representation. The offset represents the distance between the iHandU onset sample and the correspondent EMG onset. The x-axis represents the sample index of the EMG onset. The blue points are the inliers (points used for line estimation), and the green points represent the outliers (points with abnormal distance from other values).

## 5.4 Event-Related Desynchronization/Synchronization

After processing the EEG, the conditions for analyzing the brain activity during the execution of the movement are gathered. Thus, the time-frequency representation was performed to analyze the ERD/ERS.

Figure 5.25 shows the main steps performed to computed the ERD/ERS. The time-frequency representation was applied to a time interval of -3 to 3 seconds from the movement onset.

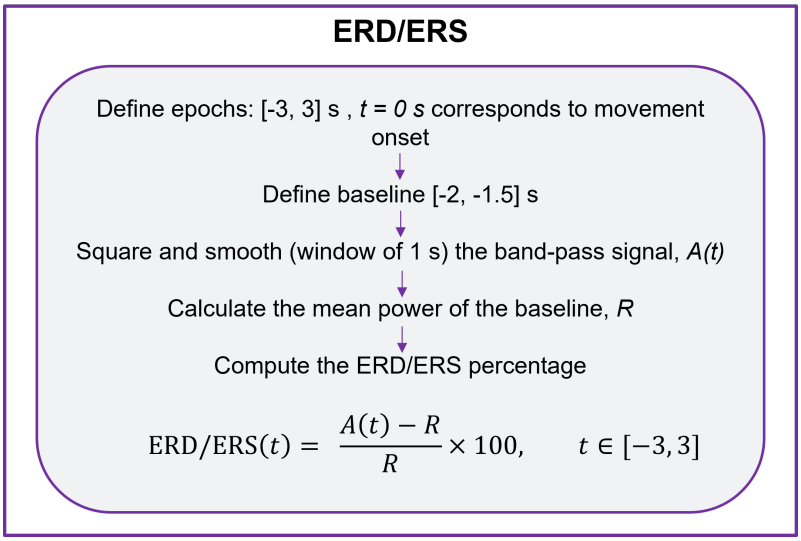


Figure 5.25: ERD/ERS methodology

After observing the results, the line plot average of ERD/ERS was computed for each subject, based on Equation 5.1. Here, A represents the power within the frequency band of interest at the instant t, and R is the mean power in the same band over a reference time interval, called the baseline. This baseline was defined as [-2, -1.5] seconds [80].

The frequency bands of interest analyzed were the $\mu$ band, 10-12 Hz, and the $\beta$ band, 18-23 Hz, since these bands were proved to be related to human movement intention [81]. Furthermore, according to the literature, it is expected to find a desynchronization (negative values) on both bands before and during the movement execution.

$$ERD/ERS(t) = \frac{A(t) - R}{R} \times 100,\ t \in [-3, 3] \tag{5.1}$$

Figure 5.26 shows an example of ERD/ERS maps that should be generated. For example, in Gudino et al. and Lopéz-Larraz et al.'s work, they performed the ERD/ERS maps in percentage (see Fig. 5.26a). The horizontal axis represents time (units of s), while the vertical axis represents frequency (units of Hz). The solid black line represents $t$=0 s or the movement onset. The blue color means desynchronization, and red means synchronization. Figure 5.26a shows a significant desynchronization ($p < 0.05$) in the motor-related $\alpha$ [8, 12] Hz and $\beta$ [14, 30] Hz frequency bands from t $\approx$ -0.5 s.

Regarding the ERD/ERS map generated using the MNE tools (see Fig. 5.26b), the output is slightly different. They mapped the ERD to red color and ERS to blue color, and they showed the map in relative values, but besides that, the logic of analyzing the map is the same.

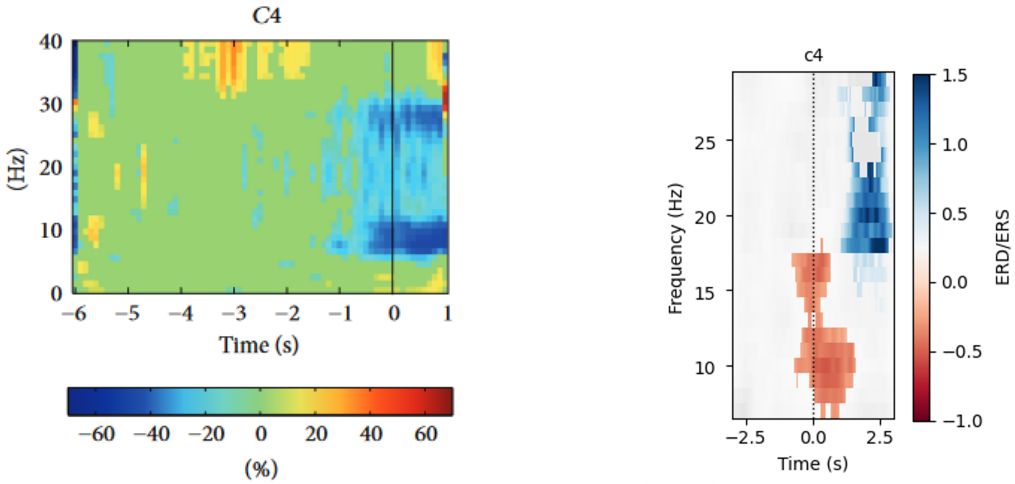


(a) ERD/ERS map from Gudino et al. [34].

(b) ERD/ERS map generated using the MNE tools[6]

Figure 5.26: ERD/ERS maps examples.

[6] https://mne.tools/dev/auto_examples/time_frequency/time_frequency_erds.html

# Chapter 6

# Results and discussion

This chapter aims to discuss the results that were obtained throughout this dissertation work.

## 6.1 Collected Dataset and its Open Access publication

From the experiment protocol, a dataset called PhysioIntent was created and published (https://doi.org/10.25747/6101-JD30) in open acess.

PhysioIntent comprises several types of data: the EEG, EMG, and ECG acquired from the openBCI Cyton board; the inertial data (9-axis) recorded on the iHandU (proprietary device from INESC TEC); and video acquired from the Logitech C270 HD camera.

The dataset is divided into two phases. The 2nd phase was performed to improve some setbacks encountered in the 1st phase, such as data loss and synchronization issues. The 1st phase study included six healthy volunteers (range of age = 22 to 25; average age = 22.3±0.9; two males and four females; all right-handed). In the 2nd phase, the study included three healthy volunteers (range of age = 20 to 26; average age = 22.6±2.5; two males and one female; all right-handed).

In phase 1, 4 different muscles EMG were measured: *bicep brachii, tricep brachii, flexor carpi radialis,* and *extensor digitorum*. For the EEG, the measured channels were: FP1, FP2, FCZ, C3, CZ, C4, CP3, CP4, P3, and P4. During phase 2, only one muscle EMG, the *extensor digitorum*, was measured. For the EEG, the channels measured were: FP1, FP2, FC3, FCz, FC4, C1, C3, Cz, C2, C4, CP3, CP4, P3, and P4.

In the end, all dataset comprises 7.41 Gigabytes of data, registered during 6 hours and 33 minutes (see Table 6.1). Besides the time spent during the protocol, it took about 45 minutes to set up all the devices and prepare each acquisition.

Table 6.1: Specifications of the dataset.

| Specification | Value |
|---|---|
| **Memory** | 7.41 Gb |
| **Participants** | 9 |
| **Age (years)** | 22.4 ± 1.64 |
| **Gender** | 5 females; 4 males |
| **Duration** | 6 h 33 min |
| **Type of data** | .csv; .mp4 |
| **Instruments** | iHandU; OpenBCI; EEG cap 64 channels; Webcam |

### 6.1.1 Data Format and Structure

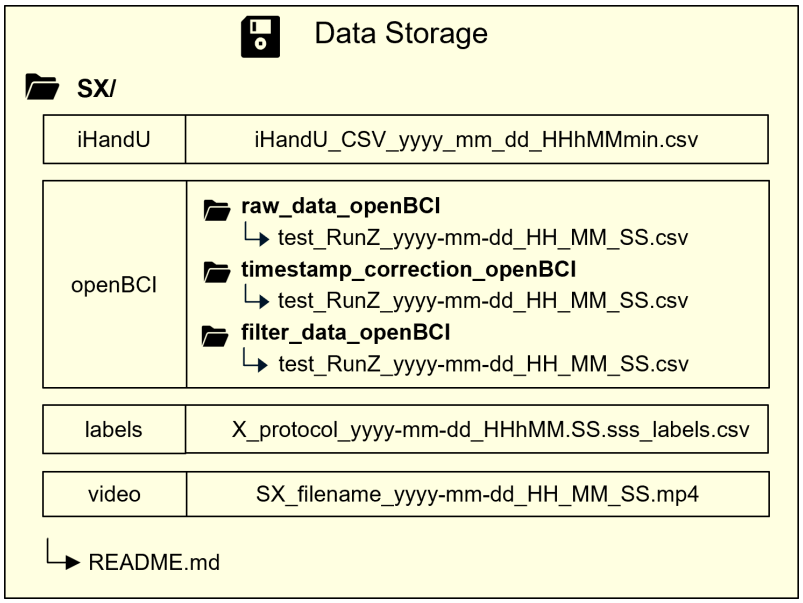


Figure 6.1: Data storage info

Each subject's data is stored in the folder *SX/*, where the X corresponds to the subject's id. For each folder, there are 4 subfolders: openBCI; iHandU; labels; and video, as presented in Figure 6.1.

Regarding the openBCI folder, there is a *raw_data_openBCI/* subfolder with the raw data of the biosignals. After obtaining the raw data, several samples were recorded with the same timestamp, so knowing the sample rate, 125 Hz, a correction was made to it, taking into account the timestamp of the initial sample (*timestamp_correction_openBCI/* folder). This was done in case users wanted to analyze and synchronize the data by timestamp.

In addition, the biosignal were preprocessed (folder *filter_data_openBCI/*). A 50 Hz notch filter was applied to remove the power line noise. Besides that, a high-pass fourth-order Butterworth

with a 10 Hz cutoff frequency was also applied to the EMG. To the ECG, a band-pass of order 0.3* *sample_rate* between 5 and 50 Hz was implemented. As for the EEG, a high-pass fourth-order Butterworth with a 0.5 Hz cutoff frequency was applied to correct the baseline.

So, within each of the 3 folders (*raw_data_openBCI/*, *timestamp_correction_openBCI/* and *filter_data_openBCI/*) there is a .csv file corresponding to the openBCI data for each Run. However, subjects who perform phase 2 of acquisitions (subjects 7, 8, and 9) have one .csv file with the raw data in *raw_data_openBCI/* folder. But in *filter_data_openBCI/* and *timestamp_correction_openBCI/* folder the data is separated by runs (one .csv file for each run).

In addition to these three subfolders related to the openBCI data, the other three folders (iHandU; labels, and video) contain the following files:

- ***labels/***: The labels file (.csv). This file contains information related to the trials, such as what stimulus was presented to the participant and in what order. -> **X_protocol_yyyy-mm-dd_HHhMM.SS.sss_labels.csv**
- ***iHandU/***: The IMU data (.csv) -> **iHandU_CSV_yyyy_mm_dd_HHhMMmin.csv**
- ***video/***: The video file (.mp4) -> S**X_filename_yyyy-mm-dd_HH_MM_SS.mp4**

### 6.1.2 Dataset open access publication

The dataset was published with open access to the whole community. Before the experiments, the participants were informed about the experimental protocols, paradigms, and purpose. After ensuring they understood the information, the participants signed a written consent following the GDPR compliance, approved by the DPO (Data Protection Officer) from INESC TEC.

The consent form contains a general description of the work and its goals. Then it has a section called "Handling of personal data", which focuses on explaining the perils and benefits of acquiring each type of data and details how the subject's data can be used. An example of written consent and the DPO approved is presented in Appendix B.

## 6.2 Synchronization and Labeling

After acquiring the data, two crucial steps to achieve the goal of predicting the human movement intention are to ensure a correct synchronization between the data from all the sensors and to label all the data. This last step aims to tag each executed movement and separate the imagery movement data from the movement execution data or rest data, thus enabling further training for these trials, using machine learning, for example.

### 6.2.1 Synchronization

Regarding the data synchronization, Section 5.3 describes the implementation's main steps for both acquisition phases (phase 1 and 2). The first approach was to sync all the data with the respective timestamp. However, the timestamp record did not equally distribute the samples as it

should. This happens because the samples are only read by the computer when it has some free time to do it, meaning that they are not read at the exact moment they are sampled.

The solution found was to readjust the timestamps. The time between each sample can be adjusted by knowing the sample rate of each device (125 Hz- openBCI; 50 Hz- iHandU). So, taking the first timestamp record, the timestamp of the remaining data will sum up to the period of each sample (8 ms - openBCI; 20 ms - iHandU). After making the timestamp correction, the iHandU and OpenBCI samples with the timestamp closest to the beginning of the protocol can be retrieved from the .csv file generated during the execution of the protocol. These two samples correspond to the beginning of the data stream of each device.

However, after further analysis, it was found that this approach would not be the most appropriate since there is always some delay between the generation of the stimulus and the actual presentation on the screen, decreasing the accuracy of the data segmentation.

For this reason, an external sensor (photoresistor) was used to determine the exact timestamp for each screen presentation. This sensor connects to the Cyton board, as explained in Section 5.3, allowing a more accurate synchronization between the biosignals and the protocol.

Figure 6.2 shows an example of the analog signal record from the beginning of the experiment until the end of the first run.

During the execution of the protocol, a square is displayed in the bottom left corner with different intensities. In this way, the photoresistor can register these differences and thus identify when a screen is displayed (see Fig. 6.2). Hence when the experiment starts, a white square is shown on the screen's lower left corner (below the photoresistor) leading to a rising edge on the photoresistor signal; this sample index will be the start of the session. After that, the delay between the record begin timestamp (registered on .csv file) and the actual begin (register in photoresistor signal) was approximately 600 ms. This significant difference may be due to computer's operating system internal processing delays. These results reveal the importance of using the analog sensor. Hence it was proved that the time register with the operating system timestamp was not precisely the time that the screen showed up.

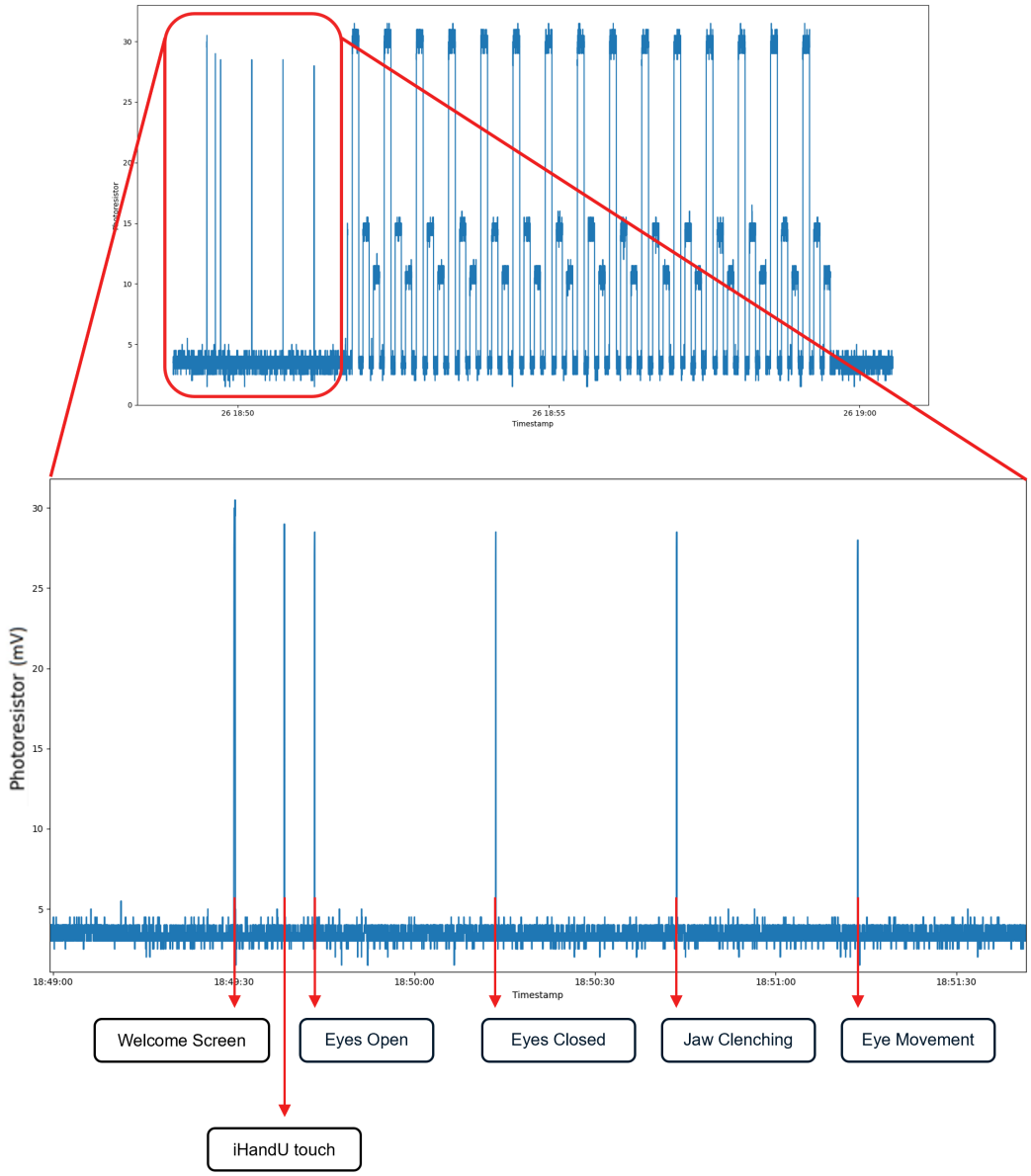


Figure 6.2: Example of photoresistor signal, Run 1, subject 6. Each peak represents the beginning of a screen.

When a trial is executed, it is essential to know when the Visual Cue, "Movement Imagery", and "Real Movement" screens are active. To distinguish between those three screens, a square with different grey levels is presented: white while the Visual Cue screen is on; light grey for "Movement Imagery", and dark grey for "Real Movement", resulting in a signal similar to the one presented in Figure 5.14.

To sum up, analyzing the results presented above, the use of a photoresistor allows the biosignals and the visual stimulus to be synchronized automatically.

However, upon further analysis, it was found that some recordings were missing data from the photoresistor, as depicted in Figure 6.3. As shown in the example, the duration of the visual cue

screen in the signal is shorter than what is shown in the video (true). One of the reasons may be that the computer's processing capacity is not high enough to perform several tasks simultaneously, and therefore data loss occurs. This problem was solved in the phase 2 of the acquisitions when two computers were used instead of one, allowing the distribution of tasks.

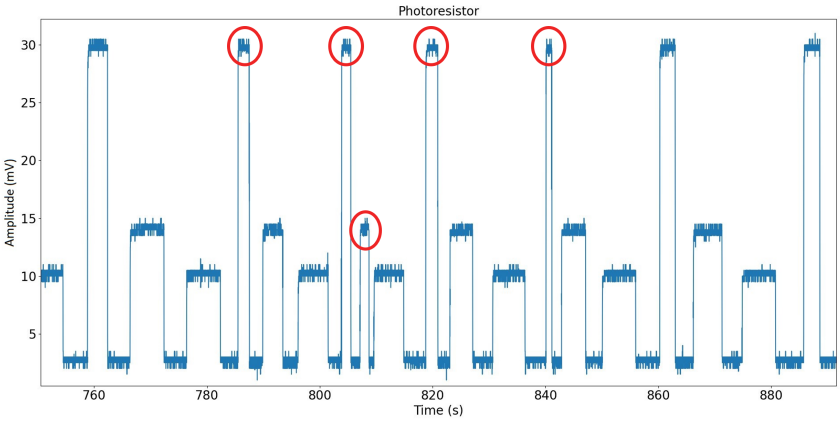


Figure 6.3: Photoresistor reading wrong (subject 2). It can be seen that the Visual Cue screen does not take the same time for all trials.

#### 6.2.1.1 iHandU synchronization

Regarding the iHandU synchronization, as detailed in Section 5.3, an iHandU sync maneuver screen was added at the beginning of the session, leading to a sudden change in the accelerometer, as shown in Figure 6.4.

(a) Example of subject touching on iHandU device.

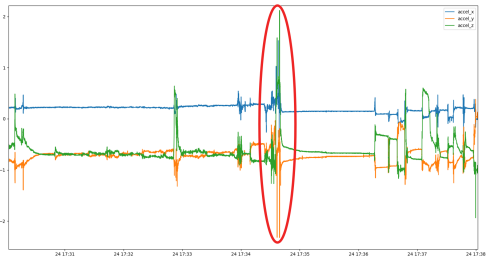

(b) Subject 2

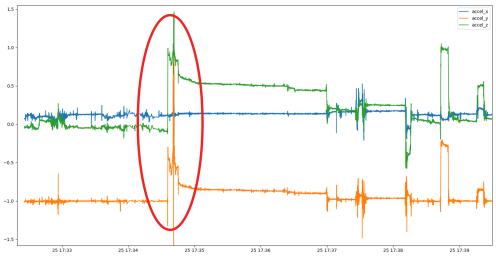

(c) Subject 4

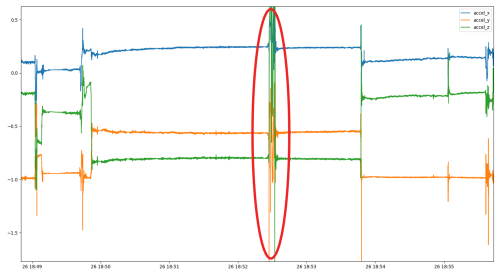

(d) Subject 6

Figure 6.4: (a): iHandU sync maneuver; (b), (c), (d): iHandU accelerometer data. The blue line represents the x-axis, the orange represents the y-axis, and the green the z-axis. The horizontal axis of the graphics represents the timestamp of each sample.

Before applying any algorithm, the iHandU data was upsampled to 125 Hz (to match the sample rate of openBCI board) using the Fast Fourier Transform (FFT). The desired length was calculate based Equation 6.1.

$$desired_length = \frac{signal_length * desired_sample_rate}{sample_rate} \tag{6.1}$$

Having all the data at the same frequency, the next step was calculating the shift between the devices and then cropping the unnecessary iHandU data, as shown in Figure 6.5.

The shift calculated is defined as the difference between the *iHandU_touch_sample* and the *iHandU_touch_sample_emg*. The *iHandU_touch_sample* will correspond to the peak found on accelerometer data related to the abrupt change in acceleration. The *iHandU_touch_sample_emg* will be the EMG onset closest to the beginning of the iHandU screen. The moment when the iHandU screen appears is recorded on the photoresistor signal and will correspond to the third index (second screen) of the edges found through the edge detection algorithm 1, as presented in Figure 6.5. It is more accurate to use the EMG onset near the iHandU screen than the index of the start of the screen since it takes some time from the beginning of the screen to the execution of the touch (information reading time + execution time).

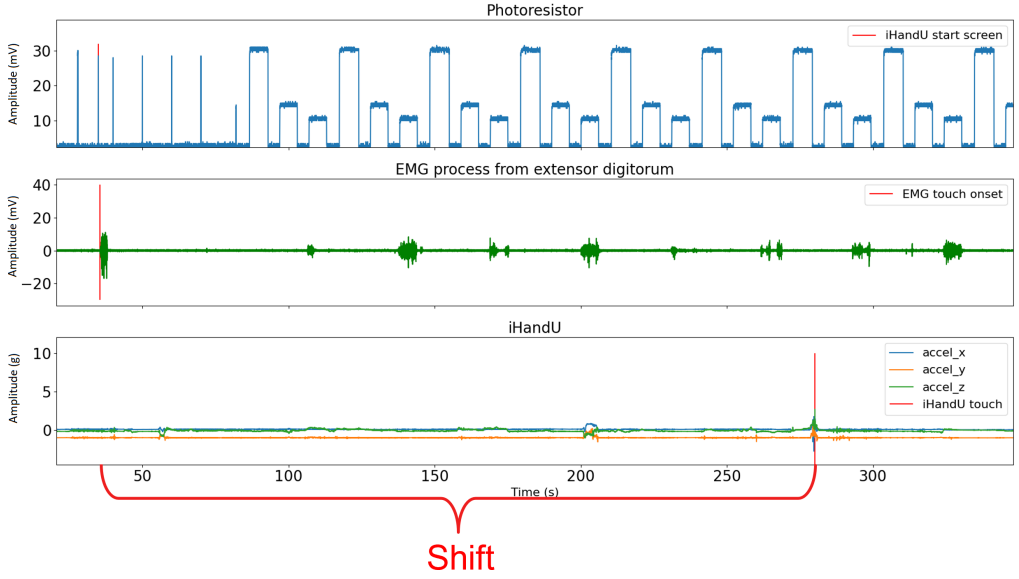


(a)

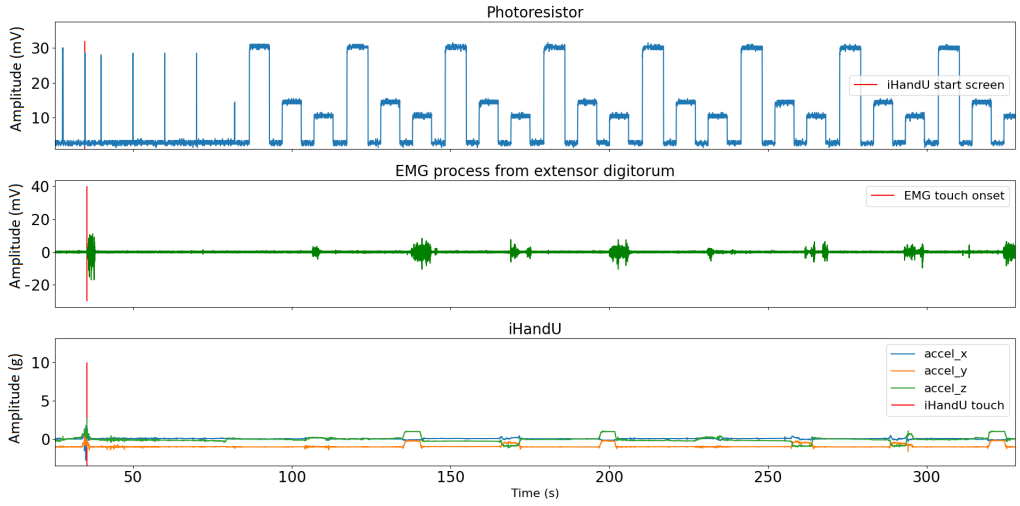


(b)

Figure 6.5: Synchronization subject 3. Shift represented in red means the difference in time that the iHandU sync maneuver is way from the correspondent EMG onset.

- **Cumulative desynchronization of iHandU data**

After making the correction based on shift, it was verified a cumulative desynchronization of iHandU data with EMG (see Fig. 6.6). One of the reasons this happens may be related to the internal error associated with the sample rate that is never precisely the value defined in the datasheet device, in this case, 50 Hz. Thus, it was necessary to perform a readjustment as described in Section 5.3.

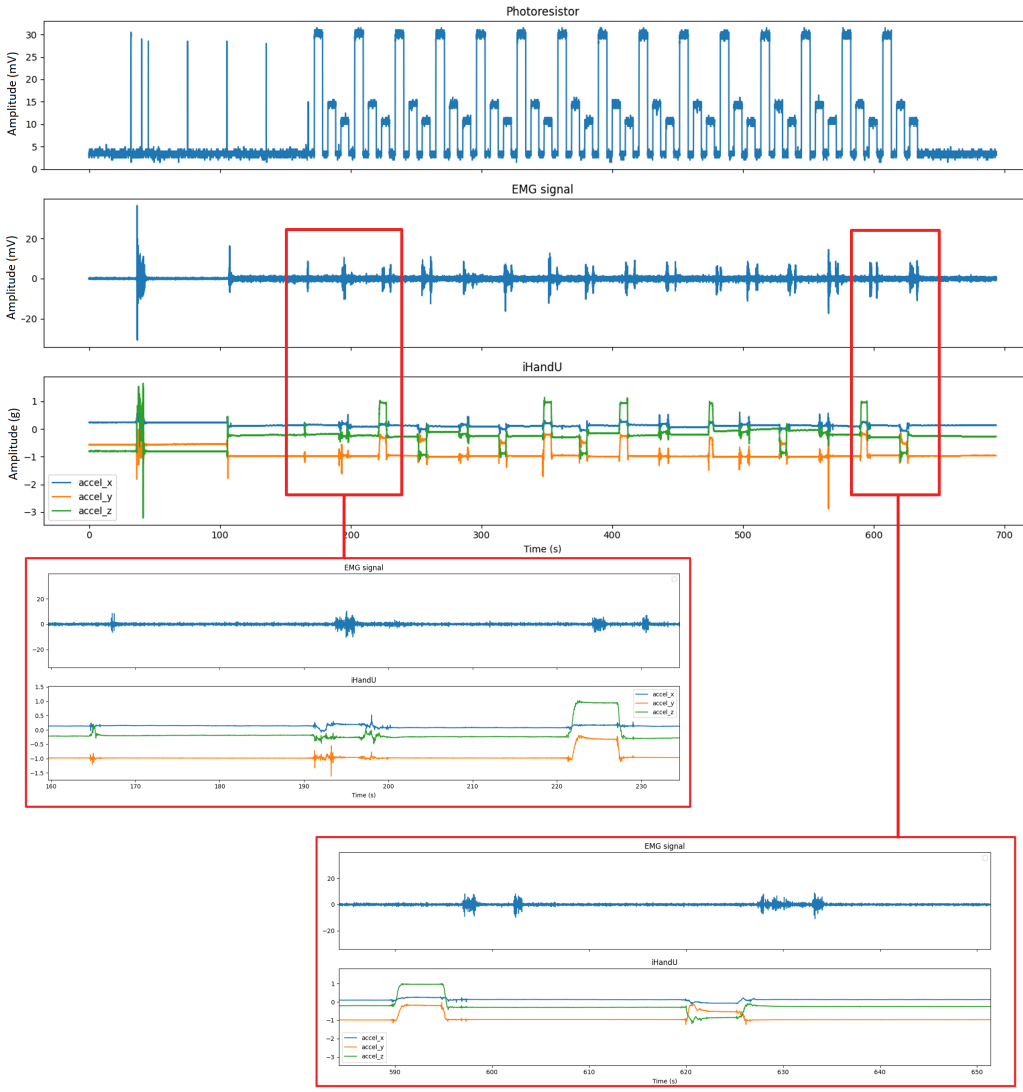


Figure 6.6: iHandU cumulative delay regarding openBCI data (subject 6).

After synchronizing the data, it was verified that some iHandU data was missing (see Fig. 6.7), the reason why the second acquisition phase was performed.

Since no method has been developed to communicate with iHandU, only the API already developed by researchers was used. Thus, there is a lack of information on how the data is being saved.

This problem has never been encountered before in this system. One of the reasons may be that so far, it has never been tested in long acquisitions with several processes running simultaneously on the same device, as was the case with the phase 1 acquisitions. Thus, after some studies, it was found that there is no data loss on systems with higher processing power, as on the computer with AMD Ryzen 7 3700X 8-Core Processor.

In order to solve this problem, the data recording was split into two computers (see Fig. 5.8)

corresponding to phase 2 of acquisitions. Figure 6.8 show the iHandU data from subject 7 (phase 2), as all the iHandU data is present.

In the future, a more straightforward communication with iHandU could be developed in a lower-level language (like C++), avoiding, for example, displaying data graphs.

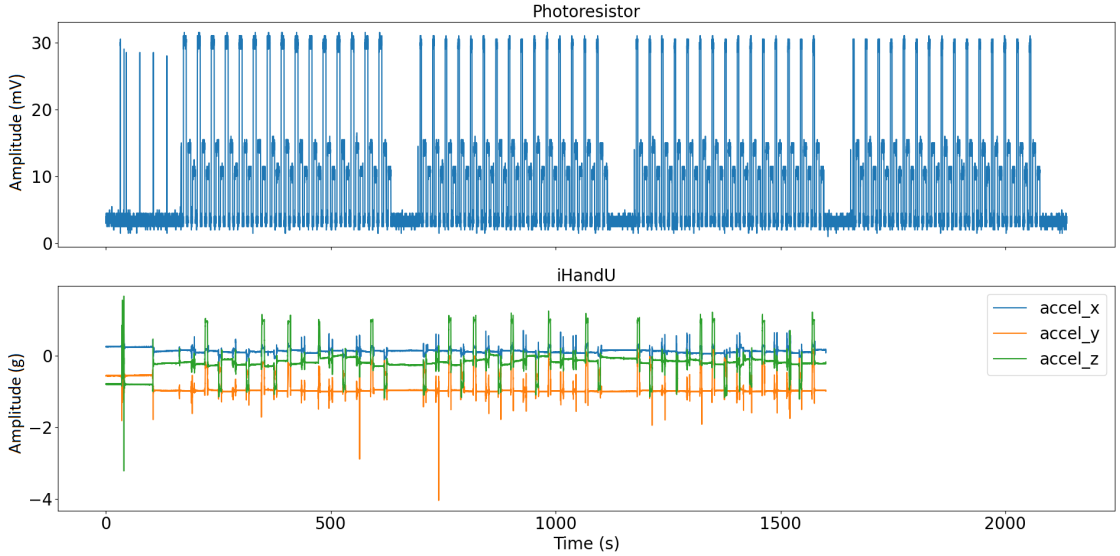


Figure 6.7: Missing iHandU data (subject 6).

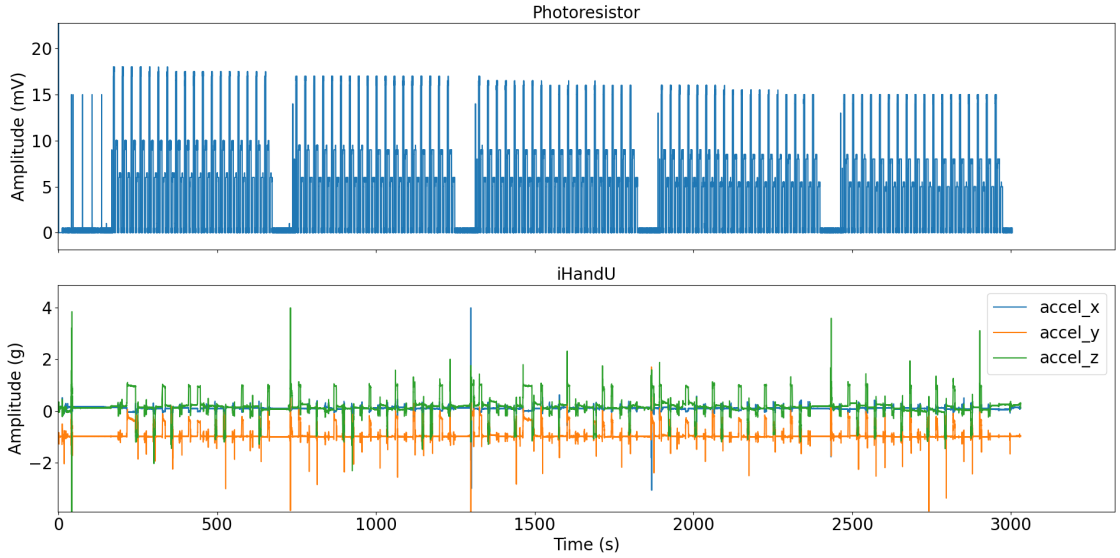


Figure 6.8: iHandU data for all runs (subject 7).

### 6.2.2 Labeling

Furthermore, it is important to know which movement the participant needs to imagine and execute. For this, complementary to the photoresistor information, during the execution of the

protocol, a .csv file is recorded. This file registers the beginning of each screen, the corresponding timestamp, and, on the visual cue screen, records the name of the file/movement shown to the subject. Figure 6.9 exemplifies how the file is structure.

Thus, by applying the edge detection algorithm (Algorithm 1) to the photoresistor signal, it is possible to know the exact beginning and end of each screen, and with the .csv file, we can know what was the movement performed in each trial and label it according to Table 6.2.

With these complementary pieces (photoresistor + labels .csv file) a new .csv (see Fig. 6.10) is generated for each subject containing the *indexes* column which represents the start and end of imagery screen (*label_index* = 1) or movement screen (*label_index* = 2). The *movement_label_index* column contains the labels of each movement according to Table 6.2.

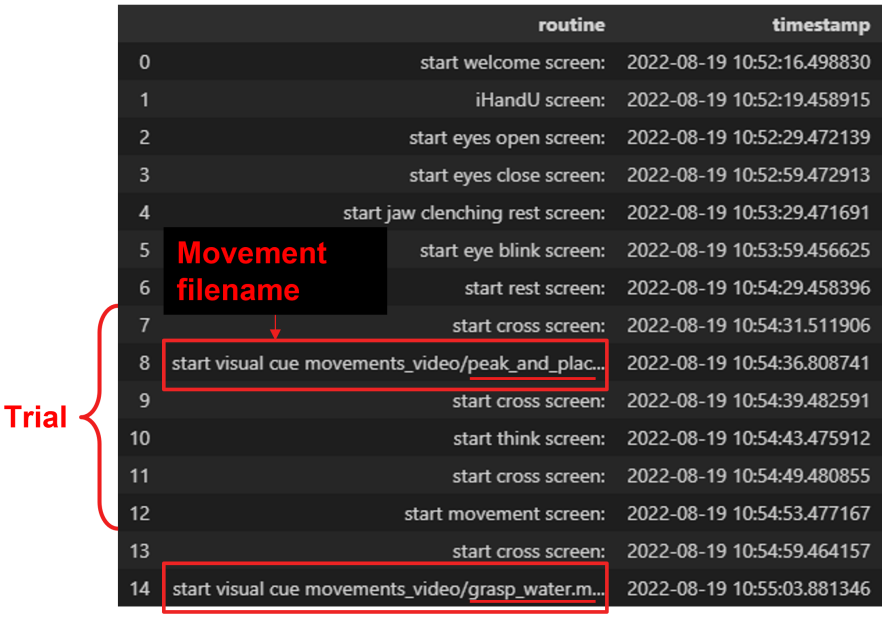


| | routine | timestamp |
|---|---|---|
| 0 | start welcome screen: | 2022-08-19 10:52:16.498830 |
| 1 | iHandU screen: | 2022-08-19 10:52:19.458915 |
| 2 | start eyes open screen: | 2022-08-19 10:52:29.472139 |
| 3 | start eyes close screen: | 2022-08-19 10:52:59.472913 |
| 4 | start jaw clenching rest screen: | 2022-08-19 10:53:29.471691 |
| 5 | start eye blink screen: | 2022-08-19 10:53:59.456625 |
| 6 | start rest screen: | 2022-08-19 10:54:29.458396 |
| 7 | start cross screen: | 2022-08-19 10:54:31.511906 |
| 8 | start visual cue movements_video/peak_and_plac... | 2022-08-19 10:54:36.808741 |
| 9 | start cross screen: | 2022-08-19 10:54:39.482591 |
| 10 | start think screen: | 2022-08-19 10:54:43.475912 |
| 11 | start cross screen: | 2022-08-19 10:54:49.480855 |
| 12 | start movement screen: | 2022-08-19 10:54:53.477167 |
| 13 | start cross screen: | 2022-08-19 10:54:59.464157 |
| 14 | start visual cue movements_video/grasp_water.m... | 2022-08-19 10:55:03.881346 |

Figure 6.9: File example of the .csv output generated during protocol acquisition.

Table 6.2: Label for each movement

| Movement | Label |
|---|---|
| **Pick and place** | 1 |
| **Grasp water** | 2 |
| **Supination** | 3 |

| index | run | indexes | label_index | movement_label_index |
|---|---|---|---|---|
| 0 | 1 | [22505, 23259] | 1 | 2 |
| 1 | 1 | [23761, 24510] | 2 | 2 |
| 2 | 1 | [26012, 26766] | 1 | 3 |
| 3 | 1 | [27268, 28017] | 2 | 3 |
| 4 | 1 | [29517, 30271] | 1 | 1 |
| 5 | 1 | [30773, 31522] | 2 | 1 |
| 6 | 1 | [33026, 33778] | 1 | 2 |
| 7 | 1 | [34278, 35029] | 2 | 2 |
| 8 | 1 | [36529, 37285] | 1 | 1 |
| 9 | 1 | [37785, 38536] | 2 | 1 |
| 10 | 1 | [40036, 40791] | 1 | 3 |

Figure 6.10: File example of the .csv created with the segmentation indexes of each screen.

## 6.3 Movements onsets

As said in the previous chapter, the movement's activation can be detected through the EMG signal or by analyzing the acceleration from the IMU.

Regarding EMG onset, for phase 1, using the *Extensor Digitorum* was enough to detect muscle activity. This was the main reason the number of muscles chosen to be used in phase 2 was reduced to just this muscle. Figure 6.11 shows an example of EMG-based onsets and offsets detection. It can be seen that the algorithm is robust, being able to discard false onsets.

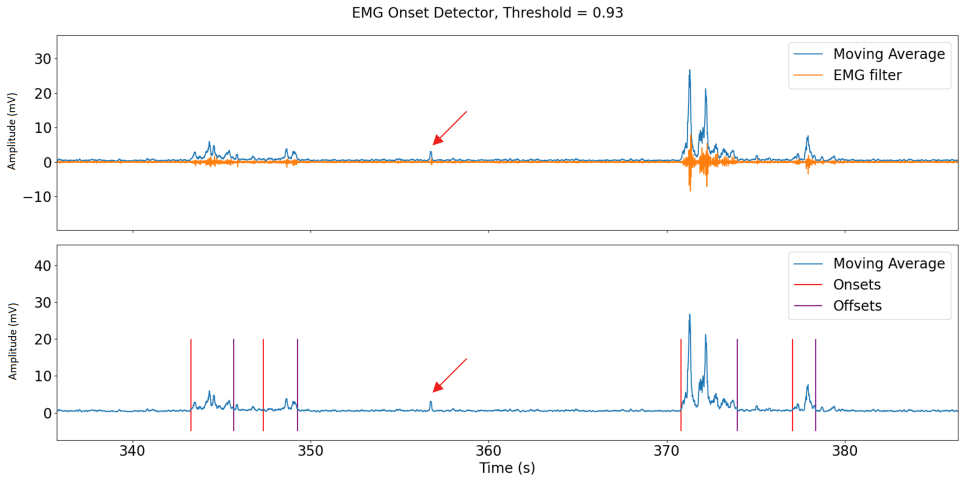


Figure 6.11: EMG activation segments detection (subject 3). The red arrow indicates a false onset that was not detected with this algorithm.

However, in phase 2, the muscle activity was too low for the algorithm to detect in some cases. Therefore, looking at the synchronized iHandU signal, it was verified that with this device, most of the movements not detectable by the EMG are caught by the acceleration, as in the case presented

in Figure 6.12a. Besides that, in some cases, like in Figure 6.12b, the movement on the EMG signal is only detected at the end, while in the iHandU is detected at the beginning.

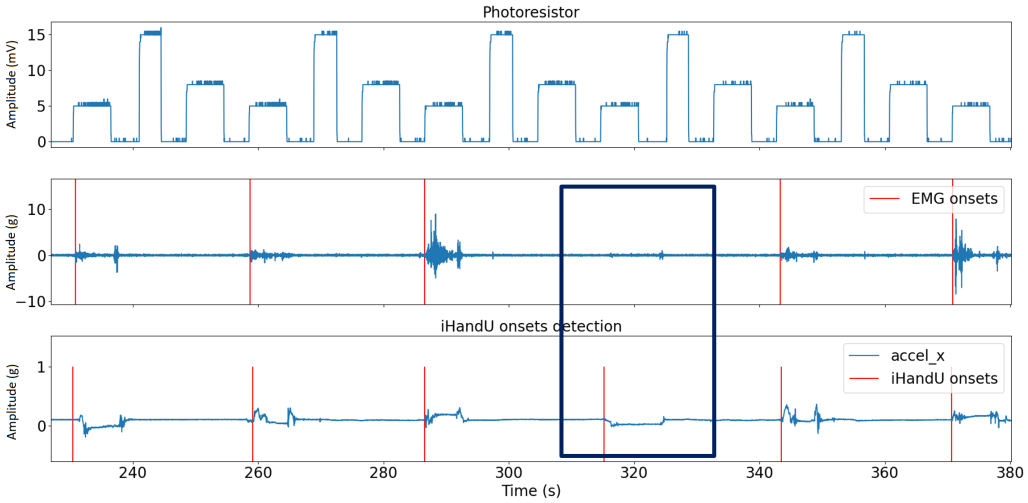


(a) Example where the iHandU detects the movement and the EMG doesn't.

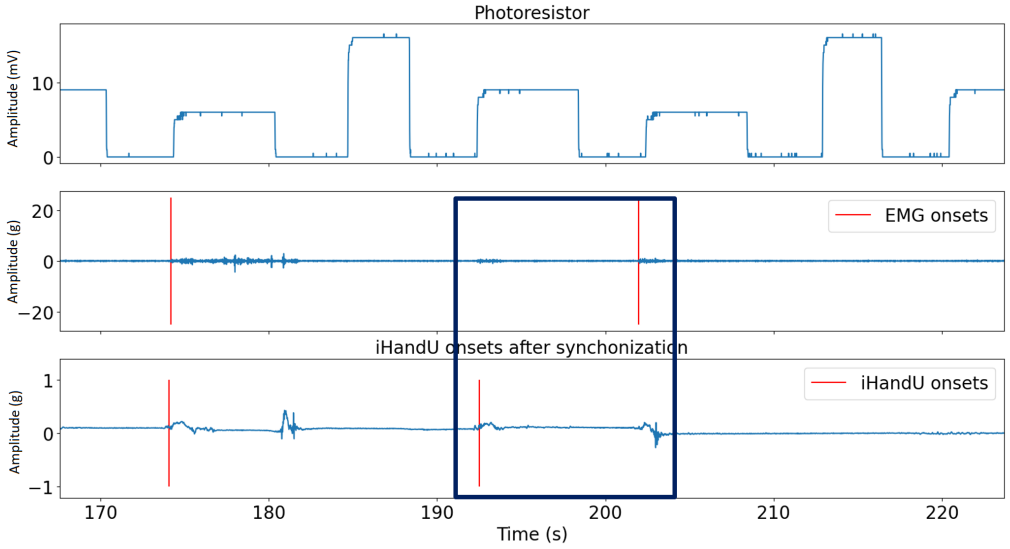


(b) Example where the iHandU detects the movement at the beginning of the movement, and the EMG detects only in the end.

Figure 6.12: Muscle activation detection through EMG signal or acceleration data (subject 7).

Therefore, a more detailed analysis was done for all subjects (see Table 6.3 and Fig. 6.13) to compare the EMG detector with the iHandU onset detector. The comparison can only be made for phase 2 of acquisition because only, for this case, there was no lack of iHandU data. By analyzing the table, the EMG onsets mostly fail in supination movements where muscle strength is lower, however, the iHandU was able to detect almost all movements correctly.

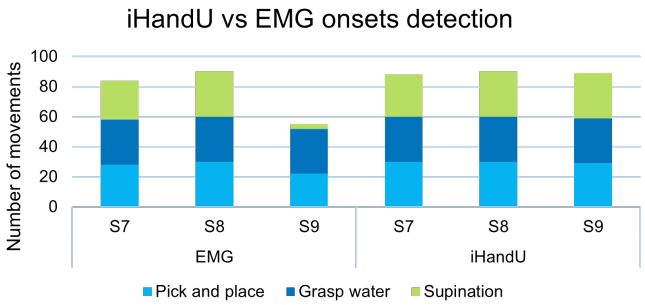


Figure 6.13: iHandU vs EMG onsets detection.

Table 6.3: Number of movements detected in each subject's session. For phase 1 each movement should be performed 20 times, and for phase 2 30 times.

| | Subject | Movement | EMG | iHandU |
|---|---|---|---|---|
| Phase 1 | **S2** | Pick and place | 20 | |
| | | Grasp water | 20 | |
| | | Supination | 20 | |
| | | **Total** | **60** | |
| | **S3**[1] | Pick and place | 10 | |
| | | Grasp water | 9 | |
| | | Supination | 10 | |
| | | **Total** | **29** | |
| | **S4** | Pick and place | 20 | |
| | | Grasp water | 20 | |
| | | Supination | 20 | |
| | | **Total** | **60** | |
| | **S5** | Pick and place | 19 | |
| | | Grasp water | 20 | |
| | | Supination | 20 | |
| | | **Total** | **59** | |
| | **S6** | Pick and place | 20 | |
| | | Grasp water | 20 | |
| | | Supination | 19 | |
| | | **Total** | **59** | |
| Phase 2 | **S7** | Pick and place | 28 | 30 |
| | | Grasp water | 30 | 30 |
| | | Supination | 26 | 28 |
| | | **Total** | **84** | **88** |
| | **S8** | Pick and place | 30 | 30 |
| | | Grasp water | 30 | 30 |
| | | Supination | 30 | 30 |
| | | **Total** | **90** | **90** |
| | **S9** | Pick and place | 23 | 29 |
| | | Grasp water | 27 | 30 |
| | | Supination | 4 | 30 |
| | | **Total** | **54** | **89** |

## 6.4 ERD/ERS maps

Regarding the study of movement intention, the correlation with the ERD/ERS maps of electrodes, C3, Cz, C4, P3, and P4, was analyzed.

### 6.4.1 Results for BCI 2000 dataset

Firstly, the analysis of the maps was done in the BCI2000 dataset to validate the implemented algorithm. The movement execution runs (3, 7, 11), consisting of closing the left or right hand (similar to the database created), were selected. The maps were separated by movement (rest, left hand, or right hand). The $t = 0$ corresponds to the start of the cue. Only the results from the right hand were analyzed since the movement was more similar to the PhysioIntent dataset created.

Following the literature, this study was done to check for $\alpha$[8, 13] Hz and $\beta$[14, 30] Hz desynchronizations. Figure 6.14 shows some of the maps obtained for different subjects. It was found that the chosen baseline influences the results obtained (see Fig. 6.15).

The maps show a significant desynchronization ($p < 0.05$) in C channels (C3, Cz, C4) for alpha and beta bands. For some subjects, desynchronization was also revealed in P3 and P4.

However, it was not possible to analyze how early the desynchronization appeared before the move because the database has no annotation regarding the beginning of the movement, being one of its limitations.

[1] Subject 3 performed 2 valid runs, in the first two runs, the photoresistor was very noisy.

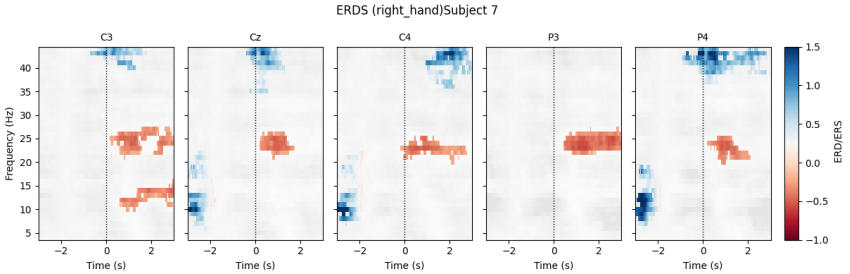


(a) ERD/ERS maps subject 7 from BCI 2000.

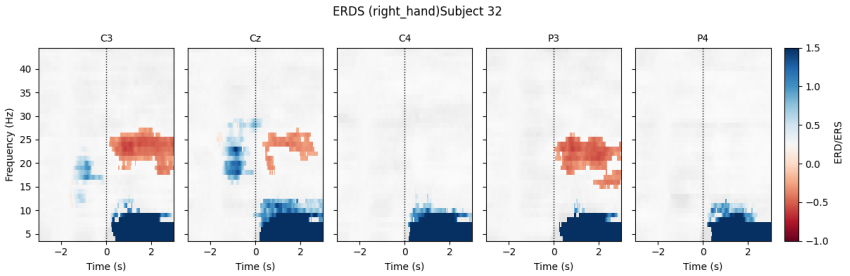


(b) ERD/ERS maps subject 32 from BCI 2000.

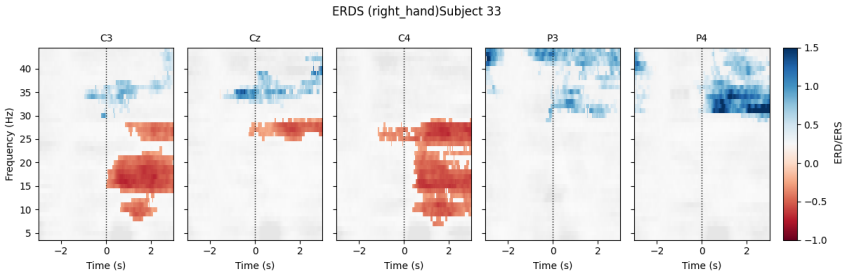


(c) ERD/ERS maps subject 33 from BCI 2000.

Figure 6.14: ERD/ERS maps examples from BCI 2000 (baseline [-2, -1.5] s). Horizontal axis represents time (units of s) while vertical axis represents frequency (units of Hz). Solid black lines in all graphs represent ($t = 0$ *s*) represent the cue onset. The ERD/ERS scale shown is relative, not in percentage. The ERD was map to red color and ERS to blue color.

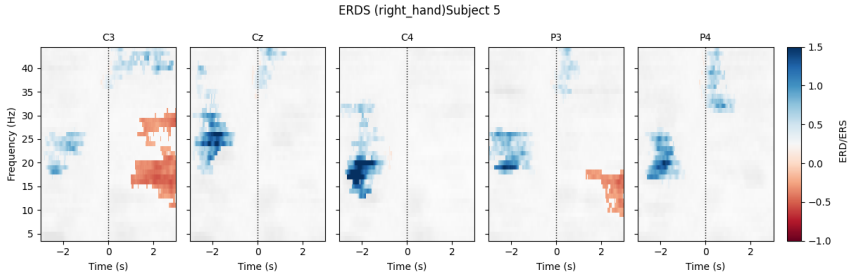


(a) Baseline [-1, 0] s.

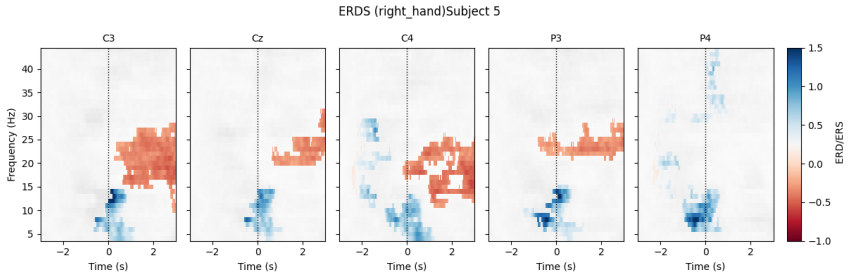


(b) Baseline [-3, -2] s.

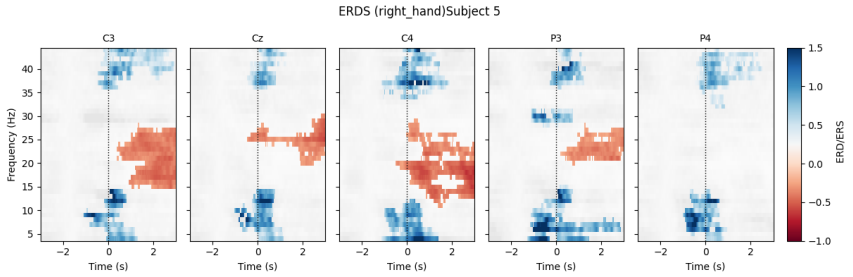


(c) Baseline [-2, -1.5] s.

Figure 6.15: ERD/ERS maps on subject 5 from BCI 2000 dataset with different baselines. The ERD was map to red color and ERS to blue color.

### 6.4.2 Results for PhysioIntent dataset

#### 6.4.2.1 ICA

According to the pipeline shown in Subsection 5.2.4, the first approach was to apply the ICA method. Figure 6.16 shows the seven components extracted for subject 6. From this analysis, it can be seen that components 0 and 1 are probably associated with the ocular activity. After computing the correlation with FP1 and FP2, it can actually be seen that components 0, 1, and 2 have the highest component of the ocular artifact (see Fig. 6.17a and 6.17b).

Regarding the cardiac artifacts, none was observed in the EEG signal (all the scores were below 10 %, see Fig. 6.17c). Figure 6.18 shows the EEG signal for subject 6 after removing the components 0, 1 and 2.

Figure 6.19 shows the influence of applying the ICA on the ERD/ERS maps. In this example, by applying the ICA method, desynchronizations in the alpha band that did not appear before are evident after removing the artifacts.

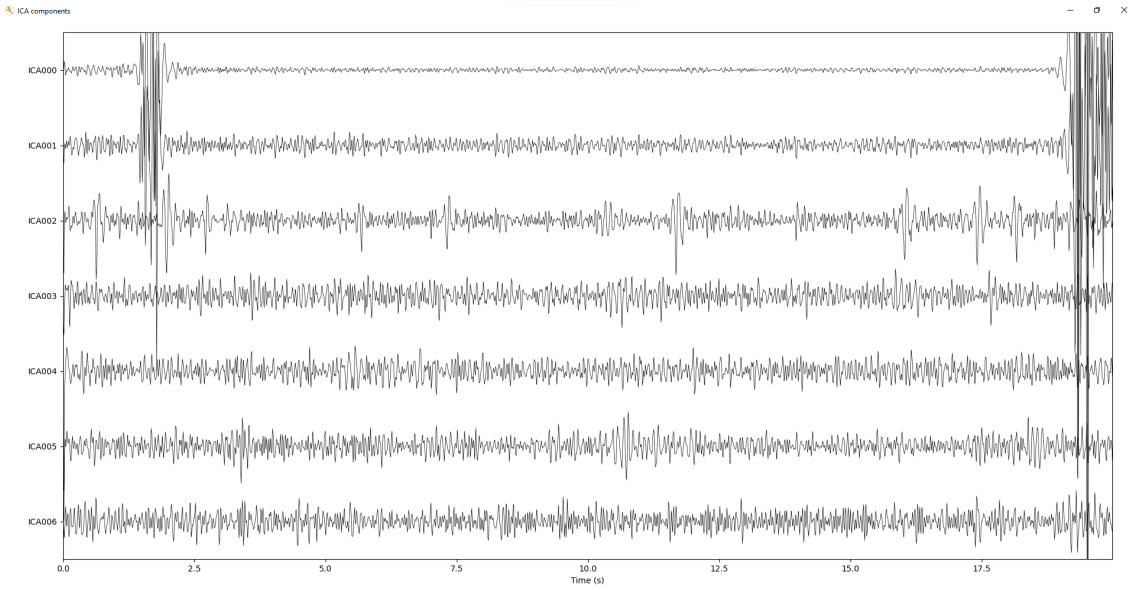


Figure 6.16: ICA components (subject 6).

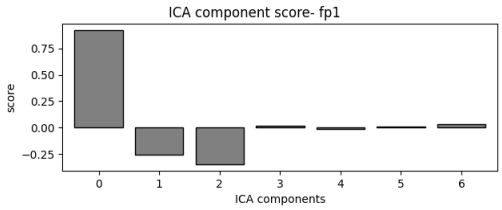


(a) ICA scores related to FP1 channel.

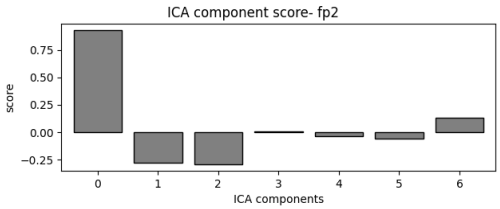


(b) ICA scores related to FP2 channel.

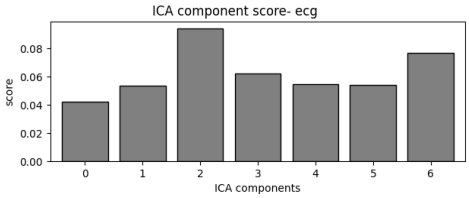


(c) ICA scores related to ECG channel.

Figure 6.17: ICA components scores for ocular and cardiac artifacts (subject 6).

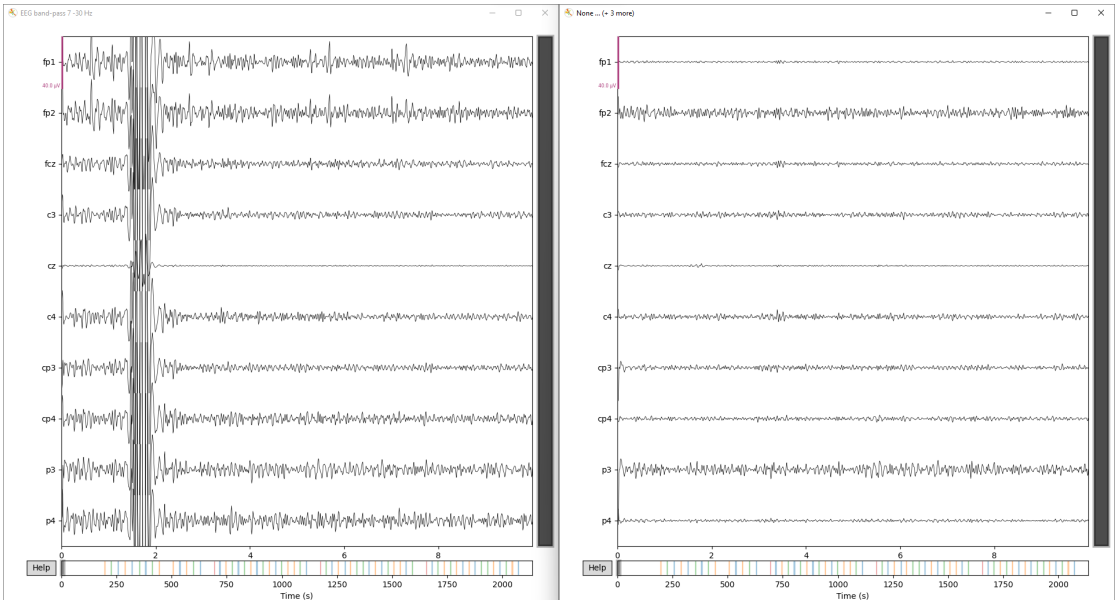


Figure 6.18: EEG signal from subject 6. Left: band-pass 7-30 Hz; Right: after removing the ICA components related with ocular artifacts.

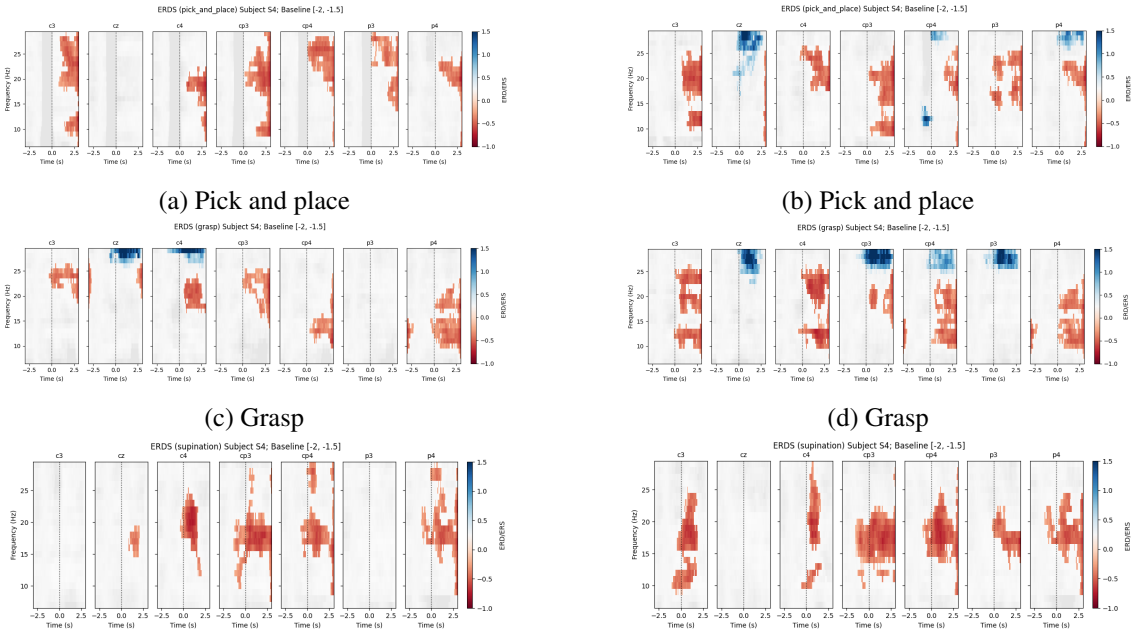


(a) Pick and place

(b) Pick and place

(c) Grasp

(d) Grasp

(e) Supination

(f) Supination

Figure 6.19: ERD/ERS maps before and after remove some ICA components (subject 4). The images on the left represent the maps before, and the images on the right represent the maps after applying ICA.

#### 6.4.2.2 ERD/ERS

The EEG analysis was not performed for subjects 1 and 5: subject 1 because there was a data loss and for subject 5 because the EEG was not recorded. The other subjects' maps are presented in Appendix C.1. The ERD/ERS maps were computed for each movement.

For subject 2, for the "Pick and place" movement, can be seen a desynchronization on the beta on the controlateral motor cortex almost 0.5 s before the movement, which is in agreement with the literature [2]. For the grasping movement, desynchronization was only found on alpha, namely in the mu band [10, 12] Hz. Regarding desynchronization on supination, it is only seen during the movement execution (after $t = 0$).

As for subject 3, only the last two runs could be analyzed. The results were not the expected. This can be explained by the fact that only ten repetitions per movement were analyzed.

Concerning subject 4, the results were promising. For all the movements, desynchronizations on mu and beta were found before and during the movement execution. Supination was the movement that could be detected earlier, -1 s before the movement.

Subject 7 (phase 2) showed promising results (see Fig. C.5). The intention can be predicted a half second before the actual movement. As for subject 8, the intention could only be predicted on pick and place and supination movement.

Despite all efforts to reduce noise, some noise/artifacts can still be picked up in the EEG, which is probably one reason why the results are not as expected for some subjects, such as subjects 6 and 9.

Thus, based on these results, we can conclude that it is possible to predict movement intention with EEG. Of the seven subjects that could be analyzed, five had desynchronizations in alpha and beta bands, although for some movements in some subjects, this was not clear. However, based on the results obtained, we cannot assume that one movement was better detected than the others. More data should be acquired in the future to further validate these results.

As future work, an algorithm based on the line plots presented in Appendix C.2 should be implemented to accurately determine the time the intention is detected. Furthermore, with more data, testing machine learning algorithms like the SVM would also be advisable.

Once we have a robust algorithm, it can be incorporated into an industry scenario, as shown in Chapter 1 - Figure 1.1, where the robot predicts human intention and avoids a possible accident.

# Chapter 7

# Conclusion

The goal of this dissertation was to be able to predict human intention through multimodal signals. The first step involved studying the devices used for data acquisition: openBCI Cyton board + Daisy module for recording EEG, EMG, and ECG, and iHandU device to register the IMU data.

Simultaneously, an experiment protocol was created, consisting of imagination and execution of some upper limb movements. Each movement was repeated several times. The protocol is split into runs to allow the subject to have a break between several trials.

This dataset has two different phases of acquisition. In phase 1, some problems, namely data loss, were encountered. Phase 2 emerged as an alternative to phase 1, aiming to overcome these problems by making a more balanced distribution of the tasks to be executed on each of the two computers.

Since different devices were used to acquire the data, it is essential to synchronize all of them. To do so, the first approach was to synchronize all the data by timestamp recording on each type of data. However, there were some limitations, the samples were not equally distributed by the timestamp as they should. Thus, a more accurate solution was implemented, which consists of an external sensor (photoresistor) connected to the Cyton board that registers precisely the time when the stimulus shows up to the user.

However, the photoresistor only allows the synchronization between the openBCI and the visual stimulus. Thus, for synchronizing the iHandU, the subject touches the device three times. These changes are registered on the iHandU and the EMG signal, allowing synchronization. Besides that, another problem was encountered: a cumulative delay on the iHandU device after synchronizing the data. This problem was solved by estimating a line equation that relates the difference between each iHandU and EMG onset with the temporal index and allows refinement of the iHandU data.

After acquiring the data, the biosignals were pre-processed to remove the noise. The EMG and IMU data were used to detect the movements onsets. A comparison between the two was made, concluding that the iHandU is a better choice because, besides detecting more movements, it is simpler and more feasible to use.

The last step of this dissertation consisted of analyzing the relation between the EEG signal and human intention. The ERD/ERS maps were analyzed on the BCI 2000 dataset and the dataset acquired during this dissertation. Desynchronizations were found on the $\alpha$, and $\beta$ bands before the subject started performing the movement. In some subjects, it can be detected almost 1 second before the movement execution.

To summarize, from this dissertation, a public dataset with nine healthy subjects was created, which was used to study human intention. Besides that, new techniques were implemented to synchronize all the data, and new algorithms were developed to detect the movements onsets. Finally, it was proved that it is possible to detect human intention earlier with the EEG, and the C3, C4, P3, and P4 channels are enough to detect it.

Thus, in the future, after having a robust algorithm that can detect human intention close to one second before the performance of the movement this information can be sent to the robot. This way, the robot will have enough time to interpret the information and actuate, preventing the robot from injuring the worker.

## 7.1 Future Work

Given the conclusions presented, some aspects can still be improved. Firstly, more data should be acquired to allow the application of machine and deep learning techniques. Besides that, recording more sessions for each subject would make it possible to study the correlation between the number of sessions and the classifier, as done by Jeong et al. [14]. These new acquisitions could also have proximal movements, allowing the relationship between distal and proximal movements to be studied, as done by Lopez-Larraz et al. [13].

In addition, an algorithm that, based on the ERD/ERS line plot, determines when the desynchronization begins (intention starts) should also be created.

To conclude, a new interface communication with iHandU could also be developed to reduce the computational load of the Google Chrome API since the current API is computationally heavy, leading to some data losses.

# Appendix A

# Code Organization

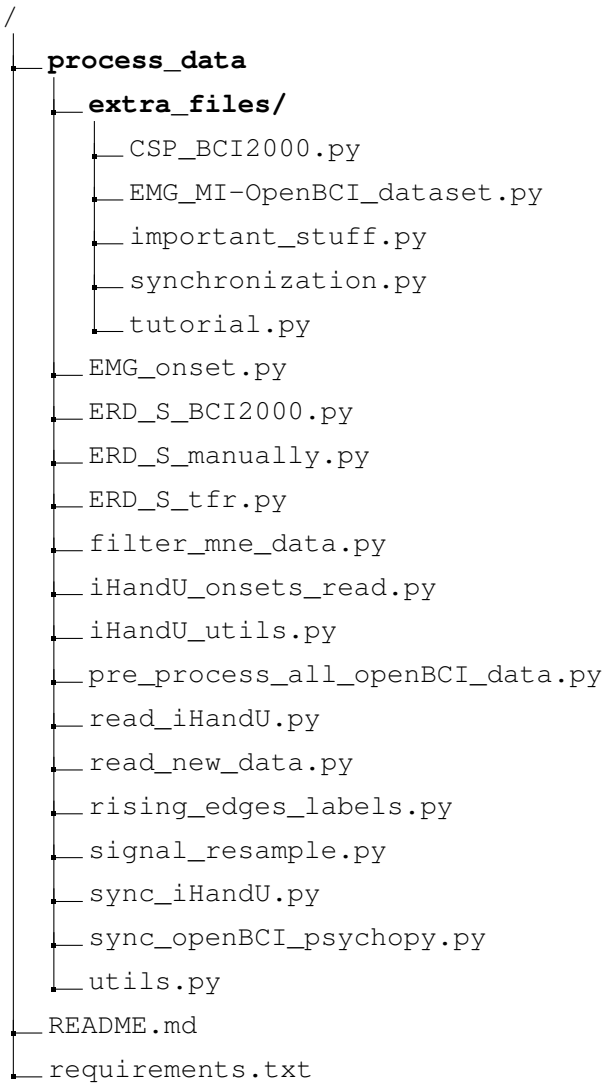


Figure A.1: Code organization.

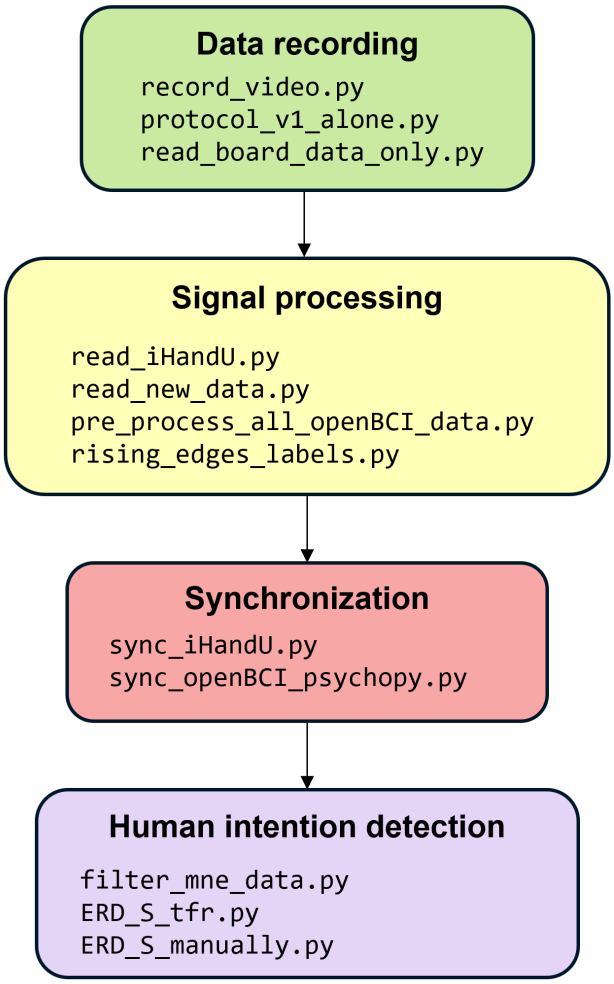


Figure A.2: Files used in each step of methodology.

# Appendix B

# Written Consent

# CONSENTIMENTO INFORMADO PARA PARTICIPAR EM ESTUDO

Por favor, leia com atenção a seguinte informação. Se achar que algo está incorreto ou pouco claro, não hesite em pedir mais informações através do email: (ana.f.sousa@inesctec.pt)

Se deseja participar no estudo solicitamos que preste o seu consentimento, assinando o documento no final.

A participação no estudo é voluntária, podendo o participante em qualquer altura cessar a sua participação sem qualquer tipo de consequência, bastando para isso contactar o responsável através do e-mail acima.

***1.DESCRIÇÃO DO ESTUDO***

**Título:** Towards Biosignal-based Robot Awareness Identification of Human Intentions

**Entidade Responsável:** INESC-TEC

**Responsável Direto:** *Nome:* Ana Filipa de Sousa Ferreira *Telemóvel:* +351910776380

**Descrição Geral:** Este estudo surge no âmbito do desenvolvimento de uma tese de mestrado no âmbito do curso Bioengenharia da FEUP para o ano letivo 2021/2022. Num mundo de tecnologia é cada vez mais importante melhorar a interação homem-máquina para que possam ser o mais natural possível. Assim, surge a importância em detetar a intenção de movimento de forma mais rápida e eficaz, para que possa haver um feedback rápido por parte do robot. Também na indústria é cada vez mais importante o uso de robots colaborativos. A intenção de movimento tem aqui um papel crucial, não só evitando alguns acidentes, mas também levando uma maior rapidez e eficácia na execução de tarefas que envolvem o robot e o homem.
Hoje em dia a deteção da intenção de movimento, é feita sobretudo com análise de vídeo ou sensores de movimento, sendo que há algum atraso na deteção desta. Este estudo pretende colmatar este problema, através da análise de sinais fisiológicos. Assim, pretendemos provar que através do eletroencefalograma (EEG) é possível fazer esta deteção de forma rápida e eficaz.

**Procedimentos gerais:** Ser-lhe-á pedido que execute alguns movimentos do membro superior de acordo com o protocolo definido. Os movimentos serão repetidos várias vezes ao longo de toda a sessão. Sendo que inicialmente é dado um período de descanso/concentração, passando para um estímulo visual do movimento que deverá ser executado, seguindo-se a execução deste. Este procedimento repetir-se-á várias vezes ao longo de todo o protocolo. Aquando à execução do protocolo a aquisição de sinais fisiológicos será realizada (Eletrocardiograma (ECG), Eletromiograma (EMG), Eletroencefalograma (EEG)) de forma contínua e não invasiva, assim como a aquisição de valores inerciais. Para além disso, será feita a gravação da sessão para efeitos de sincronização, de notar que a gravação não permitirá qualquer identificação do participante. Todas as instruções de utilização ser-lhe-ão explicadas pelo investigador.

**O Responsável:** … … … … … … … … … … … … … … … … … … … … … … … … … … … …

***O Participante:***

*Declaro ter lido e compreendido este documento, bem como as informações verbais que me foram fornecidas previamente. Desta forma, aceito participar neste estudo e permito a utilização dos dados que forneço de forma voluntária.*

Nome: … … … … … … … … … … … … … … … … … … … … … … … … … … … …

Assinatura: … … … … … … … … … … … … … … … … … … … … … … … … … … … Data: …… /…… /…….

**2. Tratamento dos dados pessoais**

**Riscos:** Os riscos e desconforto causado não serão maiores dos que está sujeito normalmente no seu dia-a-dia, na utilização de qualquer equipamento médico de ECG, EMG e EEG. Para melhorar a condutividade do sinal adquirido será aplicado uma pasta condutora sobre a pele, assim como adesivos para ajudar à fixação dos elétrodos, de modo a reduzir o ruído causada pela deslocação destes. Salienta-se que a utilização de elétrodos certificados pode causar alguma irritação na pele.

**Benefícios:** A sua participação neste estudo será de extrema importância para melhorar o estado da arte na área de intenção de movimento, pois uma rápida e eficaz deteção da intenção permite melhorar a interação homem-máquina.

**Compensações e/ou custos:** Não há qualquer compensação financeira, nem custos associados a participação neste estudo.

**Finalidade do tratamento:**
Os dados recolhidos serão tratados de acordo com a legislação nacional e da UE aplicável e apenas serão usados pelos investigadores para os fins de investigação científica.

**Responsável pelo Tratamento:**
INESC TEC – Instituto de Engenharia de Sistemas e Computadores, Tecnologia e Ciência, Campus da FEUP, Rua Dr. Roberto Frias, 4200 - 465 Porto.

**Confidencialidade:** Todos os dados adquiridos serão analisados para fins científicos no âmbito do estudo em causa; todos os envolvidos neste estudo têm um compromisso de confidencialidade e de não divulgação de dados ou informação de carácter pessoal dela retirada; os dados recolhidos serão tratados de forma pseudo-anónima e em conjunto, de forma a não ser identificada a sua participação individual no estudo; Alguns passos serão tomados para proteger a sua identidade individual, nomeadamente: a) a cada participante será atribuído um código; b) todos os dados recolhidos serão guardados num servidor local do INESC TEC (instituição acolhedora do estudo) com acesso restrito e limitado apenas aos membros do grupo de investigação envolvidos; c) qualquer vídeo contendo imagens que identifiquem os participantes serão guardados de forma segura e apenas é permitido o seu acesso a investigadores autorizados. No entanto, os participantes podem, ou não, permitir esta partilha anónima de dados a investigadores terceiros, indicando "SIM" ou "NÃO" na frase seguinte:
- Compreendo que os investigadores possam querer utilizar alguma parte de um vídeo para questões ilustrativas, apenas para fins científicos e/ou educativos. Dou autorização para tal, desde que o meu nome e rosto não sejam visíveis.

Por favor indique: _____SIM _____ NAO

**Partilha de Dados Pessoais:** Os dados/resultados anónimos e em conjunto poderão ser divulgados/publicados no âmbito de publicações científicas, podendo envolver equipas de investigação de diversas instituições.

**Encarregado de Proteção de Dados:** Para quaisquer questões, exercício de direitos do titular dos dados pessoais, pedidos ou reclamações relativas ao tratamento de dados pessoais, contacte por favor, o nosso encarregado de proteção de dados, através do contacto: dpo@inesctec.pt

**Direitos do Titular dos Dados**:
Enquanto titular dos dados, a lei reconhece-lhe os seguintes direitos: Informação, Acesso, Retificação, Apagamento, Oposição e Portabilidade. No caso de desistência não há prejuízo no tratamento de dados recolhidos até então, sendo estes tornados totalmente anonimizados. Para qualquer questão relacionada com o estudo pode contactar o Investigador Responsável: Duarte Dias (duarte.f.dias@inesctec.pt).

O exercício dos direitos poderá ver-se afastado ou limitado, no respeito pelos termos e condições previstos na legislação nacional e da UE aplicável, na medida em que tal exercício seja suscetível de tornar impossível ou

# Appendix C

# ERD/ERS

## C.1 ERD/ERS maps

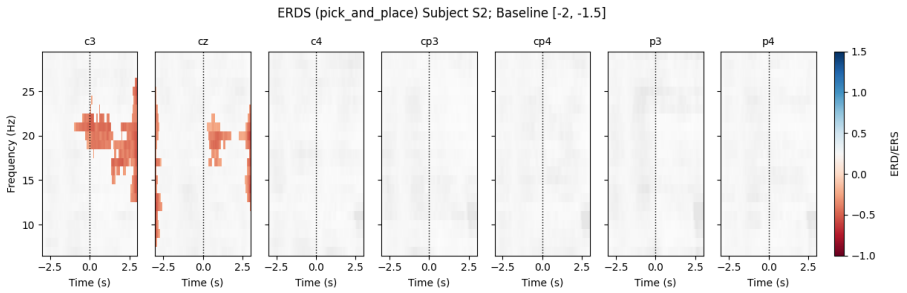


(a) Pick and place

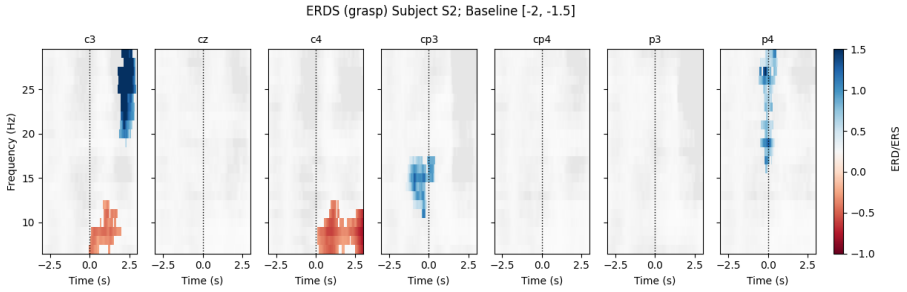


(b) Grasp

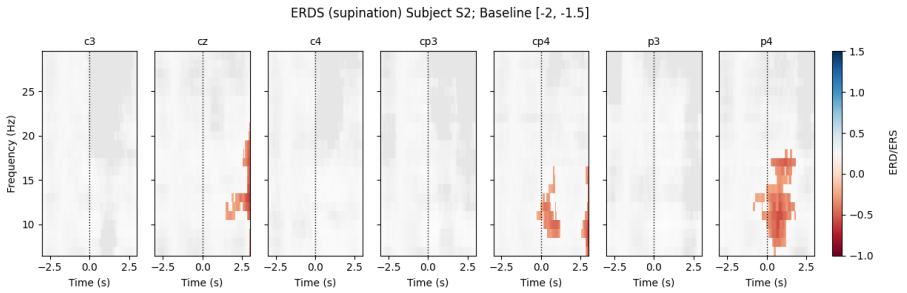


(c) Supination

Figure C.1: ERD/ERS maps subject 2.

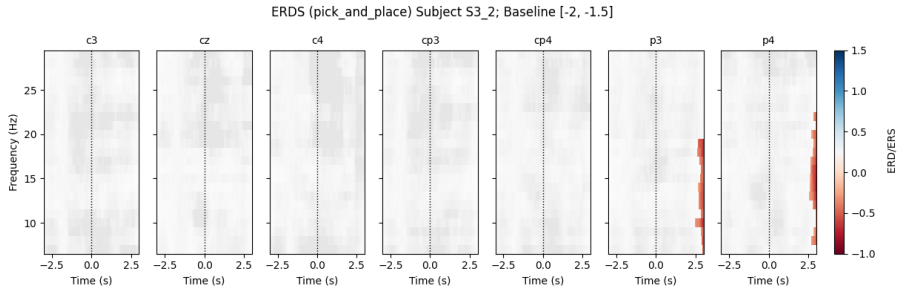


(a) Pick and place

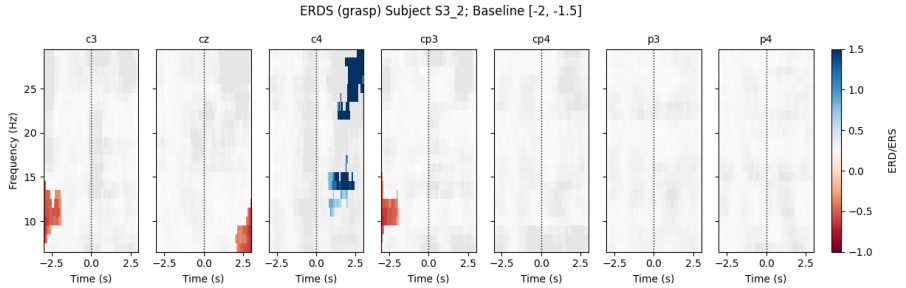


(b) Grasp

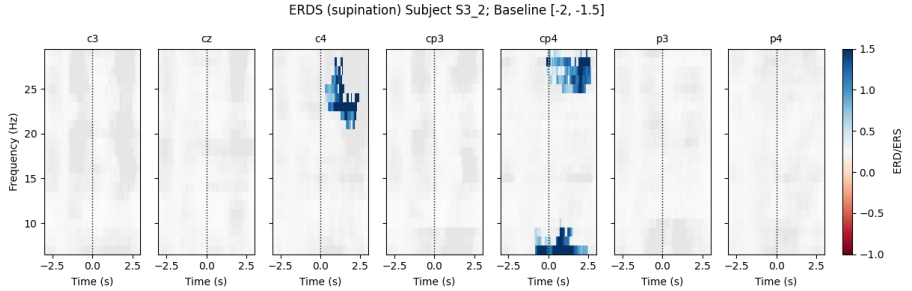


(c) Supination

Figure C.2: ERD/ERS maps subject 3.

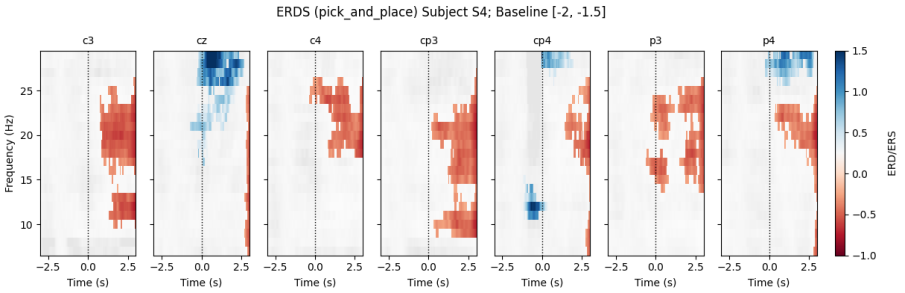


(a) Pick and place

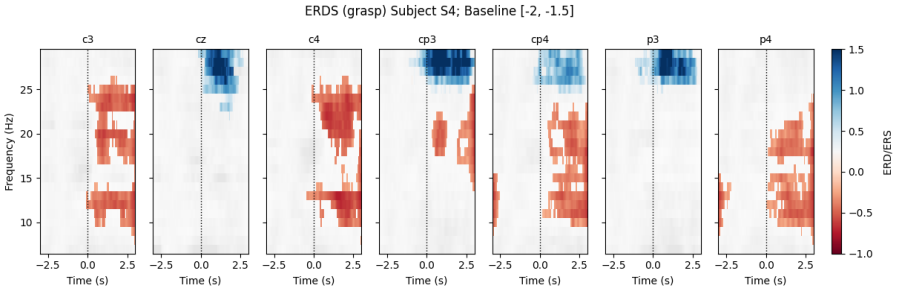


(b) Grasp

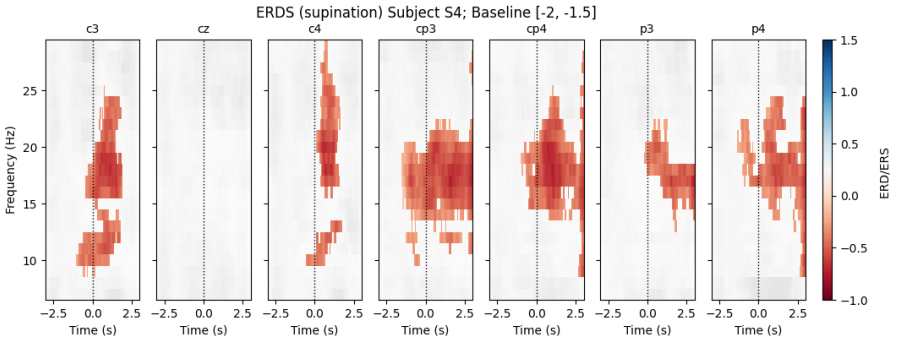


(c) Supination

Figure C.3: ERD/ERS maps subject 4.

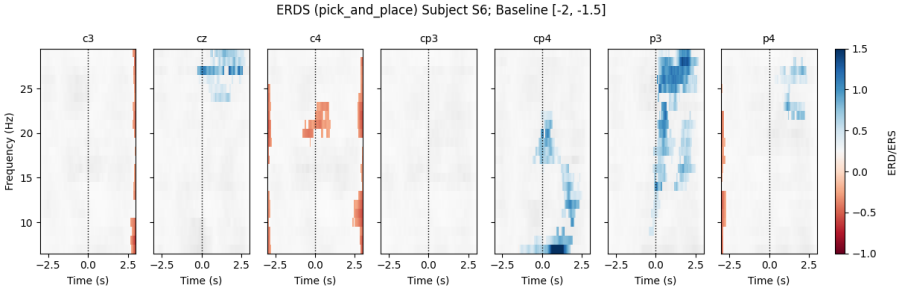


(a) Pick and place

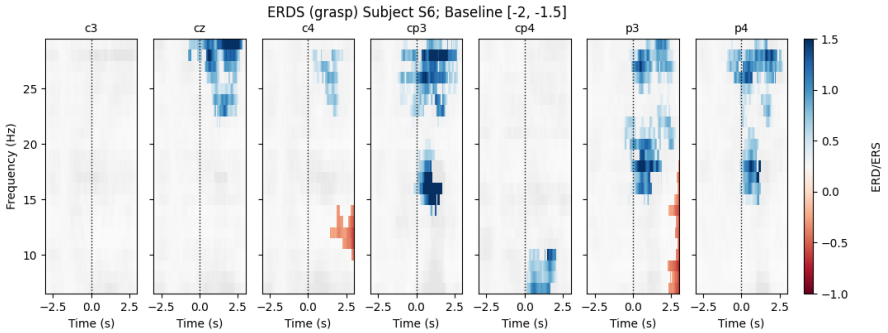


(b) Grasp

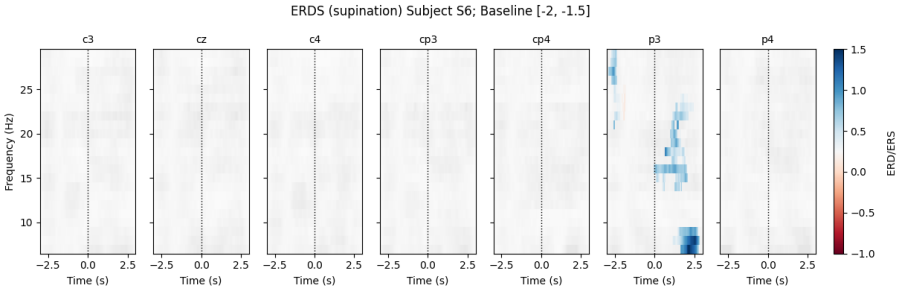


(c) Supination

Figure C.4: ERD/ERS maps subject 6.

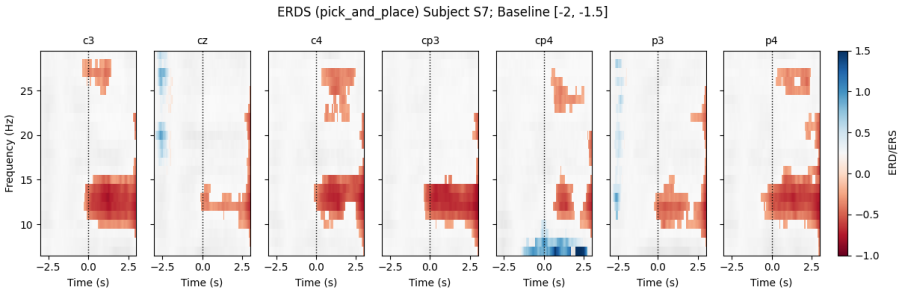


(a) Pick and place

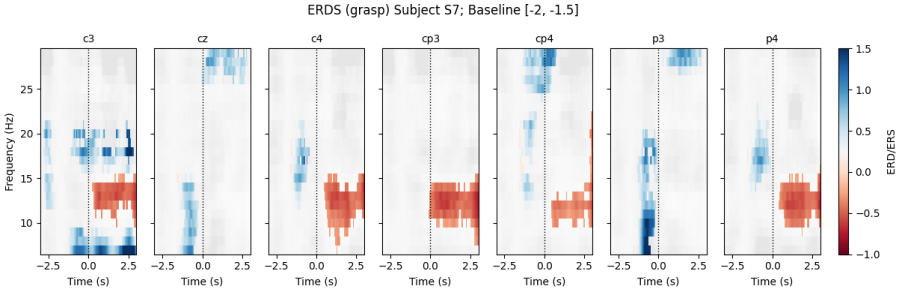


(b) Grasp

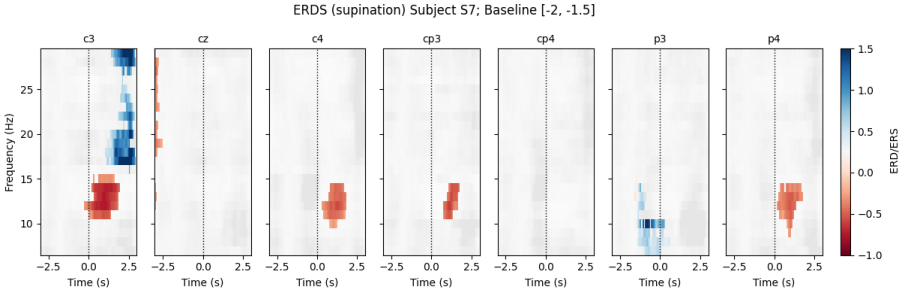


(c) Supination

Figure C.5: ERD/ERS maps subject 7.

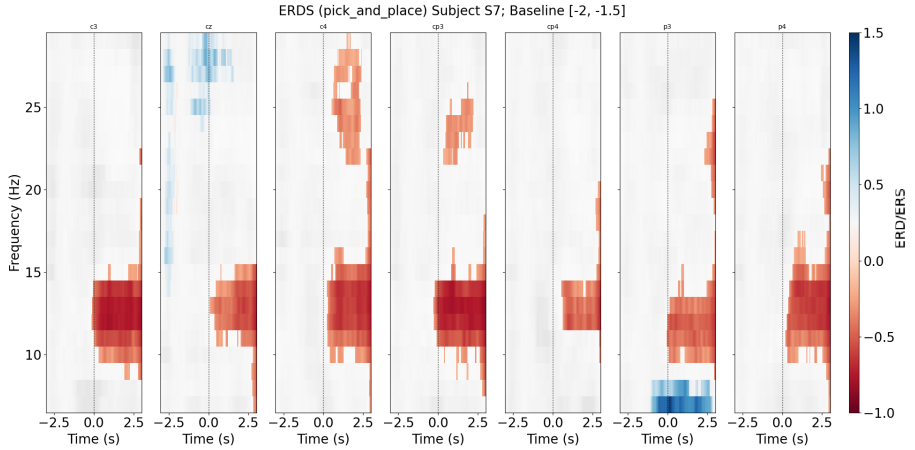


(a) Pick and place

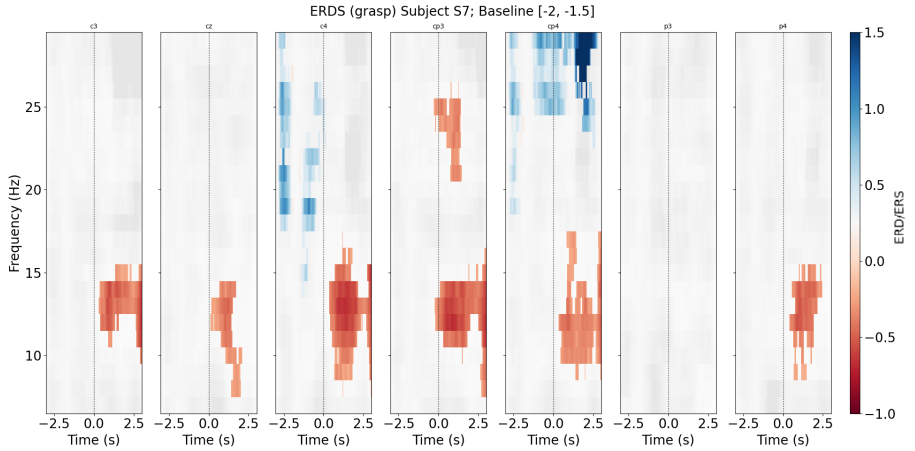


(b) Grasp

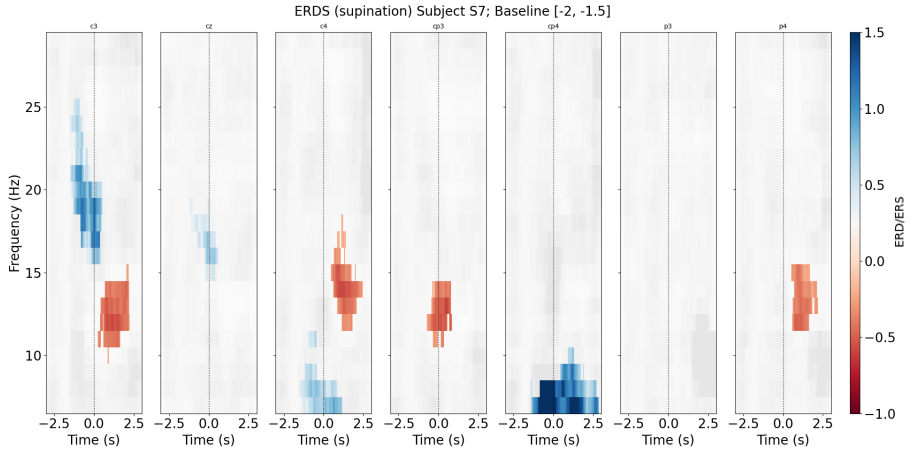


(c) Supination

Figure C.6: ERD/ERS maps subject 7 with iHandU marking the onsets (t = 0).

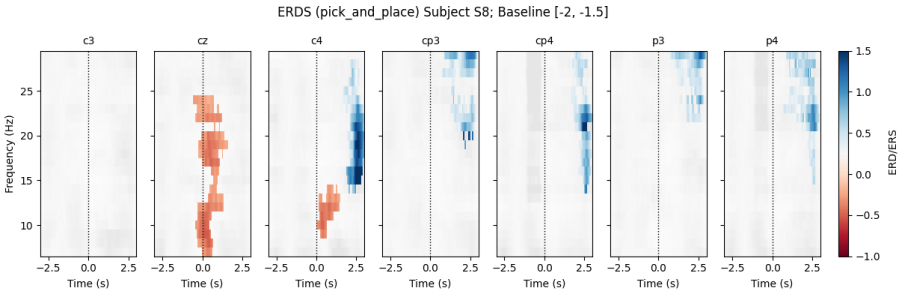


(a) Pick and place

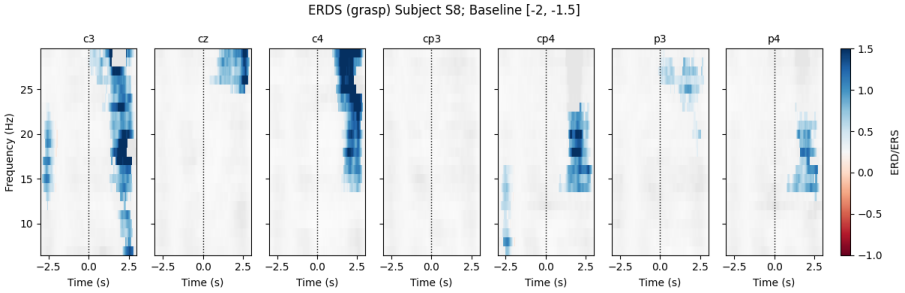


(b) Grasp

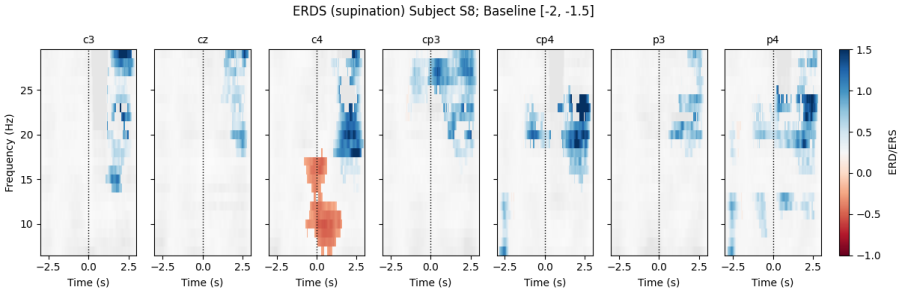


(c) Supination

Figure C.7: ERD/ERS maps subject 8.

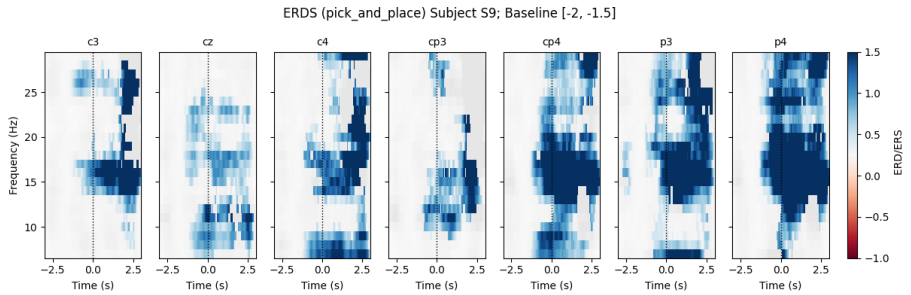


(a) Pick and place

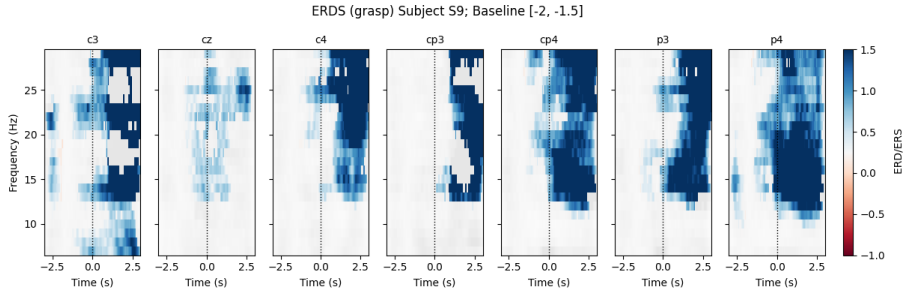


(b) Grasp

Figure C.8: ERD/ERS maps subject 9.

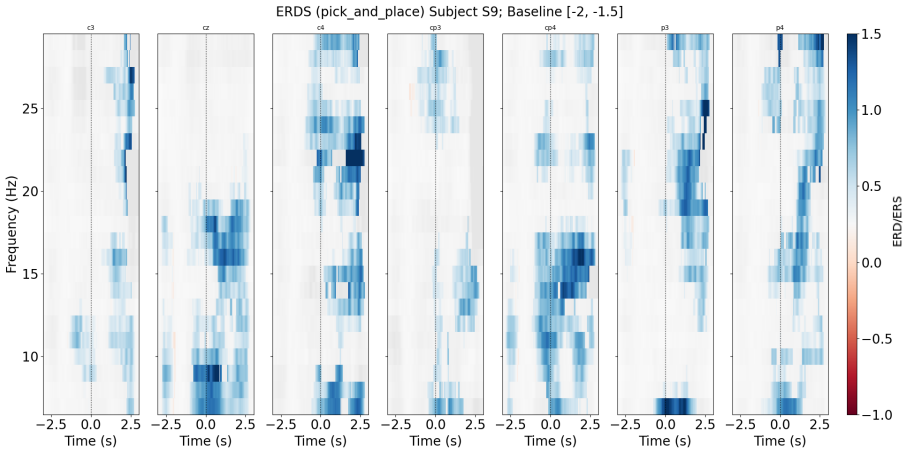


(a) Pick and place

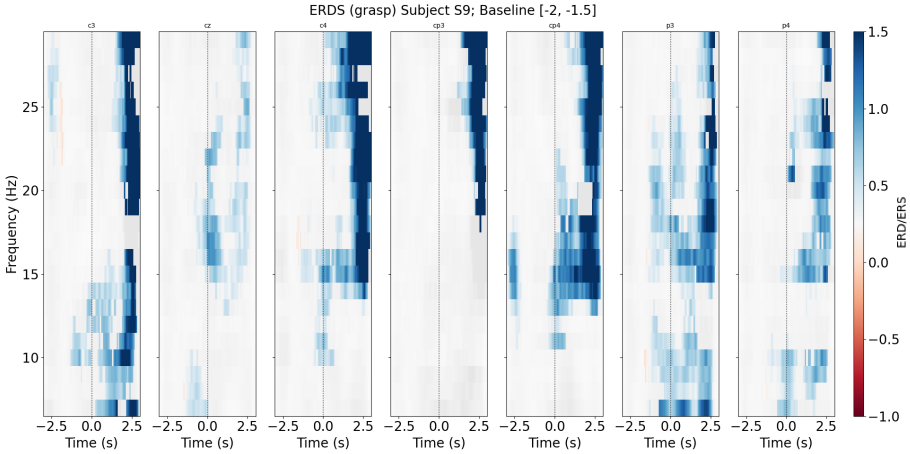


(b) Grasp

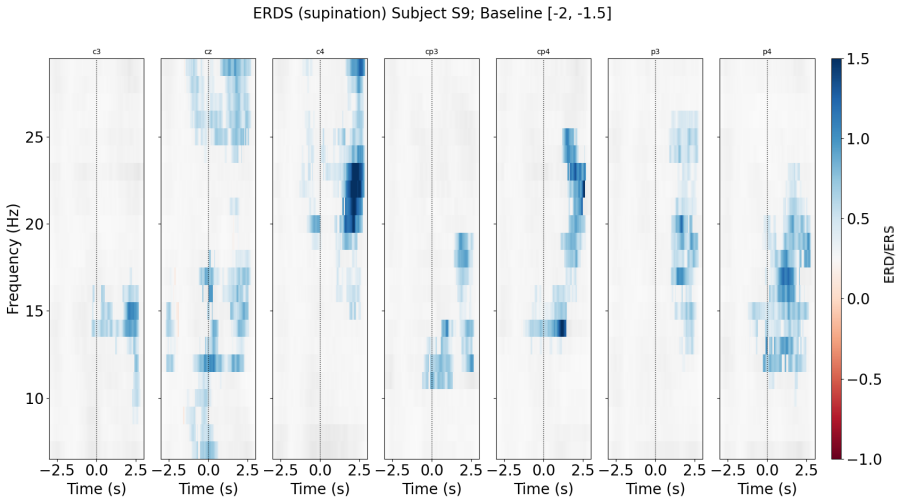


(c) Supination

Figure C.9: ERD/ERS maps subject 9 with iHandU marking the onsets (t = 0).

## C.2 ERD/ERS line plots

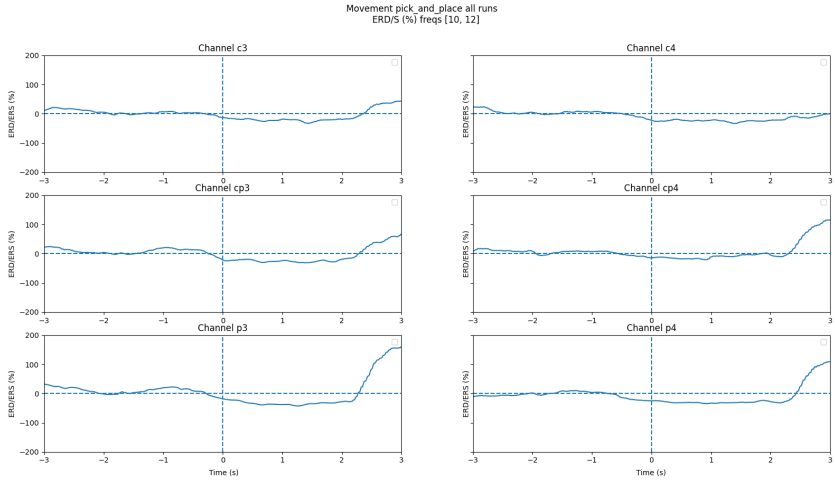


(a) Pick and place

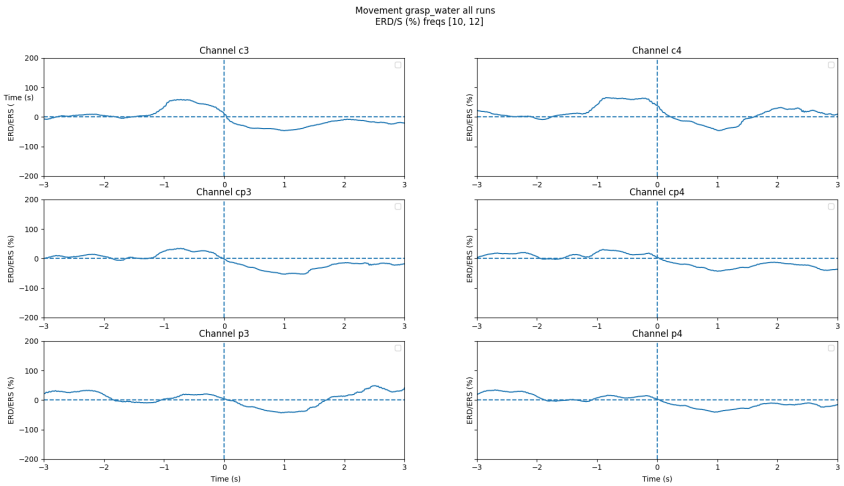


(b) Grasp

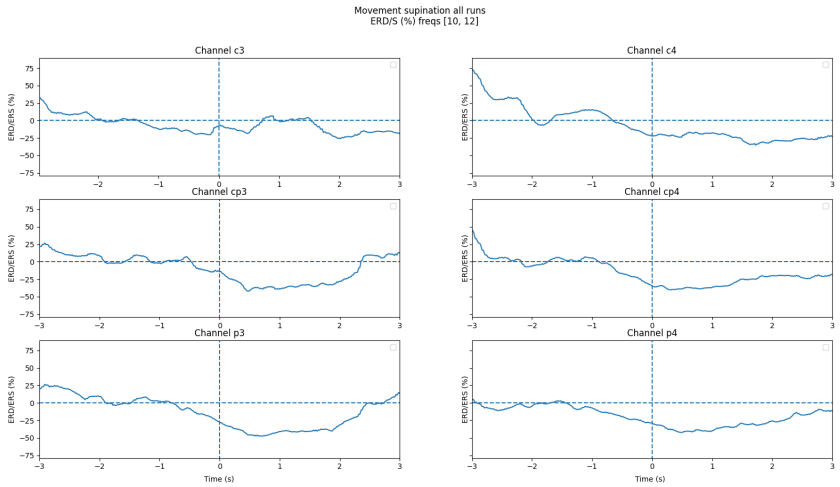


(c) Supination

Figure C.10: ERD/ERS line plot subject 2 for $\mu$ band [10, 12] Hz

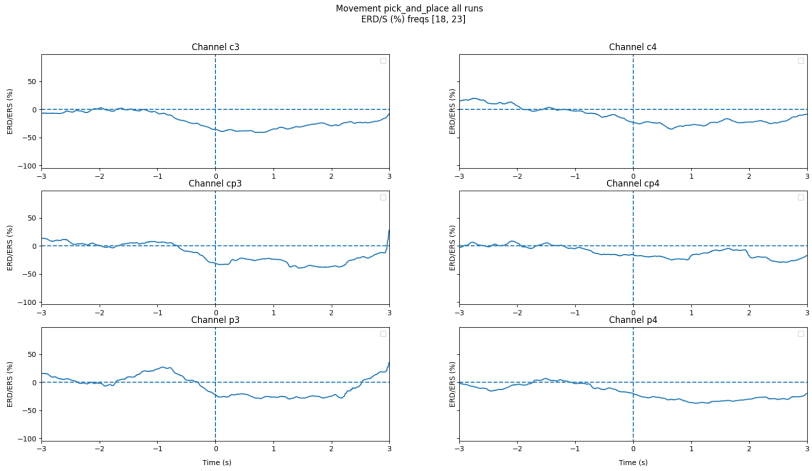


(a) Pick and place

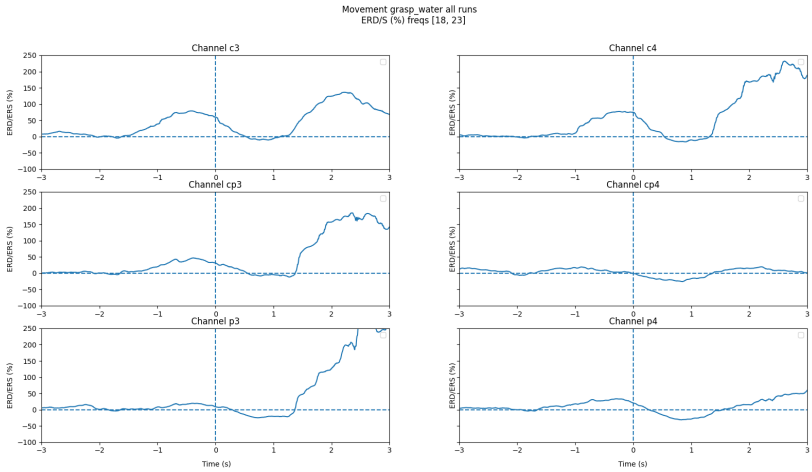


(b) Grasp

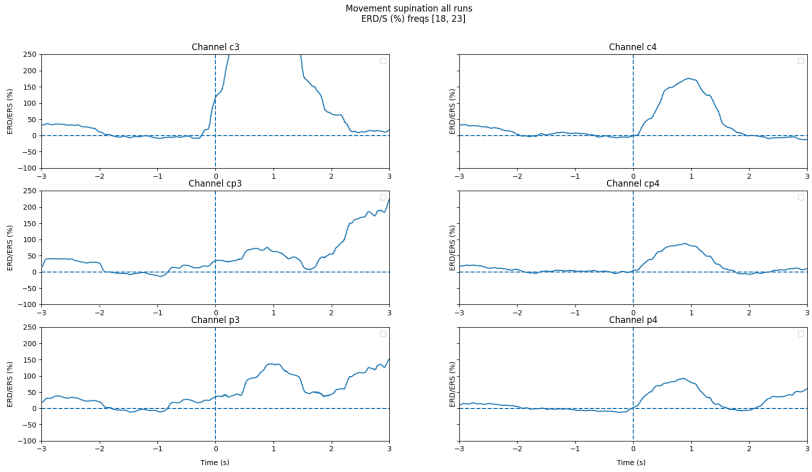


(c) Supination

Figure C.11: ERD/ERS line plot subject 2 for $\beta$ band [18, 23] Hz

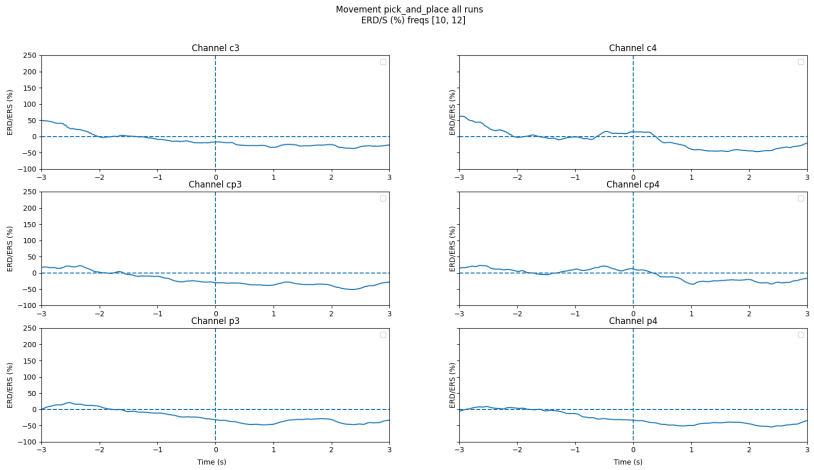


(a) Pick and place

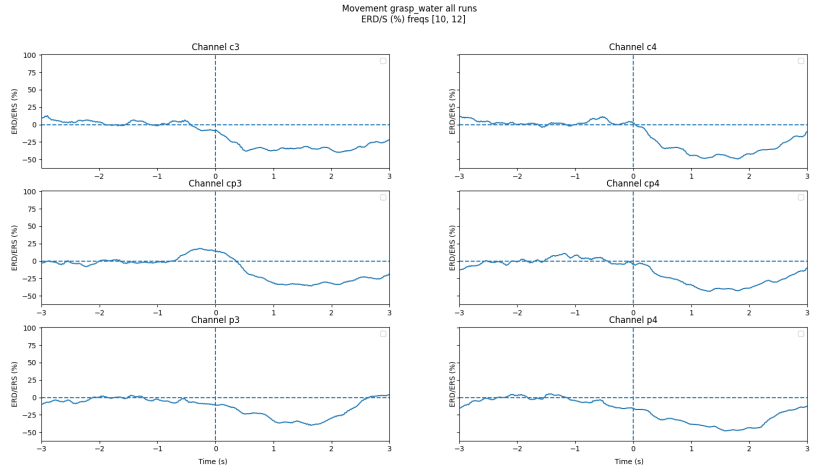


(b) Grasp

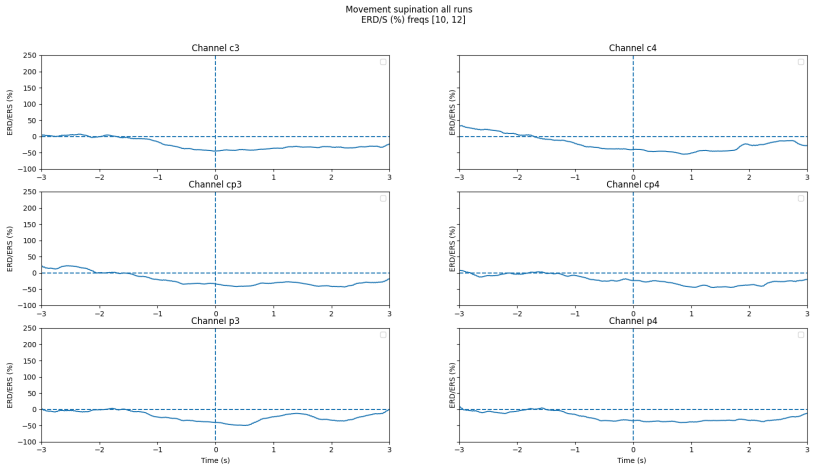


(c) Supination

Figure C.12: ERD/ERS line plot subject 4 for $\mu$ band [10, 12] Hz

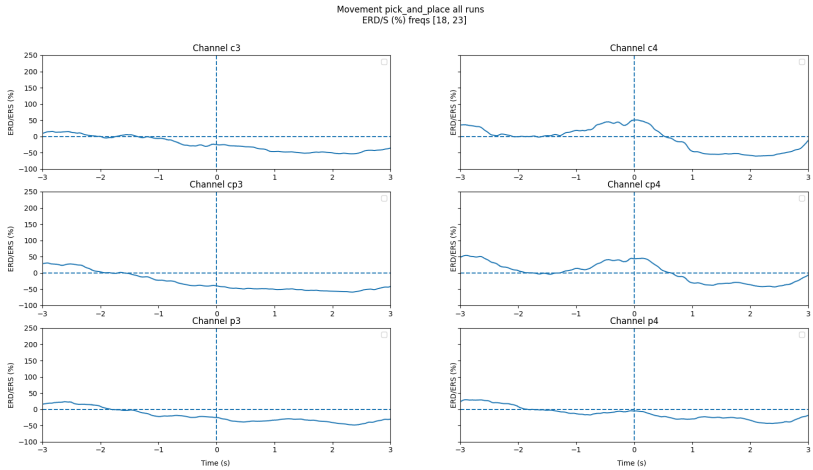


(a) Pick and place

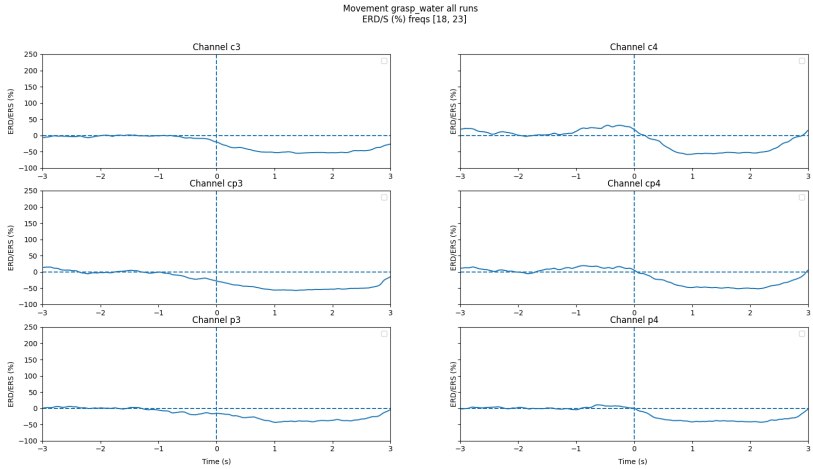


(b) Grasp

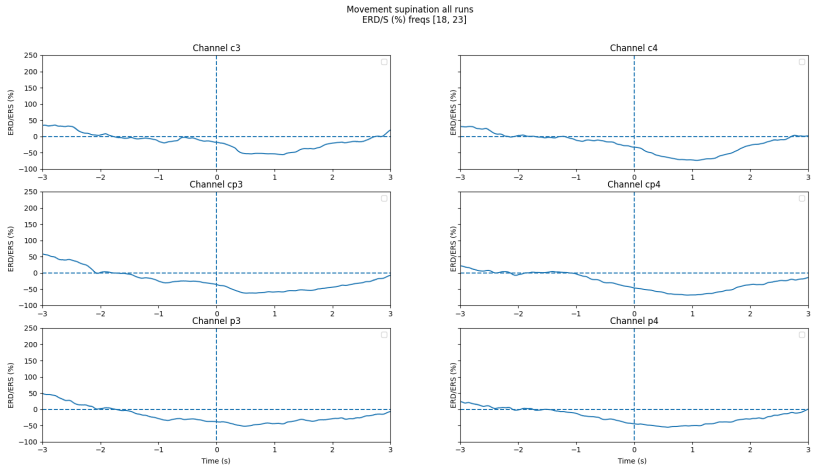


(c) Supination

Figure C.13: ERD/ERS line plot subject 4 for $\beta$ band [18, 23] Hz

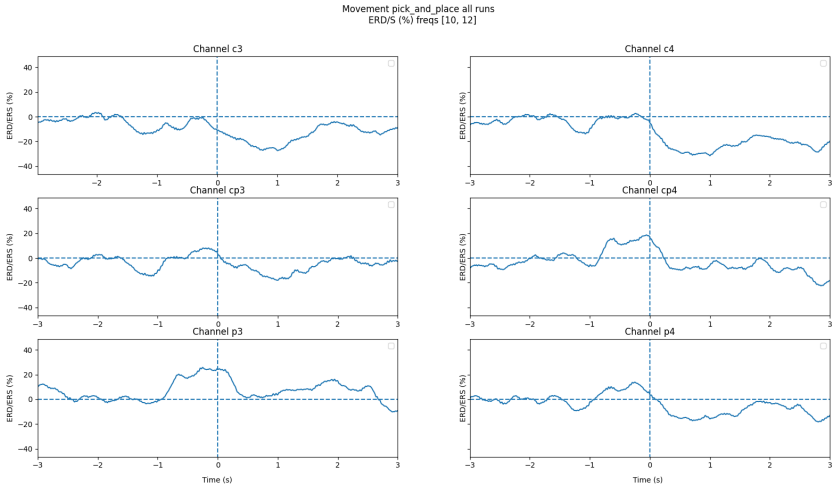


(a) Pick and place

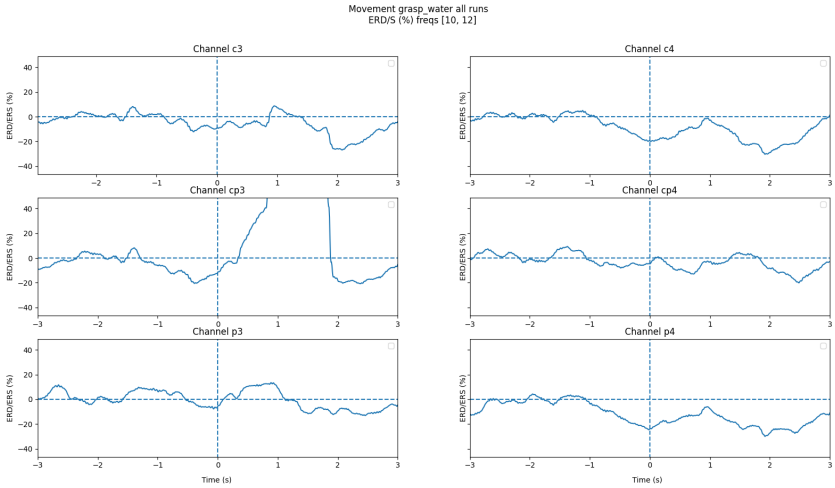


(b) Grasp

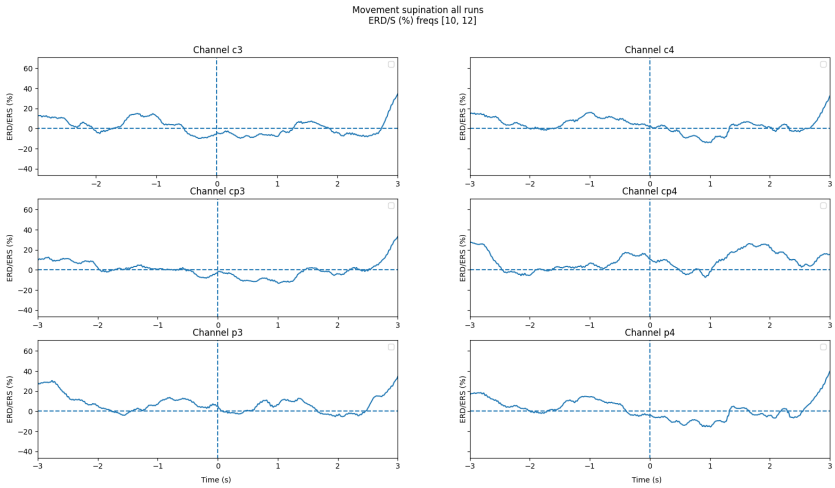


(c) Supination

Figure C.14: ERD/ERS line plot subject 6 for $\mu$ band [10, 12] Hz

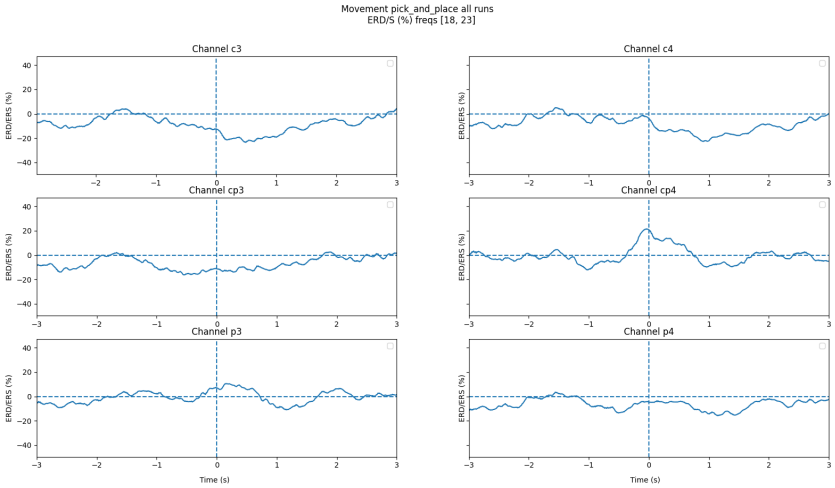


(a) Pick and place

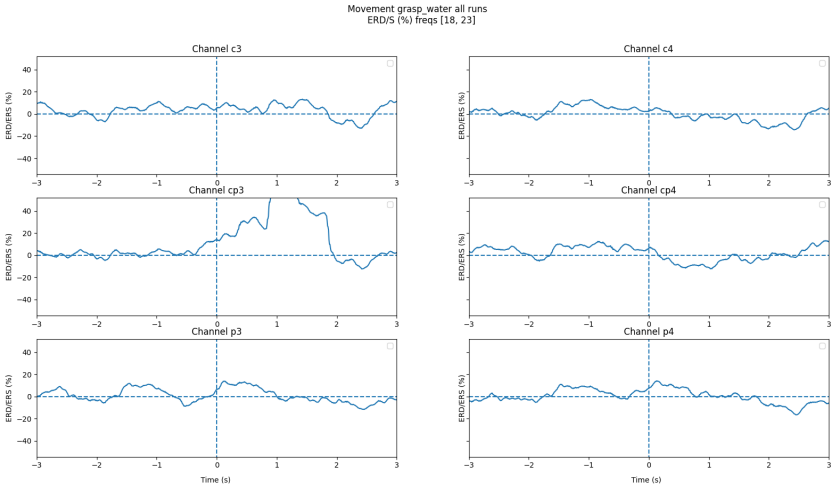


(b) Grasp

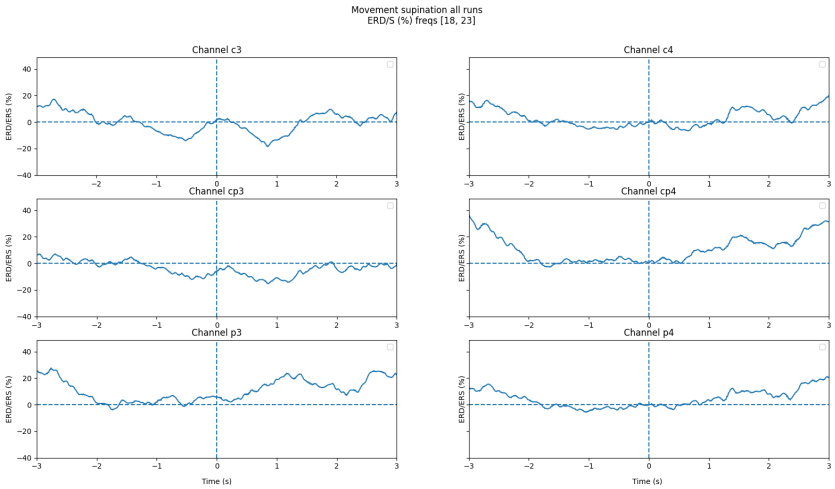


(c) Supination

Figure C.15: ERD/ERS line plot subject 6 for $\beta$ band [18, 23] Hz

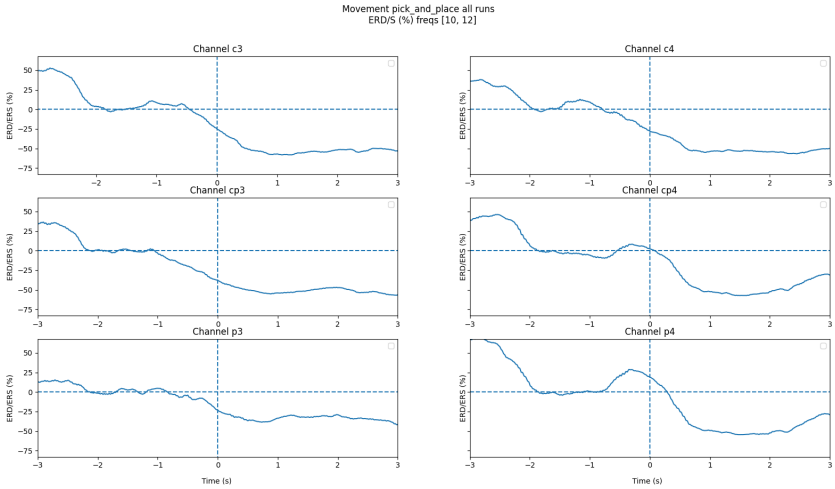


(a) Pick and place

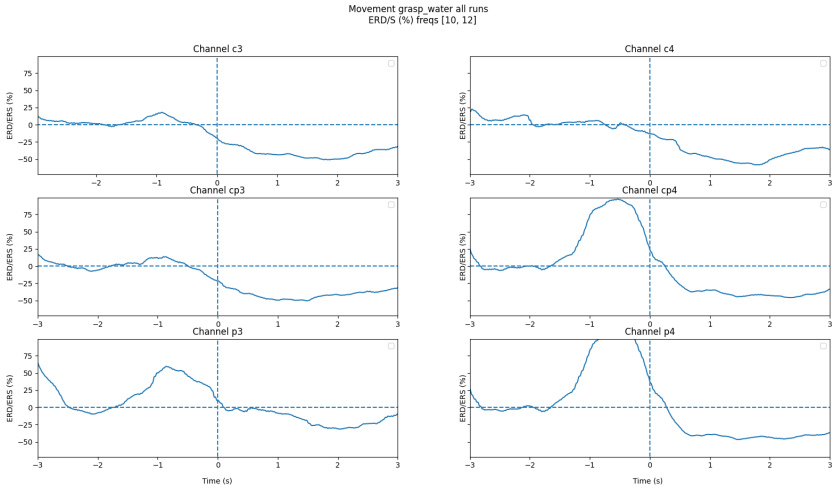


(b) Grasp

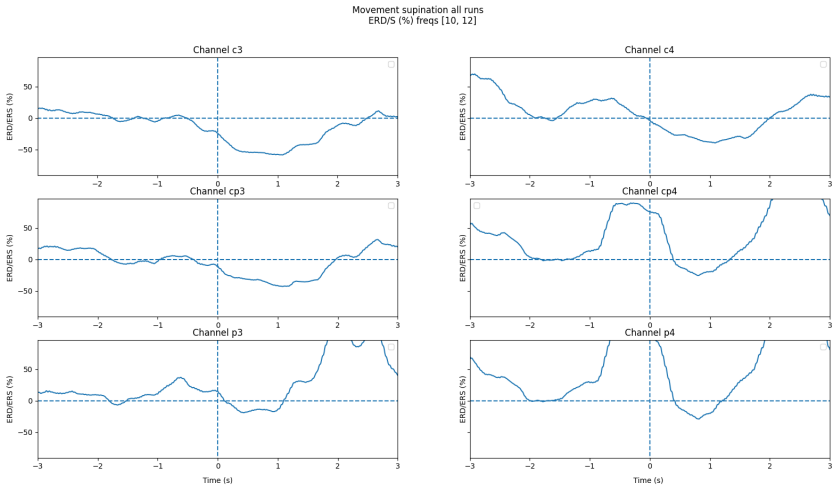


(c) Supination

Figure C.16: ERD/ERS line plot subject 7 for $\mu$ band [10, 12] Hz

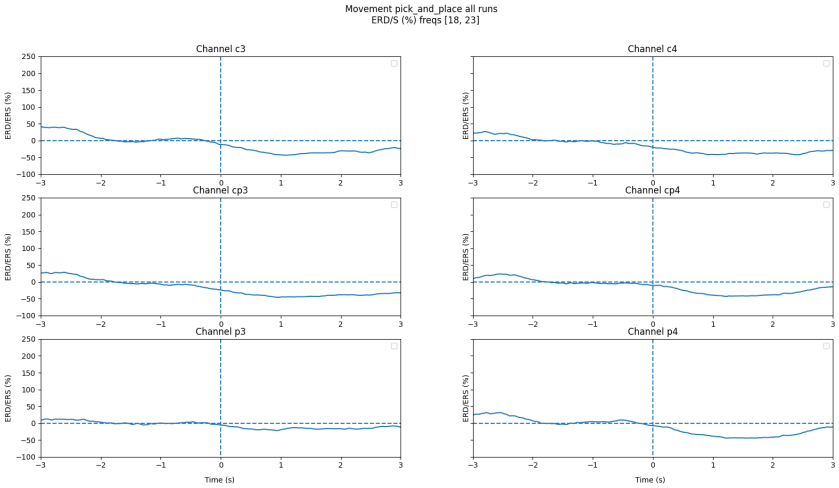


(a) Pick and place

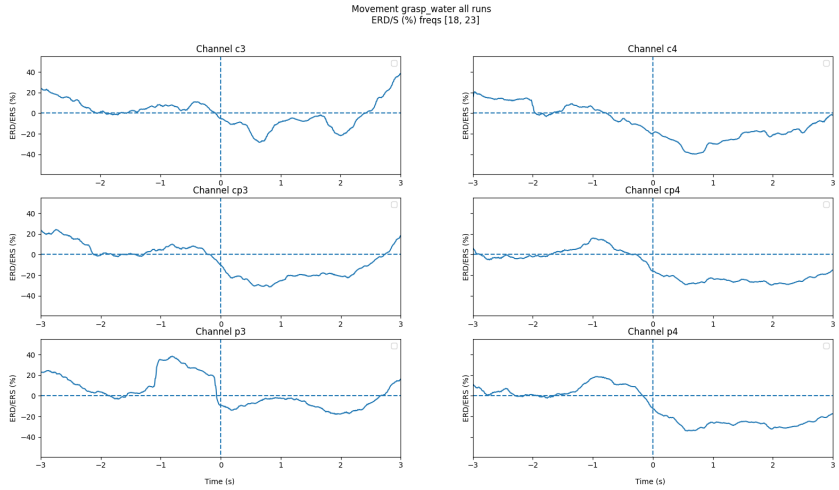


(b) Grasp

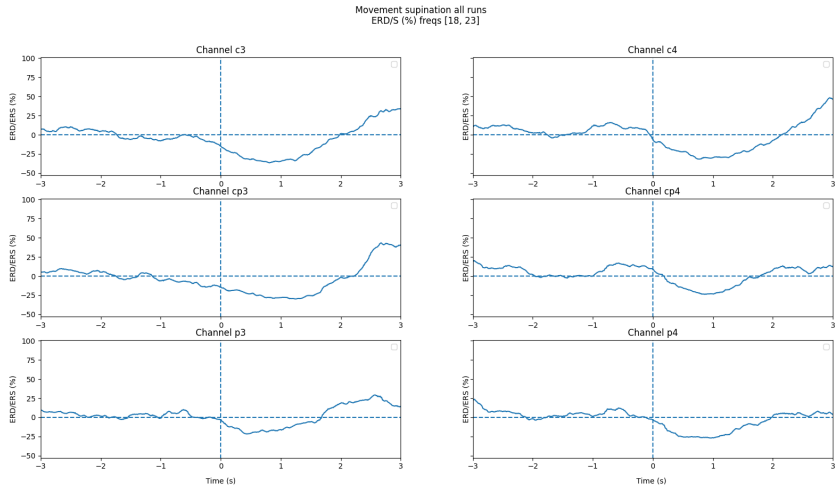


(c) Supination

Figure C.17: ERD/ERS line plot subject 7 for $\beta$ band [18, 23] Hz

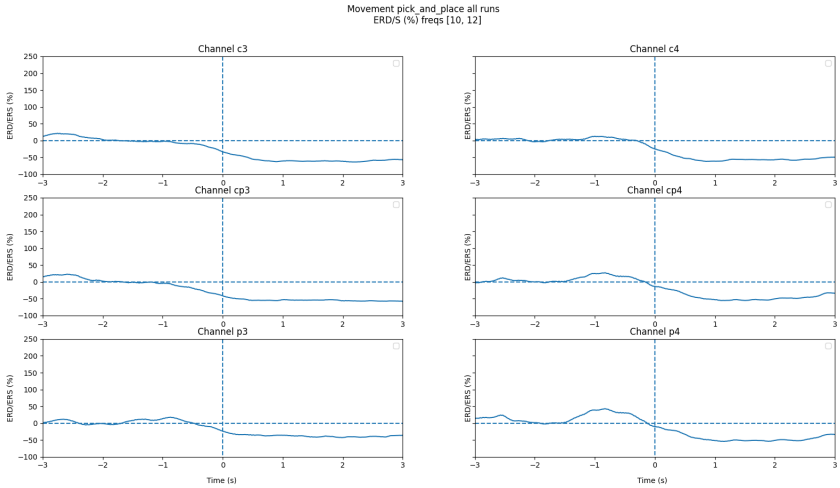


(a) Pick and place

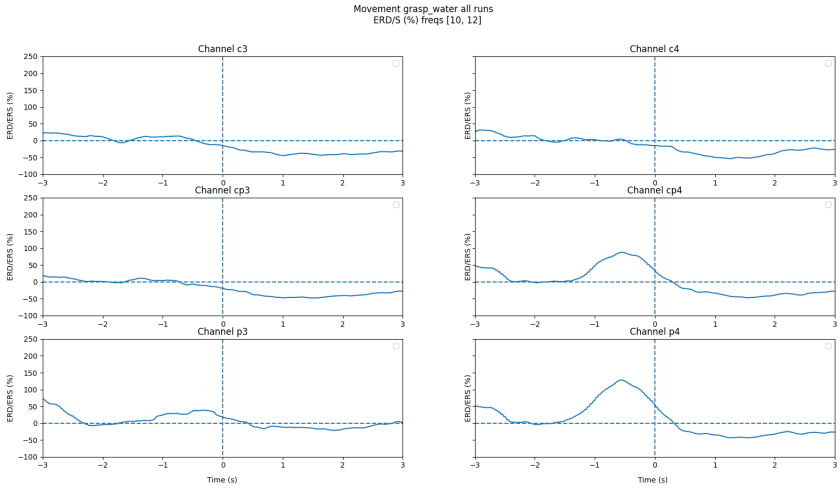


(b) Grasp

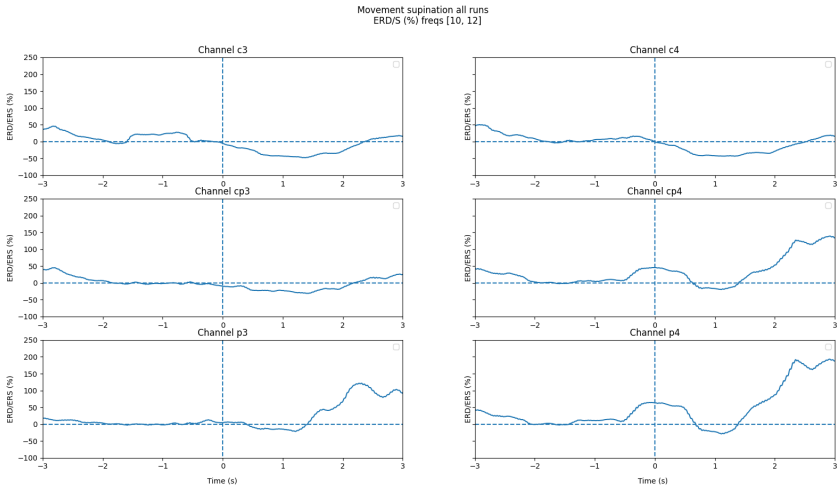


(c) Supination

Figure C.18: ERD/ERS line plot subject 7 for $\mu$ band [10, 12] Hz (with iHandU onsets as t= 0)

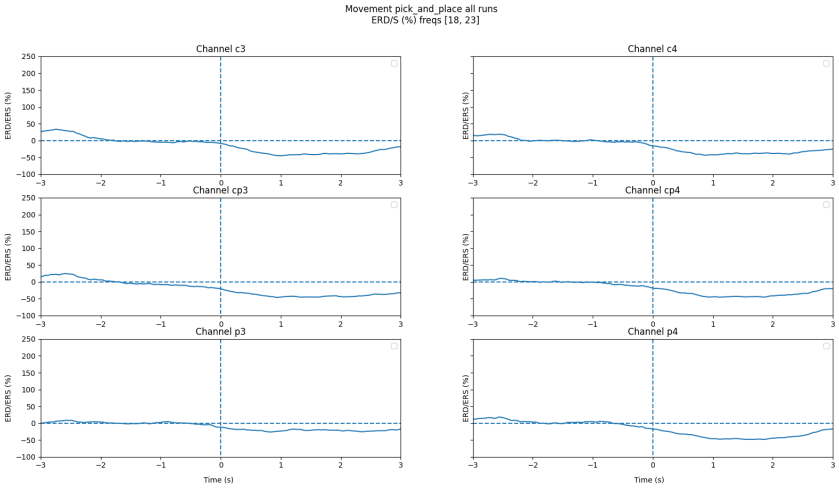


(a) Pick and place

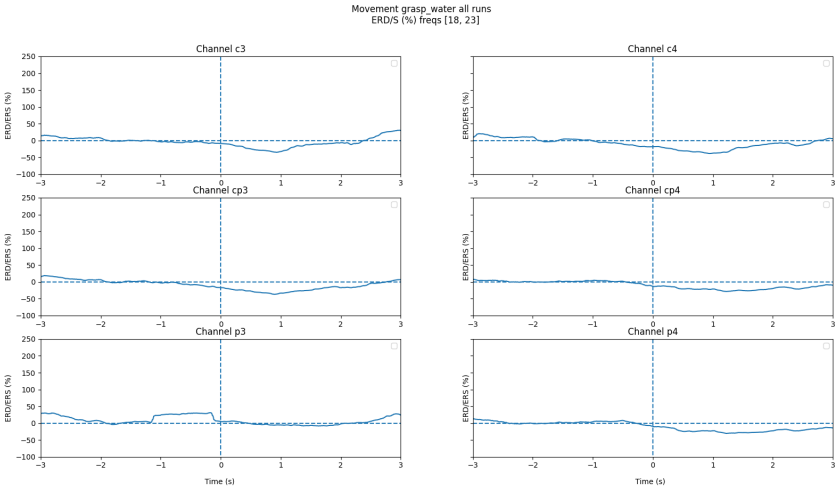


(b) Grasp

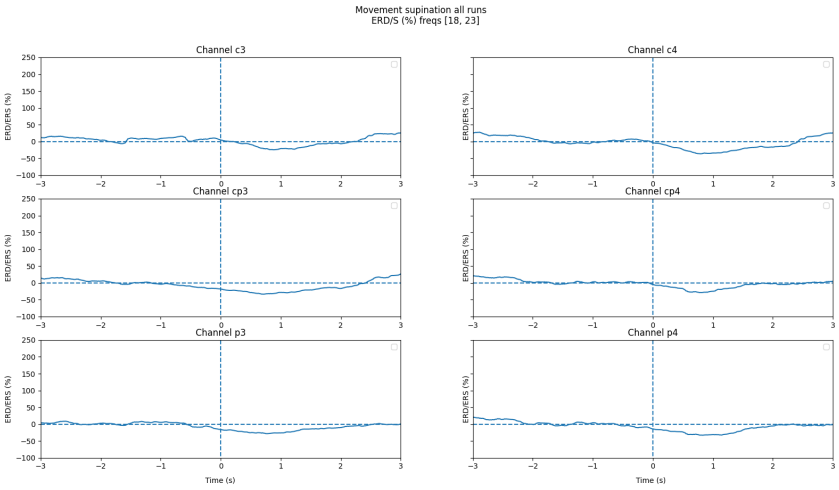


(c) Supination

Figure C.19: ERD/ERS line plot subject 7 for $\beta$ band [18, 23] Hz (with iHandU onsets as t= 0)

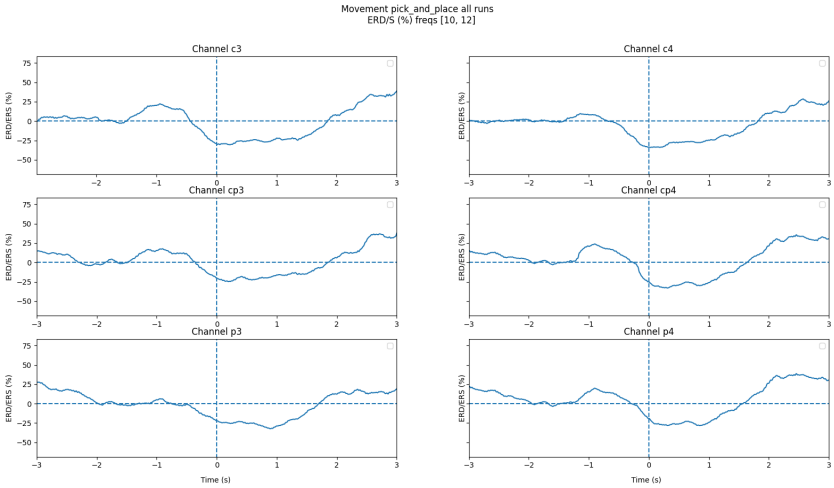


(a) Pick and place

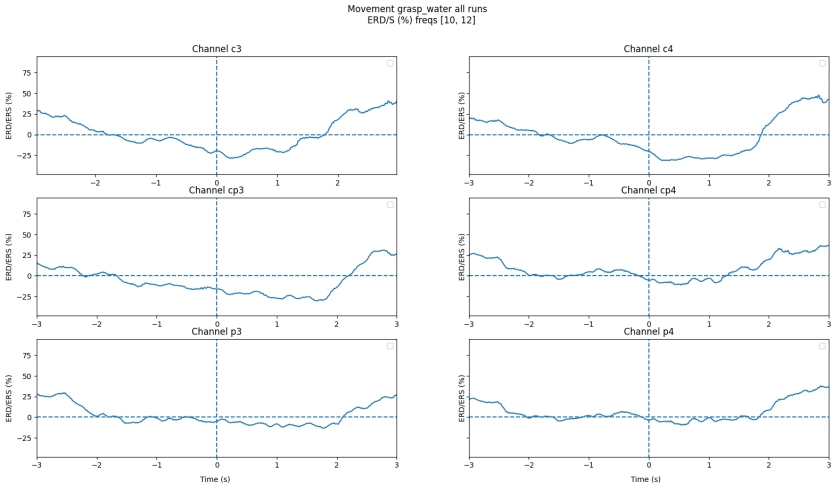


(b) Grasp

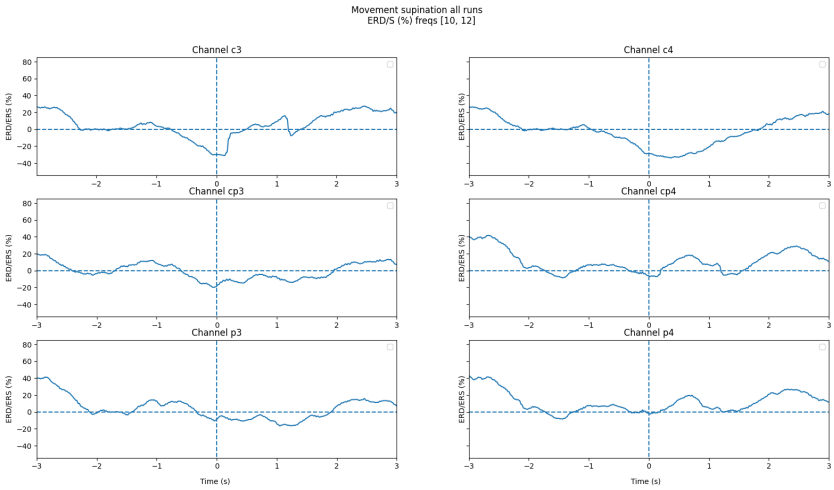


(c) Supination

Figure C.20: ERD/ERS line plot subject 8 for $\mu$ band [10, 12] Hz

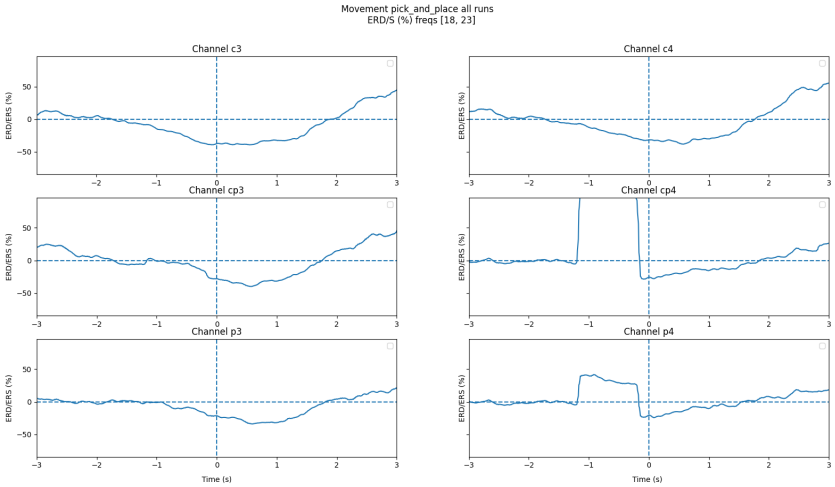


(a) Pick and place

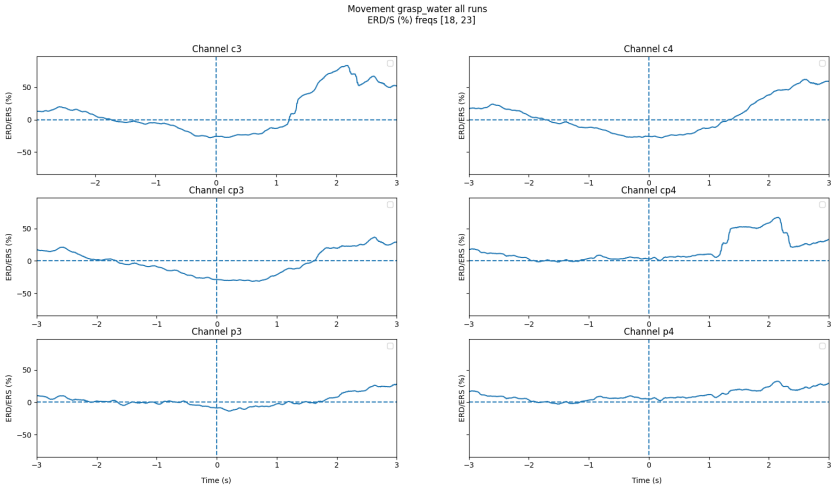


(b) Grasp

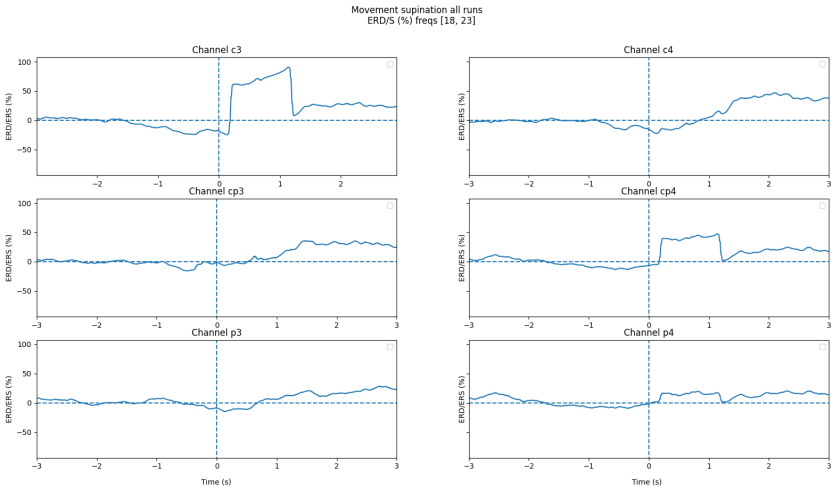


(c) Supination

Figure C.21: ERD/ERS line plot subject 8 for $\beta$ band [18, 23] Hz

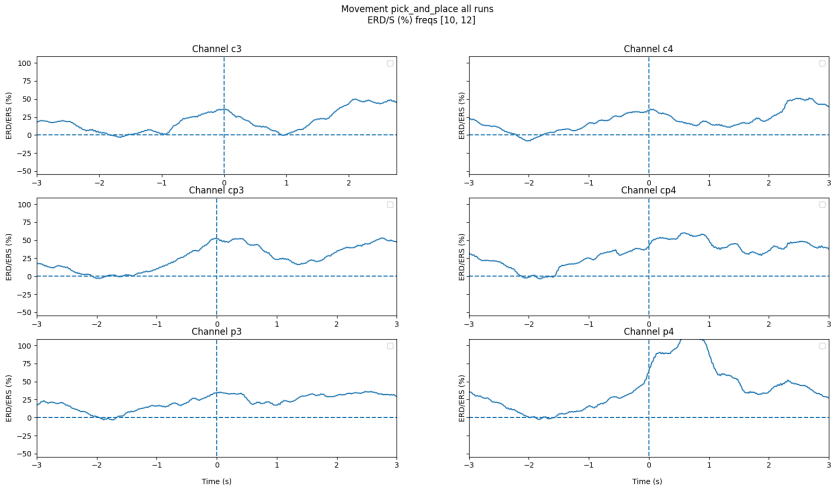


(a) Pick and place

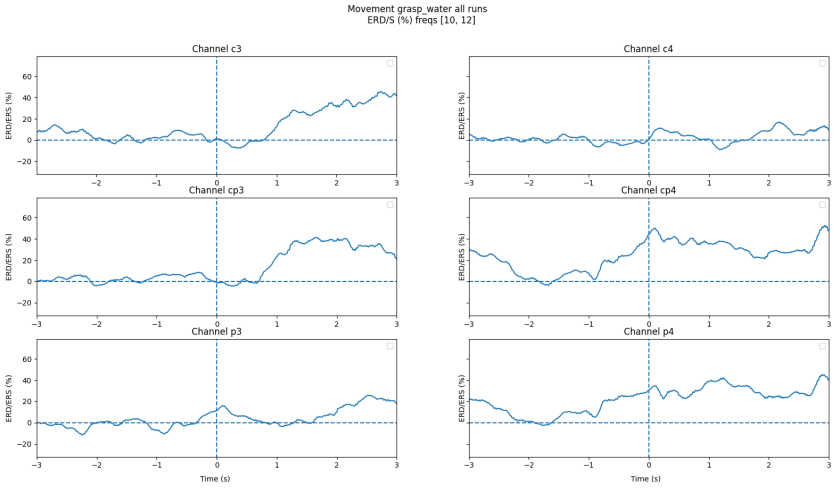


(b) Grasp

Figure C.22: ERD/ERS line plot subject 9 for $\mu$ band [10, 12] Hz

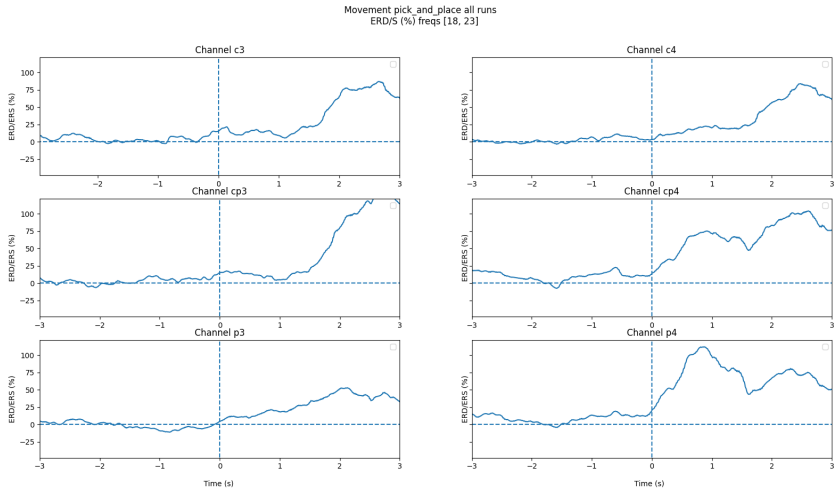


(a) Pick and place

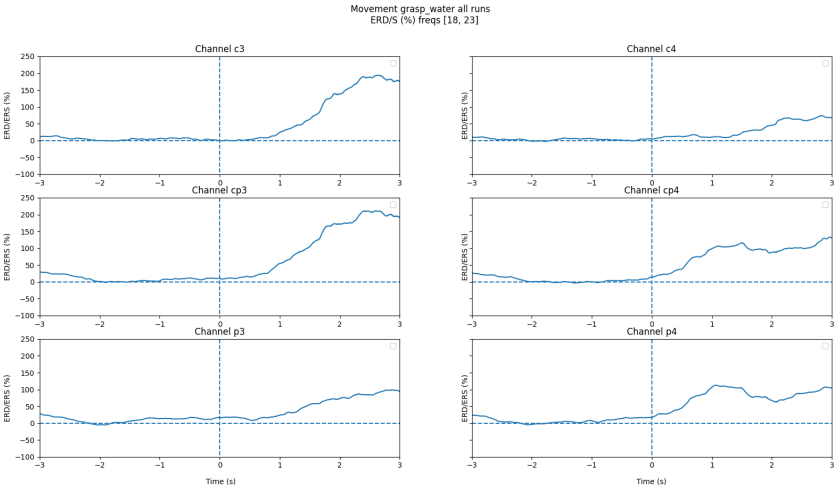


(b) Grasp

Figure C.23: ERD/ERS line plot subject 9 for $\beta$ band [18, 23] Hz

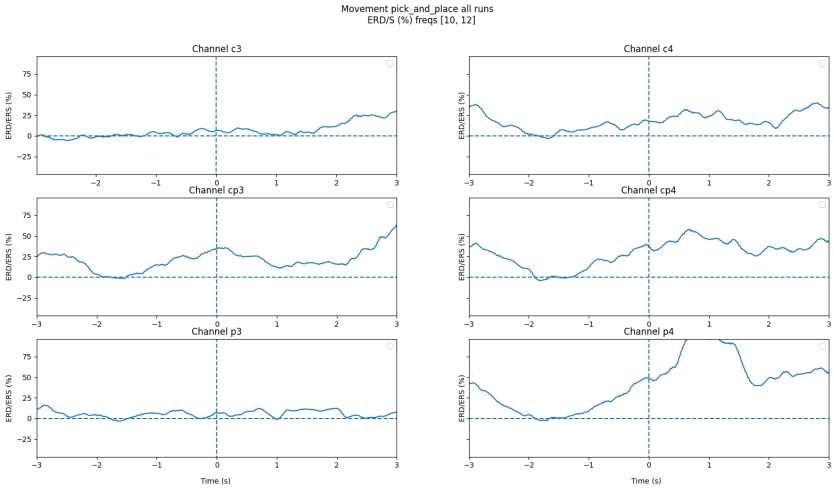


(a) Pick and place

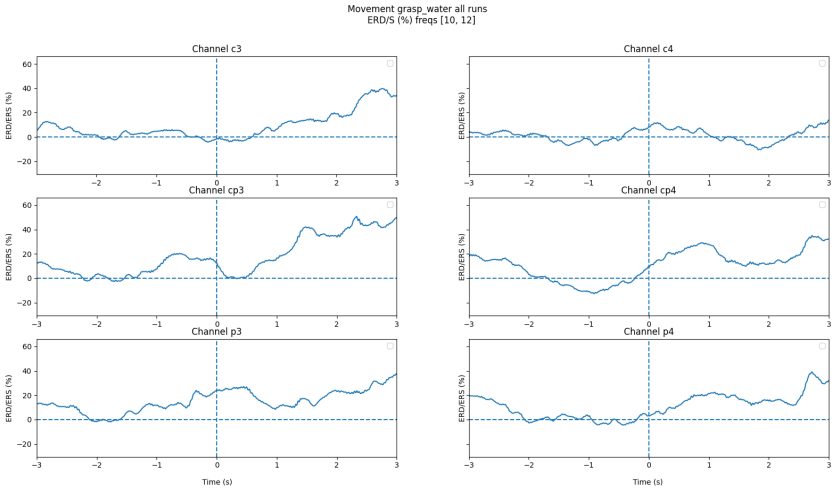


(b) Grasp

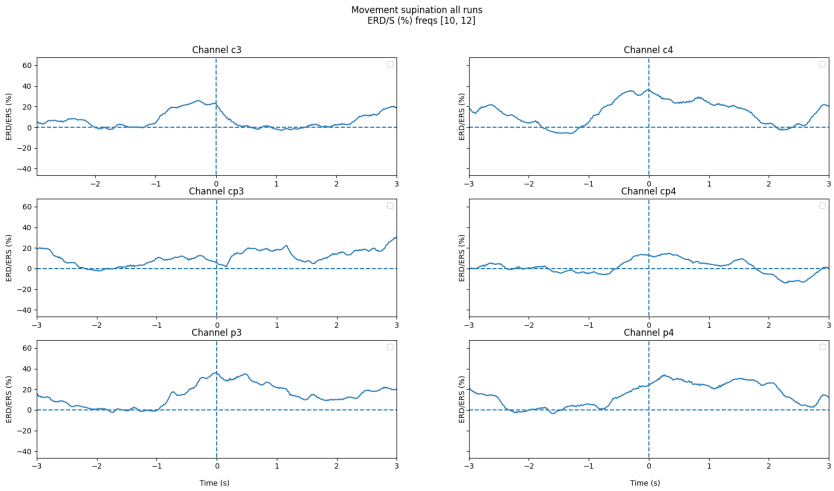


(c) Supination

Figure C.24: ERD/ERS line plot subject 9 for $\mu$ band [10, 12] Hz (with iHandU onsets as t= 0)

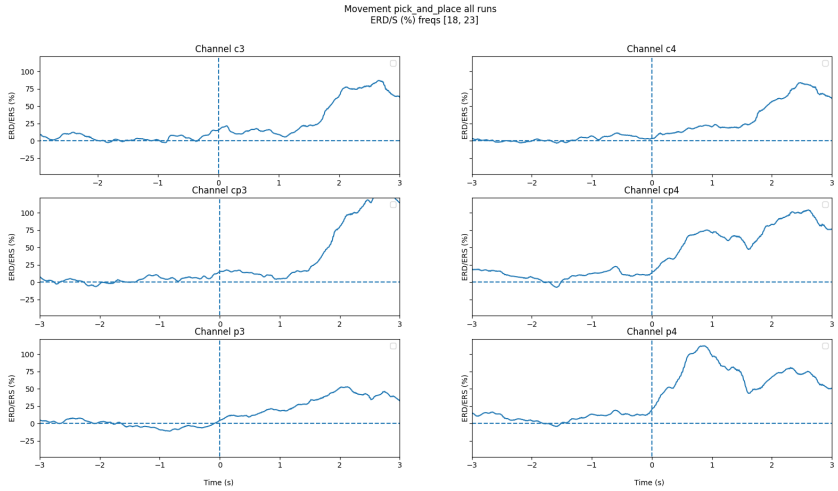


(a) Pick and place

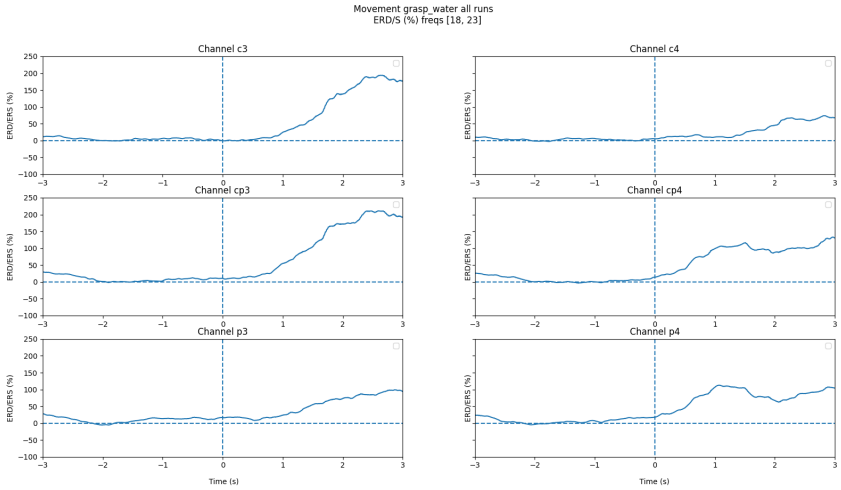


(b) Grasp

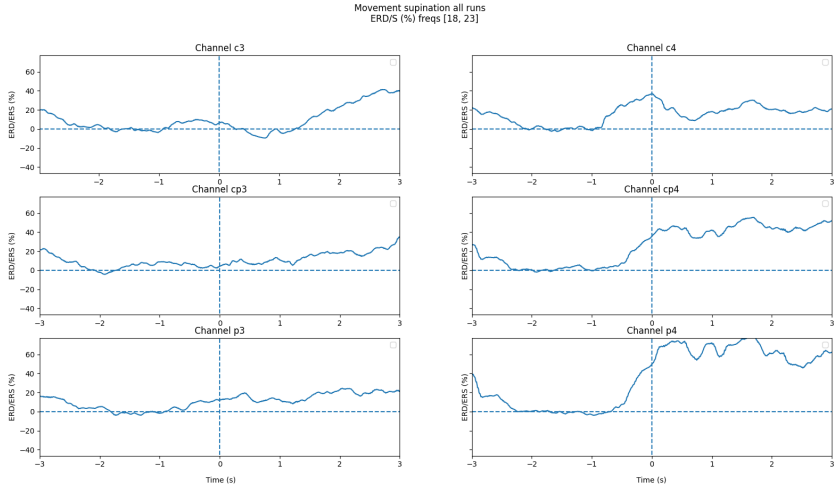


(c) Supination

Figure C.25: ERD/ERS line plot subject 9 for $\beta$ band [18, 23] Hz (with iHandU onsets as t= 0)

# References


[1] Luzheng Bi, A. Feleke, and Cuntai Guan. A review on EMG-based motor intention prediction of continuous human upper limb motion for human-robot collaboration, may 2019. doi:10.1016/j.bspc.2019.02.011.

[2] Achim Buerkle, William Eaton, Niels Lohse, Thomas Bamber, and Pedro Ferreira. EEG based arm movement intention recognition towards enhanced safety in symbiotic Human-Robot Collaboration. *Robotics and Computer-Integrated Manufacturing*, 70:102137, aug 2021. doi:10.1016/j.rcim.2021.102137.

[3] Yao Guo, Xiao Gu, and Guang-Zhong Yang. Human–Robot Interaction for Rehabilitation Robotics. pages 269–295, 2021. doi:10.1007/978-3-030-65896-0_23.

[4] Junyao Wang, Yuehong Dai, and Xiaxi Si. Analysis and recognition of human lower limb motions based on electromyography (Emg) signals. *Electronics (Switzerland)*, 10(20), oct 2021. doi:10.3390/electronics10202473.

[5] Miguel Simao, Nuno Mendes, Olivier Gibaru, and Pedro Neto. A Review on Electromyography Decoding and Pattern Recognition for Human-Machine Interaction. *IEEE Access*, 7:39564–39582, 2019. doi:10.1109/ACCESS.2019.2906584.

[6] Cristina Brambilla, Ileana Pirovano, Robert Mihai Mira, Giovanna Rizzo, Alessandro Scano, and Alfonso Mastropietro. Combined use of emg and eeg techniques for neuromotor assessment in rehabilitative applications: A systematic review, nov 2021. doi:10.3390/s21217014.

[7] Andrés F. Ruiz-Olaya. On the use of wearable sensors to enhance motion intention detection for a contralaterally controlled FES system. In *BSN 2016 - 13th Annual Body Sensor Networks Conference*, pages 324–328. Institute of Electrical and Electronics Engineers Inc., jul 2016. doi:10.1109/BSN.2016.7516282.

[8] Doganay Sirintuna, Idil Ozdamar, Yusuf Aydin, and Cagatay Basdogan. Detecting Human Motion Intention during pHRI Using Artificial Neural Networks Trained by EMG Signals. In *29th IEEE International Conference on Robot and Human Interactive Communication, RO-MAN 2020*, pages 1280–1287. Institute of Electrical and Electronics Engineers Inc., aug 2020. doi:10.1109/RO-MAN47096.2020.9223438.

[9] Arul V H Amrutha N. A Review on Noises in EMG Signal and its Removal. *International Journal of Scientific and Research Publications*, 7(5):23, 2017. URL: www.ijsrp.org.

[10] Nuradebah Burhan, Mohammad Afif Kasno, Rozaimi Ghazali, Mohd Hafiz Jali, and Radzai Said. Discrete Wavelet Transform Approach on the Electromyography Signal Processing during Rehabilitation Exercise. (03), 2017. URL: https://www.semanticscholar.

org/paper/Discrete-Wavelet-Transform-Approach-on-the-Signal-Burhan-Kasno/73f8c5e8cdc6102a940aef03443400dcc0f71446.

[11] OpenStax. Muscles of the pectoral girdle and upper limbs, 2015. https://courses.lumenlearning.com/suny-ap1/chapter/muscles-of-the-pectoral-girdle-and-upper-limbs/, Accessed 2022-05-31.

[12] Shuxiang Guo, Muye Pang, Baofeng Gao, Hideyuki Hirata, and Hidenori Ishihara. Comparison of sEMG-based feature extraction and motion classification methods for upper-limb movement. *Sensors (Switzerland)*, 15(4):9022–9038, apr 2015. doi:10.3390/s150409022.

[13] Eduardo López-Larraz, Luis Montesano, Ángel Gil-Agudo, and Javier Minguez. Continuous decoding of movement intention of upper limb self-initiated analytic movements from pre-movement EEG correlates. *Journal of NeuroEngineering and Rehabilitation*, 11(1):1–15, nov 2014. URL: https://jneuroengrehab.biomedcentral.com/articles/10.1186/1743-0003-11-153, doi:10.1186/1743-0003-11-153.

[14] Ji Hoon Jeong, Jeong Hyun Cho, Kyung Hwan Shim, Byoung Hee Kwon, Byeong Hoo Lee, Do Yeun Lee, Dae Hyeok Lee, and Seong Whan Lee. Multimodal signal dataset for 11 intuitive movement tasks from single upper extremity during multiple recording sessions. *GigaScience*, 9(10):1–15, 2020. doi:10.1093/GIGASCIENCE/GIAA098.

[15] Muhammad Zahak. Signal Acquisition Using Surface EMG and Circuit Design Considerations for Robotic Prosthesis. In *Computational Intelligence in Electromyography Analysis - A Perspective on Current Applications and Future Challenges*. IntechOpen, oct 2012. doi:10.5772/52556.

[16] Towards Hybrid EEG-EMG-Based Control Approaches to be Used in Bio-robotics Applications: Current Status, Challenges and Future Directions. *Paladyn, Journal of Behavioral Robotics*, 4(2):147–154, dec 2015. doi:10.2478/pjbr-2013-0009.

[17] Mayfield brain. Brain anatomy, Anatomy of the human brain | Mayfield Brain & Spine Cincinnati, Ohio. *Mayfield Brain & Spine.*, 2007. URL: https://mayfieldclinic.com/pe-anatbrain.htm.

[18] S Sreeja, Debasis Samanta, Pabitra Mitra, and Monalisa Sarma. Motor Imagery EEG Signal Processing and Classification using Machine Learning Approach. *Jordanian Journal of Computers and Information Technology*, (0):80, 2018. doi:10.5455/jjcit.71-1512555333.

[19] James Knierim. Motor Cortex (Section 3, Chapter 3) Neuroscience Online: An Electronic Textbook for the Neurosciences | Department of Neurobiology and Anatomy - The University of Texas Medical School at Houston, 2018. https://nba.uth.tmc.edu/neuroscience/m/s3/chapter03.html, Accessed 2022-04-16.

[20] K. S. Rockland. Anatomy of the Cerebral Cortex. In *The Cerebral Cortex in Neurodegenerative and Neuropsychiatric Disorders: Experimental Approaches to Clinical Issues*, pages 3–36. 2017. doi:10.1016/B978-0-12-801942-9.00001-X.

[21] Catherine L. Ojakangas, Ammar Shaikhouni, Gerhard M. Friehs, Abraham H. Caplan, Mijail D. Serruya, Maryam Saleh, Daniel S. Morris, and John P. Donoghue. Decoding movement intent from human premotor cortex neurons for neural prosthetic applications. *Journal*

*of Clinical Neurophysiology*, 23(6):577–584, dec 2006. doi:10.1097/01.wnp.0000233323.87127.14.

[22] S. M. Shafiul Hasan, Masudur R. Siddiquee, Roozbeh Atri, Rodrigo Ramon, J. Sebastian Marquez, and Ou Bai. Prediction of gait intention from pre-movement EEG signals: A feasibility study. *Journal of NeuroEngineering and Rehabilitation*, 17(1):1–16, apr 2020. URL: https://jneuroengrehab.biomedcentral.com/articles/10.1186/s12984-020-00675-5, doi:10.1186/s12984-020-00675-5.

[23] Yongwoong Jeon, Chang S. Nam, Young Joo Kim, and Min Cheol Whang. Event-related (De)synchronization (ERD/ERS) during motor imagery tasks: Implications for brain-computer interfaces. *International Journal of Industrial Ergonomics*, 41(5):428–436, sep 2011. doi:10.1016/j.ergon.2011.03.005.

[24] Gert Pfurtscheller and Christa Neuper. Motor imagery direct communication. *Proceedings of the IEEE*, 89(7):1123–1134, 2001. doi:10.1109/5.939829.

[25] Irene Vigué-Guix. Brain Computer Interfaces (BCIs)based-on Movement Related CorticalPotentials (MRCPs), 2016. URL: https://www.dropbox.com/s/3833u9u6dr8dcvv/Thesis.pdf?dl=0.

[26] Gonzalo M. Rojas, Carolina Alvarez, Carlos E. Montoya, María de la Iglesia-Vayá, Jaime E. Cisternas, and Marcelo Gálvez. Study of resting-state functional connectivity networks using EEG electrodes position as seed. *Frontiers in Neuroscience*, 12(APR):235, apr 2018. doi:10.3389/fnins.2018.00235.

[27] Wikipedia. Inertial measurement unit - Wikipedia, 2021. https://en.wikipedia.org/wiki/Inertial_measurement_unit, Accessed 2022-01-29.

[28] What is an IMU Sensor? https://www.ceva-dsp.com/ourblog/what-is-an-imu-sensor/, Accessed 2022-01-29.

[29] Xiao Jiang, Gui Bin Bian, and Zean Tian. Removal of Artifacts from EEG Signals: A Review. *Sensors 2019, Vol. 19, Page 987*, 19(5):987, feb 2019. URL: https://www.mdpi.com/1424-8220/19/5/987, doi:10.3390/S19050987.

[30] Rubana H. Chowdhury, Mamun B.I. Reaz, Mohd Alauddin Bin Mohd Ali, Ashrif A.A. Bakar, K. Chellappan, and T. G. Chang. Surface Electromyography Signal Processing and Classification Techniques. *Sensors 2013, Vol. 13, Pages 12431-12466*, 13(9):12431–12466, sep 2013. doi:10.3390/S130912431.

[31] E. A. Clancy, E. L. Morin, and R. Merletti. Sampling, noise-reduction and amplitude estimation issues in surface electromyography. In *Journal of Electromyography and Kinesiology*, volume 12, pages 1–16. Elsevier, feb 2002. doi:10.1016/S1050-6411(01)00033-5.

[32] Maria Carolina Tigre Avelar. Intellwheels–Controlling an Intelligent Wheelchair using a Brain Computer Interface. Master's thesis, FEUP, 2019.

[33] Victoria Peterson, Catalina Galván, Hugo Hernández, and Ruben Spies. A feasibility study of a complete low-cost consumer-grade brain-computer interface system. *Heliyon*, 6(3):e03425, mar 2020. doi:10.1016/j.heliyon.2020.e03425.

[34] Berenice Gudiño-Mendoza, Gildardo Sanchez-Ante, and Javier M. Antelis. Detecting the Intention to Move Upper Limbs from Electroencephalographic Brain Signals. *Computational and Mathematical Methods in Medicine*, 2016, 2016. doi:10.1155/2016/3195373.

[35] Jia Liang Ren, Ya Hui Chien, En Yu Chia, Li Chen Fu, and Jin Shin Lai. Deep learning based motion prediction for exoskeleton robot control in upper limb rehabilitation. In *Proceedings - IEEE International Conference on Robotics and Automation*, volume 2019-May, pages 5076–5082. Institute of Electrical and Electronics Engineers Inc., may 2019. doi:10.1109/ICRA.2019.8794187.

[36] MyoWare™Muscle Sensor (AT-04-001) Datasheet by SparkFun Electronics | Digi-Key Electronics. https://www.digikey.com/htmldatasheets/production/1897318/0/0/1/myoware-muscle-sensor-at-04-001-.html, Accessed 2022-01-29.

[37] EmotiBit. EmotiBit – Wearable emotion sensing for any project, 2019. https://www.emotibit.com/, Accessed 2022-01-29.

[38] Hiroki Ohashi, Mohammad Al-Naser, Sheraz Ahmed, Takayuki Akiyama, Takuto Sato, Phong Nguyen, Katsuyuki Nakamura, and Andreas Dengel. Augmenting wearable sensor data with physical constraint for dnn-based human-action recognition. 08 2017.

[39] Ana Oliveira, Duarte Dias, Elodie Murias Lopes, Maria Do Carmo Vilas-Boas, and Joao Paulo Silva Cunha. A Textile Embedded Wearable Device for Movement Disorders Quantification. In *Proceedings of the Annual International Conference of the IEEE Engineering in Medicine and Biology Society, EMBS*, volume 2020-July, pages 4559–4562. Institute of Electrical and Electronics Engineers Inc., jul 2020. doi:10.1109/EMBC44109.2020.9175772.

[40] Welcome to the OpenBCI Community · OpenBCI Documentation. https://docs.openbci.com/, Accessed 2022-01-29.

[41] Emotiv. https://www.emotiv.com/epoc/, Accessed 2022-01-24.

[42] EEG cap. URL: https://besdatatech.com/eeg-caps/.

[43] Evan D. Crotty, Laura Anne M. Furlong, Kevin Hayes, and Andrew J. Harrison. Onset detection in surface electromyographic signals across isometric explosive and ramped contractions: A comparison of computer-based methods. *Physiological Measurement*, 42(3), 2021. doi:10.1088/1361-6579/abef56.

[44] Stanislaw Solnik, Patrick Rider, Ken Steinweg, Paul Devita, and Tibor Hortobágyi. Teager-Kaiser energy operator signal conditioning improves EMG onset detection. *European Journal of Applied Physiology*, 110(3):489–498, oct 2010. doi:10.1007/s00421-010-1521-8.

[45] Robert Leeb, Hesam Sagha, Ricardo Chavarriaga, and José Del R. Millán. Multimodal fusion of muscle and brain signals for a Hybrid-BCI. In *2010 Annual International Conference of the IEEE Engineering in Medicine and Biology Society, EMBC'10*, pages 4343–4346, 2010. doi:10.1109/IEMBS.2010.5626233.

[46] M. B.I. Reaz, M S Hussain, and F Mohd-Yasin. Techniques of EMG signal analysis: Detection, processing, classification and applications. *Biological Procedures Online*, 8(1):11–35, 2006. URL: www.biologicalprocedures.com, doi:10.1251/bpo115.

[47] William Rose. Mathematics and Signal Processing for Biomechanics: Electromyogram Analysis. *Mathematics and Signal Processing for Biomechanics*, 2014.

[48] EMG page. http://www.soe.uoguelph.ca/webfiles/mleuniss/Biomechanics/EMG.html, Accessed 2022-04-10.

[49] Dennis J. McFarland. The advantages of the surface Laplacian in brain-computer interface research. *International Journal of Psychophysiology*, 97(3):271–276, sep 2015. URL: https://www.ncbi.nlm.nih.gov/pmc/articles/PMC4312749/, doi:10.1016/j.ijpsycho.2014.07.009.

[50] Josep Mouriño, José Del R. Millán, Febo Cincotti, Silvia Chiappa, Raimon Jané, and Fabio Babiloni. Spatial filtering in the training process of a brain computer interface. In *Annual Reports of the Research Reactor Institute, Kyoto University*, volume 1, pages 639–642, 2001. doi:10.1109/iembs.2001.1019016.

[51] Sajjad Afrakhteh and Mohammad Reza Mosavi. Applying an efficient evolutionary algorithm for EEG signal feature selection and classification in decision-based systems. In *Energy Efficiency of Medical Devices and Healthcare Applications*, pages 25–52. Academic Press, jan 2020. doi:10.1016/b978-0-12-819045-6.00002-9.

[52] Terrence D Lagerlund, Frank W Sharbrough, and Neil E Busacker. Use of principal component analysis in the frequency domain for mapping electroencephalographic activities: Comparison with phase-encoded Fourier spectral analysis. *Brain Topography*, 17(2):73–84, 2004. doi:10.1007/s10548-004-1005-4.

[53] Abdulhamit Subasi and M. Ismail Gursoy. EEG signal classification using PCA, ICA, LDA and support vector machines. *Expert Systems with Applications*, 37(12):8659–8666, dec 2010. doi:10.1016/j.eswa.2010.06.065.

[54] Nikesh Bajaj. Wavelets for EEG Analysis. In *Wavelet Theory*. IntechOpen, nov 2021. URL: undefined/state.item.id, doi:10.5772/intechopen.94398.

[55] Ed Burns. What is Machine Learning and Why is it Important? (July):1–23, 2016. URL: https://www.techtarget.com/searchenterpriseai/definition/machine-learning-ML.

[56] Marc Peter, Deisenroth A Aldo, Faisal Cheng, and Soon Ong. MATHEMATICS FOR MACHINE LEARNING. In *INTED2022 Proceedings*, volume 1, pages 8354–8354, 2022. URL: https://mml-book.com., doi:10.21125/inted.2022.2134.

[57] Geoffrey I. Webb, Claude Sammut, Claudia Perlich, Tamás Horváth, Stefan Wrobel, Kevin B. Korb, William Stafford Noble, Christina Leslie, Michail G. Lagoudakis, Novi Quadrianto, Wray L. Buntine, Novi Quadrianto, Wray L. Buntine, Lise Getoor, Galileo Namata, Lise Getoor, Jiawei Han, Xin Jin, Jo-Anne Ting, Sethu Vijayakumar, Stefan Schaal, and Luc De Raedt. Leave-One-Out Cross-Validation. In *Encyclopedia of Machine Learning*, pages 600–601. Springer, Boston, MA, 2011. URL: https://link.springer.com/referenceworkentry/10.1007/978-0-387-30164-8{_}469, doi:10.1007/978-0-387-30164-8_469.

[58] Yi Hui Zhou and Paul Gallins. A review and tutorial of machine learning methods for microbiome host trait prediction. *Frontiers in Genetics*, 10(JUN):579, 2019. doi:10.3389/fgene.2019.00579.

[59] Sergios Theodoridis. *Machine Learning: A Bayesian and Optimization Perspective*. 2015. doi:10.1016/C2013-0-19102-7.

[60] J. A.K. Suykens and J. Vandewalle. Least squares support vector machine classifiers. *Neural Processing Letters*, 9(3):293–300, 1999. https://link.springer.com/article/10.1023/A:1018628609742, Accessed 2022-08-18. doi:10.1023/A:1018628609742.

[61] 1.4. Support Vector Machines — scikit-learn 1.1.2 documentation. https://scikit-learn.org/stable/modules/svm.html, Accessed 2022-08-17.

[62] Drew Wilimitis. The Kernel Trick in Support Vector Classification | by Drew Wilimitis | Towards Data Science, 2018. https://towardsdatascience.com/the-kernel-trick-c98cdbcaeb3f, Accessed 2022-08-17.

[63] Raman Bhadauria. ML | Linear Discriminant Analysis - GeeksforGeeks, 2019. https://www.geeksforgeeks.org/ml-linear-discriminant-analysis/, Accessed 2022-08-17.

[64] Scikit-learn.org. 1.2. Linear and Quadratic Discriminant Analysis — scikit-learn 0.20.1 documentation, 2018. https://scikit-learn.org/stable/modules/lda{_}qda.html?highlight=linear+discriminant+analysis, Accessed 2022-08-17.

[65] Vitor Minhoto. Man-Machine Symbiosis - EEG and other biosignal man-machine interaction. Master's thesis, FEUP, 2019.

[66] N. J. Sairamya, L. Susmitha, S. Thomas George, and M. S.P. Subathra. Hybrid approach for classification of electroencephalographic signals using time-frequency images with wavelets and texture features. In *Intelligent Data Analysis for Biomedical Applications: Challenges and Solutions*, pages 253–273. Academic Press, jan 2019. doi:10.1016/B978-0-12-815553-0.00013-6.

[67] Wikipedia. Long short-term memory - Wikipedia. https://en.wikipedia.org/wiki/Long{_}short-term{_}memory, Accessed 2022-08-17.

[68] Shipra Saxena. LSTM | Introduction to LSTM | Long Short Term Memory, 2021. https://www.analyticsvidhya.com/blog/2021/03/introduction-to-long-short-term-memory-lstm/, Accessed 2022-08-17.

[69] Alon Lekhtman. Data Science in Medicine — Precision & Recall or Specificity & Sensitivity? | by Alon Lekhtman | Towards Data Science, 2019. https://towardsdatascience.com/should-i-look-at-precision-recall-or-specificity-sensitivity-3946158aace1, Accessed 2022-08-18.

[70] Sarang Narkhede. Understanding AUC - ROC Curve | by Sarang Narkhede | Towards Data Science, 2018. https://towardsdatascience.com/understanding-auc-roc-curve-68b2303cc9c5, Accessed 2022-08-18.

[71] Setting up for EEG, EMG, and ECG at the same time · OpenBCI Documentation. https://docs.openbci.com/GettingStarted/Biosensing-Setups/ExGSetup/, Accessed 2022-03-03.

[72] Gold Cup Electrodes – OpenBCI Online Store. https://shop.openbci.com/products/openbci-gold-cup-electrodes?variant=37345591591070, Accessed 2022-01-24.

[73] Ultracortex mark iv. https://docs.openbci.com/AddOns/Headwear/MarkIV/, Accessed 2022-01-24.

[74] Ana Oliveira, Duarte Dias, Elodie Múrias Lopes, Maria Do Carmo Vilas-Boas, and João Paulo Silva Cunha. Snapki—an inertial easy-to-adapt wearable textile device for movement quantification of neurological patients. *Sensors (Switzerland)*, 20(14):1–20, jul 2020. URL: https://www.mdpi.com/1424-8220/20/14/3875/htmhttps://www.mdpi.com/1424-8220/20/14/3875, doi:10.3390/s20143875.

[75] Vinicius Horn Cene, Mauricio Tosin, Juliano Machado, and Alexandre Balbinot. Open database for accurate upper-limb intent detection using electromyography and reliable extreme learning machines. *Sensors (Switzerland)*, 19(8), apr 2019. doi:10.3390/s19081864.

[76] Baofeng Gao, Chao Wei, Hongdao Ma, Shu Yang, Xu Ma, and Songyuan Zhang. Real-time evaluation of the signal processing of sEMG used in limb exoskeleton rehabilitation system. *Applied Bionics and Biomechanics*, 2018, 2018. doi:10.1155/2018/1391032.

[77] Network time protocol. https://en.wikipedia.org/wiki/Network_Time_Protocol, Accessed 2022-04-24.

[78] M. Lidierth. A computer based method for automated measurement of the periods of muscular activity from an EMG and its application to locomotor EMGs. *Electroencephalography and Clinical Neurophysiology*, 64(4):378–380, oct 1986. doi:10.1016/0013-4694(86)90163-X.

[79] Martin A. Fischler and Robert C. Bolles. Random sample consensus: A paradigm for model fitting with applications to image analysis and automated cartography. *Commun. ACM*, 24(6):381–395, jun 1981. URL: https://doi.org/10.1145/358669.358692, doi:10.1145/358669.358692.

[80] Andrej Savić, Romulus Lontis, Ning Jiang, Mirjana Popović, Dario Farina, Kim Dremstrup, and Natalie Mrachacz-Kersting. Movement related cortical potentials and sensory motor rhythms during self initiated and cued movements. *Biosystems and Biorobotics*, 7:701–707, 2014. URL: https://link.springer.com/chapter/10.1007/978-3-319-08072-7{_}98, doi:10.1007/978-3-319-08072-7_98.

[81] G. Pfurtscheller and F. H. Lopes Da Silva. Event-related EEG/MEG synchronization and desynchronization: Basic principles. *Clinical Neurophysiology*, 110(11):1842–1857, 1999. doi:10.1016/S1388-2457(99)00141-8.